


2021

Understanding the relationship between local environmental changes and the function of the pH Low Insertion Peptide

Violetta Burns Casamayor
West Virginia University, vb0009@mix.wvu.edu

Follow this and additional works at: <https://researchrepository.wvu.edu/etd>

 Part of the [Biochemistry Commons](#), [Biophysics Commons](#), [Molecular Biology Commons](#), and the [Physical Chemistry Commons](#)

Recommended Citation

Burns Casamayor, Violetta, "Understanding the relationship between local environmental changes and the function of the pH Low Insertion Peptide" (2021). *Graduate Theses, Dissertations, and Problem Reports*. 10156.

<https://researchrepository.wvu.edu/etd/10156>


This Dissertation is protected by copyright and/or related rights. It has been brought to you by the The Research Repository @ WVU with permission from the rights-holder(s). You are free to use this Dissertation in any way that is permitted by the copyright and related rights legislation that applies to your use. For other uses you must obtain permission from the rights-holder(s) directly, unless additional rights are indicated by a Creative Commons license in the record and/ or on the work itself. This Dissertation has been accepted for inclusion in WVU Graduate Theses, Dissertations, and Problem Reports collection by an authorized administrator of The Research Repository @ WVU. For more information, please contact researchrepository@mail.wvu.edu.

2021

Understanding the relationship between local environmental changes and the function of the pH Low Insertion Peptide

Violetta Burns Casamayor

Follow this and additional works at: <https://researchrepository.wvu.edu/etd>

 Part of the [Biochemistry Commons](#), [Biophysics Commons](#), [Molecular Biology Commons](#), and the [Physical Chemistry Commons](#)

Understanding the relationship between local environmental changes and the function of the pH Low Insertion Peptide

Violetta Burns

Dissertation submitted
to the Eberly College of Arts and Sciences
at West Virginia University

in partial fulfillment for the
degree of Doctor of Philosophy in Chemistry

Blake Mertz, PhD, chair

Brian Popp, PhD

Justin Legleiter, PhD

Jonathan Boyd, PhD

Valery Khramtsov, PhD

[C. Eugene Bennett Department of Chemistry](#)

Morgantown, West Virginia

2021

Keywords: pHLIP, pH Low Insertion Peptide, Molecular dynamics, Intrinsically
disordered proteins

Copyright 2021 Violetta Burns

Abstract

Understanding the relationship between local environmental changes and the function of the pH Low Insertion Peptide

Violetta Burns

Cancer is the second leading cause of death in the US with over 1.7 million new cases each year. Current cancer treatments tend to also target healthy tissues due to similarities with cancerous ones, resulting in acute side effects. Early detection is the best approach towards defeating cancer, however, modern imaging techniques require sizeable samples, often implying a late stage in the disease. One common attribute of tumors is their acidic microenvironment, which can be taken advantage of.

The pH Low Insertion Peptide (pHLIP) is a membrane-active peptide that can take advantage of the acidic microenvironment surrounding cancer cells. pHLIP can spontaneously fold and insert unidirectionally as a transmembrane into lipid membranes under acidic conditions. Thus, pHLIP is able to transport drugs across cancerous membranes and deliver it to the interior of the cell. Although the mechanism of insertion and exit of the peptide has been thoroughly studied through experimental and computational approaches, there are still elements of the peptide and its behavior that are not fully understood.

This dissertation focuses on all-atoms molecular dynamics (MD) simulations to study the interactions between pHLIP and its environmental factors. Through High Performance Computing (HPC) at West Virginia University (WVU), we were able to map the initial stages of exit of pHLIP, determine the effect of peptide insertion on the dynamics of a complex lipid bilayer and provide new insights into the environmental factors affecting pHLIP in solution. The results reported in this dissertation will aid the future development of pHLIP-based early detection and targeting agents.

Declaration of Authorship

I, Violetta Burns, declare that this thesis titled, ‘Understanding the relationship between local environmental changes and the function of the pH Low Insertion Peptide’ and the work presented in it are my own. I confirm that:

- This work was done wholly or mainly while in candidature for a research degree at this University.
- Where any part of this thesis has previously been submitted for a degree or any other qualification at this University or any other institution, this has been clearly stated.
- Where I have consulted the published work of others, this is always clearly attributed.
- Where I have quoted from the work of others, the source is always given. With the exception of such quotations, this thesis is entirely my own work.
- I have acknowledged all main sources of help.
- Where the thesis is based on work done by myself jointly with others, I have made clear exactly what was done by others and what I have contributed myself.

Signed: Violetta Burns

Date: 08/09/2021

“No matter what they tell you, words and ideas can change the world”

Robin Williams

Acknowledgements

I would like to take the opportunity to thank a few people without whom this work would not have been possible.

Firstly, I would like to thank my advisor, Dr. Blake Mertz, for his continuous support throughout these years and his guidance, not only in work related matters, but also in every day life challenges. Joining Dr. Mertz's research group was, without a question, one of the best decisions I have ever made, and it has made me a better scientist. I would also like to thank past and present lab members and colleagues, for their patience, guidance and fun times. I would also like to thank my committee members, Dr. Brian Popp, Dr. Justin Legleiter, Dr. Jonathan Boyd and Dr. Valery Khramtsov for their feedback and support throughout these years.

I would like to thank my LANL mentor, Dr. Chris Neale, for giving me the opportunity to become part of an amazing team and help me develop my coding and scientific skills.

I would like to thank my family, both here and overseas, for the unconditional support and love, including the tough love moments, as they have tough me so much about life and success.

Finally, I would also like to thank my friends, without whom I would have never thought myself capable of achieving this. Thank you to the Cattermole family for lifting me up and never doubting my capabilities, and for the never ending love. Thank you to my dear friend Kristin Kelly, for showing me how to survive and adapt in a brand new place, and for always believing in me. Thank you to my friends Bill Feeney and Halle Edwards for the laughter, the trips and the "we can do this moments". And thank you to my friends Ana Devesa and Raul Lopez for the weekly calls and thoughtful messages.

Contents

Abstract	ii
Declaration of Authorship	iii
Acknowledgements	v
List of Figures	viii
List of Tables	xiii
1 Introduction	1
1.1 Cell membrane lipids	1
1.2 Characteristics of cancer cells	5
1.3 The pH Low Insertion Peptide	6
1.3.1 Origins and discovery	6
1.3.2 pHLIP's mechanism	7
1.3.3 pHLIP cancer studies	8
2 Methods	18
3 Using Simulation to Understand the Role of Titration on the Stability of a Peptide–Lipid Bilayer Complex	24
3.1 Abstract	24
3.2 Introduction	26
3.3 Computational Methods	28
3.3.1 System setup	28
3.3.2 MD simulations	28
3.3.3 Analysis	29
3.4 Results and Discussion	30
3.4.1 pHLIP repositions in the bilayer in distinct ways to compensate for deprotonation	31

3.4.2	Localized destabilization of the bilayer is closely coupled to deprotonation of pHLIP and hydration of the hydrophobic interior	33
3.4.3	Implications of results on understanding of pHLIP in state III	36
3.5	Conclusion	40
4	The Transmembrane Helix of pHLIP Slows Down Membrane Thickness Fluctuations and Translational Diffusion	47
4.1	Abstract	47
4.2	Introduction	49
4.3	Results	51
4.3.1	Effect of pHLIP on bilayer dynamics in its SA and TM states.	51
4.3.2	Average bilayer thickness is not affected by pHLIP.	55
4.3.3	TM pHLIP increases lipid acyl chain snorkeling.	57
4.4	Discussion	59
4.4.1	pHLIP suppresses membrane thickness fluctuations by increasing lipid viscosity.	60
4.4.2	TM pHLIP reduces lipid translational diffusion more than rotational diffusion.	61
4.4.3	Lipid tails exhibit more snorkeling in the presence of TM pHLIP.	62
4.5	Conclusion	63
5	Understanding the effects of salt concentration on state I of pHLIP	77
5.1	Abstract	77
5.2	Introduction	78
5.3	Computational Methods	79
5.3.1	MD simulations	80
5.3.2	Analysis	80
5.4	Results and Discussion	80
5.4.1	Salt concentration affects helicity of N-terminus.	80
5.4.2	Deprotonated pHLIP expands as a function of salt concentration.	82
5.4.3	Number of contacts increases with salt.	83
5.5	Conclusion	84
6	Future directions	93

List of Figures

1.1	Schematic of lipid bilayer. Lipid bilayer formed by spontaneous self-assembly of amphipathic lipids, with hydrophobic tails secluding themselves by positioning at the center of the bilayer and hydrophilic headgroups staying at the lipid-solvent interfaces.	2
1.2	Chemical structure of a glycerophospholipid. One of the main structural polar lipids found in mammalian cells. Primarily composed of two fatty acyl chains, glycerol backbone and charged headgroup. [2]	2
1.3	Chemical structure of a sphingolipid. Structural polar lipid type found in mammalian cells. Composed by a sphingoid base backbone, N-Acyl hydrocarbon chain and charged headgroup.[2]	3
1.4	Chemical structure of a cholesterol. Non-polar lipid found in mammalian cells. Structure defined by a hydroxyl group, fused rings and a hydrocarbon tail. Specially important in affecting the viscosity of the lipid bilayer.[2]	4
1.5	Warburg effect. <i>Left:</i> Oxidative phosphorylation and anaerobic glycolysis processes of healthy cells. <i>Right:</i> Aerobic glycolysis process of cancer cells.[22]	6
1.6	Mechanism of folding and insertion of pHLIP. pHLIP has three distinctive states: unstructured in solution (state I), embedded in the membrane (state II) both a $\text{pH} > 7$ and inserted as a transmembrane helix (state III) at $\text{pH} < 6.5$.[23]	7
1.7	Folding and insertion events through CD and fluorescence spectroscopy. <i>Figure A:</i> CD spectroscopy of pHLIP at $\text{pH} 7.4$ (<i>black</i>), 6.4 (<i>blue</i>) and 5.3 (<i>red</i>). Results show how pHLIP's conformation changes from a coil conformation (<i>blue and black</i>) to helical at acidic pH (<i>red</i>). <i>Figure B:</i> Fluorescence spectroscopy of pHLIP as a function of pH . Blue shift is observed from $\text{pH} 7.87$ to 5.70 , which indicates that pHLIP's tryptophans have progressed from being in contact with the solvent to be inserted into the membrane.[29]	8
1.8	Generalized model of insertion and exit mechanism of pHLIP. Single-tryptophan pHLIP variants at positions 6 (<i>green</i>), 17 (<i>blue</i>) and 30 (<i>red</i>). Insertion of pHLIP via initial embedding, partial folding and finally, insertion to transmembrane conformation. Exit pathway involves destabilization of the transmembrane peptide followed by exit. [37]	9

2.1	Molecular dynamics as a higher resolution technique. Graphical depiction of the resolution of current experimental versus molecular dynamics (MD) simulations. MD allows to research short biological processes at the atomic level, hence avoiding loss of detailed information of the system.[1]	18
3.1	Overview of systems studied. <i>Left:</i> Snapshot of pHLIP (<i>yellow</i>) folded and inserted into a POPC bilayer (<i>surface, green and red</i>). <i>Inset:</i> Close-up of pHLIP highlighting the acidic residues that are either protonated or deprotonated in this study.	28
3.2	Sequential deprotonation of pHLIP leads to localized and global changes in helicity. <i>Top:</i> Representative conformation of pHLIP in the fully folded state. Primary amino acid sequence of pHLIP, with putative transmembrane segment underlined. A) Per-residue helicity of pHLIP as a function of protonation state. B) Total helical content of pHLIP as a function of protonation state.	31
3.3	Deprotonation of acidic residues triggers expansion of pHLIP. A) Average radius of gyration (r_g) of the TM segment of pHLIP as a function of deprotonation of acidic residues. B) distribution of r_g of the TM segment of pHLIP as a function of deprotonation of acidic residues.	32
3.4	Hydrophobic effect leads to compensating motions of N- and C-terminal halves of pHLIP TM helix as acidic residues are progressively deprotonated. A) Helix tilt angle with respect to the membrane normal, as defined by the vector from residues 8-30 in pHLIP. B) Helix tilt angle with respect to the membrane normal, as defined by the vector from residues 8-19 in pHLIP. C) Helix tilt angle with respect to the membrane normal, as defined by the vector from residues 21-30 in pHLIP. D) Hinge angle as measured between the vectors formed by the N-terminal (residues 10 to 19) and C-terminal (residues 21 to 30) halves of the transmembrane (TM) helix of pHLIP. <i>Lower right:</i> schematic showing the corresponding change in tilt angle of each TM segment of pHLIP as it is fully deprotonated.	33
3.5	Deprotonation has subtle localized and global effects on positioning of pHLIP in state III. Per-residue distance distribution of pHLIP with respect to the midplane of the POPC bilayer (zero corresponds to the projection onto the z-axis of the center of mass of the bilayer). Heat bar indicates the probability of per-residue distance. Thick black vertical lines indicate the boundaries of the TM segment of pHLIP.	34

- 3.6 **Destabilization of hydrophobic interior of bilayer is coupled to deprotonation of pHLIP in state III.** **(A)** Maximum value of the first shell of the radial distribution function (RDF) of water with respect to pHLIP. **(B)** Explicit count of the number of times a water molecule diffuses into the membrane interior, shown as the number of crossing events. **(C)** Probability distribution of the time a given water molecule spends in the hydrophobic region of the bilayer. **(D)** Molecular order parameter (MOP) of pHLIP. 35
- 3.7 **Deprotonation of acidic residues leads to penetration of water molecules into interior of the bilayer.** Volumetric representation of average water density for each protonation state in pHLIP. Average structure of pHLIP is used to show the gradual invasion of waters as pHLIP is sequentially deprotonated. *Red and green surface:* headgroups of upper and lower leaflets of POPC bilayer; *blue surface:* water; *yellow cartoon:* pHLIP. 36
- 4.1 **TM pHLIP slows down the rate of membrane thickness fluctuations and increases membrane viscosity.** **(A)** NSE schematic, where lipid vesicles scatter neutrons with a scattering angle 2θ and wavevector transfer \vec{q} . **(B)** NSE data, showing the normalized relaxation rate, $\frac{\Gamma}{q^3}$, as a function of q for tail perdeuterated membranes. Data are shown in the absence (black) and presence of pHLIP in its SA (blue, pH 8) or TM (red, pH 4) states. Peak height is associated with the rate of thickness fluctuations, while peak width describes the fluctuation amplitude. Lines are fits to the data using Eq. 2. **(C)** CG-MD simulation of membrane Fluctuation signals as detected by NSE, for vesicles without (black) and with (red) TM peptide incorporated. The suppression of thickness Fluctuations with TM pHLIP, compared to peptide-free membranes, is manifested in differences in the $\frac{\Gamma}{q^3}$ vs. q plots. **(D)** The rates of thickness fluctuations, extracted from fits to the data in (B), show remarkable suppression in the presence of TM pHLIP relative to the peptide-free membrane, and no changes with SA pHLIP. **(E)** Membrane viscosity changes exhibit a similar trend, as only TM pHLIP increases viscosity. **(F)** Atomistic MD simulations show a decrease in the mean-squared displacement (MSD) of the lipid headgroups in the presence (red) of pHLIP compared to lipid-only membranes (black). Error bars represent ± 1 S.D. 54

- 4.2 **Solid-state NMR cross-relation rates and the effect of pHLIP.** (A) Schematic of a DOPC lipid molecule showing the PC headgroup α and β carbons, and the two terminal CH_3 groups. (B) 1D slices at different mixing times showing the build-up of cross-relaxation peaks between acyl chain terminal methyl group protons and the PC headgroup α and β carbons in vesicles of DOPC/DOPS/Chol with containing pHLIP at pH 8. (C-E) Experimental peak volumes (symbols) and simulated build-up curves (lines) for three sets of cross peaks: (C) $\text{CH}_3 - \beta$ H, (D) $\text{CH}_3 - \alpha$ H, and (E) $\alpha - \beta$. Legend: Black + Squares, lipid only; Blue + Circles: pHLIP pH 8; Red + Diamonds, pHLIP pH 4. (F) Best-fit cross-relaxation rates for individual H spin-pairs (i.e. $\alpha - \beta$, $\text{CH}_3 - \alpha$ and $\text{CH}_3 - \beta$. Colors/markers are the same as in plots C-F. 56
- 4.3 **TM pHLIP increases snorkeling of lipid tails to the water-bilayer interface.** (A) Probability distribution of the distance between the CH_3 groups of oleoyl chains and the plane formed by the C_α of the choline headgroups. Black lines show data from neat bilayers, and red lines consider only lipids within 15 Å of pHLIP (*top*), or between 15 and 25 Å from the helix (*bottom*). *Insets* show the subtraction between red and black lines. (B) Representative snapshots of a DOPC/DOPC/Chol bilayer containing TM pHLIP. Phospholipid headgroups are shown in blue, and tails in yellow. CH_3 groups are shown as green spheres. Cholesterol molecules are shown in a ball and stick representation. (C) A representative DOPC molecule with fully extended acyl chains can snorkel reducing the distance to the choline headgroup in the presence of TM pHLIP. C_α (yellow) and CH_3 (green) are shown in spheres and are used for distance measurements. (D) Schematic of the effect of snorkeling on the DOPC oleoyl chain, depicting a structural change that enables nearby acyl chains to explore a larger conformation space and experience more entanglement. This manifest itself in increased membrane viscosity and slower thickness fluctuations compared to neat membranes. 58
- 5.1 **pHLIP in state I.** pHLIP is represented as coil (*yellow*), surrounded by Na^+ (*red*) and Cl^- (*green*) ions, and solvated in a water box. 79
- 5.2 **Deprotonation of all acidic residues leads to high helical content.** *Left:* Per residue helical content for fully deprotonated pHLIP as a function of the salt concentration for deprotonated pHLIP. *Right:* Per residue helical content of protonated pHLIP as a function of salt concentration. 81

5.3	Increased salt concentration induces extended conformations of deprotonated pHLIP. <i>Left:</i> Radius of gyration of deprotonated pHLIP as a function of the distance between residues 1 and 36 of the peptide. <i>Right:</i> Radius of gyration of protonated pHLIP as a function of the distance between residues 1 and 36 of the peptide.	82
5.4	Salt concentration directly affects contacts. A) Average number of contacts as a function of salt concentration, for deprotonated (<i>black</i>) and protonated (<i>red</i>) pHLIP. B) Contact times for deprotonated (<i>top</i>) and protonated (<i>bottom</i>) pHLIP as a function of salt concentration.	83

List of Tables

3.1	List of protonation states of pHLIP in this study.	29
5.1	List of states of pHLIP and salt concentrations in this study.	79

*Dedicated to every person out there who does not think
they have what it takes to make it. The sky is the limit!
Learn to fly!*

Chapter 1

Introduction

The human body is composed of trillions of cells, each designed to fulfill specific functions that keep the body alive and working. Each cell has a plasma membrane that separates the interior organelles and cytoplasm from the extracellular environment. Cell membranes are typically made of around 50% lipids[1], specifically phospholipids and sterols, and 50% proteins. In membranes, lipids act as structural components, barriers and platforms for biological processes, and proteins behave as gateways for nutrient transport, energy conversion and as part of the signaling cascades for processes such as cell proliferation. Local and global lipid composition of the membrane influences lipid-lipid and lipid-protein interactions, hence dictating the functionality of the system.

1.1 Cell membrane lipids

Cell membranes are amphipathic in nature, meaning that they possess both hydrophobic and hydrophilic regions. This characteristic is due to the spontaneous self-assembly of the amphipathic lipids that form the membrane, where the hydrophobic moieties self-associate to avoid the solvent while the hydrophilic domains interact with the solvent, forming lipid bilayers (**Fig. 1.1**).

Most membrane lipids in eukaryotic cells can be classified as glycerophospholipids (GPLs), sphingolipids or sterols[1, 2]. GPL's and sphingolipids have a polar hydrophilic headgroup region, usually localized at the lipid-water interface of the membrane, and non-polar hydrophobic tails, normally located in the interior of

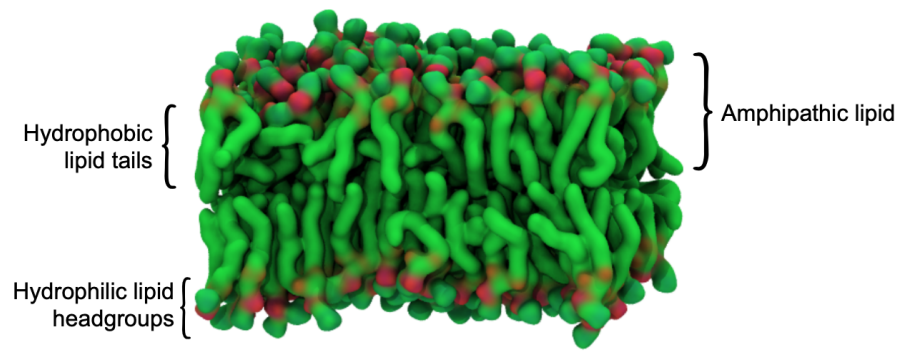


FIGURE 1.1: **Schematic of lipid bilayer.** Lipid bilayer formed by spontaneous self-assembly of amphipathic lipids, with hydrophobic tails secluding themselves by positioning at the center of the bilayer and hydrophilic headgroups staying at the lipid-solvent interfaces.

the bilayer, while sterols are non-polar and tend to stay in the hydrophobic region of the bilayer[1–3]. GPL’s and sphingolipids are both structural lipids and can be differentiated between them by their hydrophobic domains, specifically due to their variations in chain length, number of double bonds, position of double bonds and hydroxylation. Variations between headgroups and tails of GPL’s and sphingolipids allow the existence of >1000 different lipids.

GPL’s hydrophobic moieties consist of a pair of acyl chains, also known as diacylglycerol (DAG). These tails are connected to the headgroup region by the glycerol backbone, at positions denoted as *sn-1* and *sn-2*. Fatty acyl chains linked at *sn-1* tend to be either saturated or *cis*-monounsaturated, and with the *sn-2* chain being *cis*-monounsaturated or polyunsaturated [2, 3](Fig. 1.2).

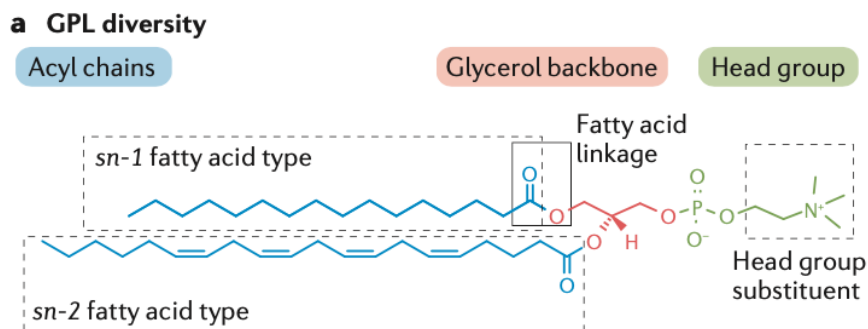


FIGURE 1.2: **Chemical structure of a glycerophospholipid.** One of the main structural polar lipids found in mammalian cells. Primarily composed of two fatty acyl chains, glycerol backbone and charged headgroup. [2]

Phosphatidylcholine (PC) is a GPL that makes >50% of phospholipids found in eukaryotic cell membranes[3], and one of its main characteristics is that it increases fluidity thanks to possessing at least one *cis*-unsaturated fatty acyl chain. This increase in fluidity is a consequence of the kink found in the fatty acyl chains, which prevents close packing of the lipids.

Sphingolipids hydrophobic tails are a sphingoid base backbone, made from ceramides (Cer), and a N-acyl chain. The sphingoid backbone can adopt various lengths and types and the N-acyl chains are mostly saturated and longer than GPL's fatty acyl chains[3, 4](Fig. 1.3).

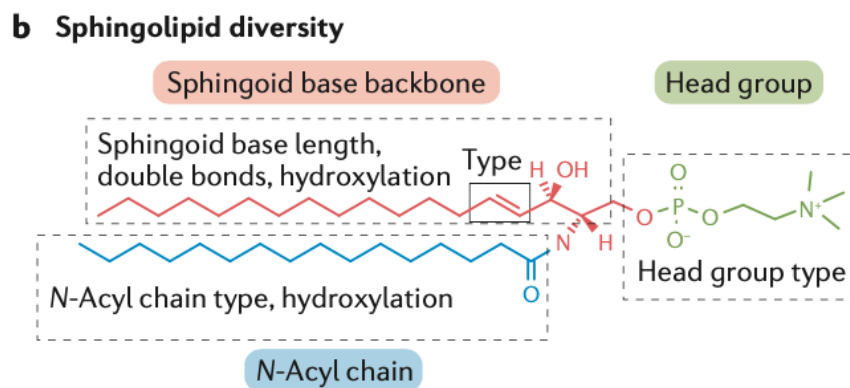


FIGURE 1.3: **Chemical structure of a sphingolipid.** Structural polar lipid type found in mammalian cells. Composed by a sphingoid base backbone, N-Acyl hydrocarbon chain and charged headgroup.[2]

Sterols are non-polar lipids with cholesterol being the main one found in mammalian cells. Sterols can adopt various structures, and one of their principal characteristics is their capability to ease phase transitions of the membrane from gel to lipid-crystalline[5](Fig. 1.4).

The differences in the chemical structure of lipids affects the physical properties of the cell membrane. Lipids with long, saturated tails, such as sphingolipids, decrease the fluidity of the membrane and increase thickness, as the lipid tails allow for close packing. In contrast, lipids with unsaturated tails, such as GPL's, tend to kink and prevent tight packing of the lipids. This is important as proteins interact with membranes by sensing the physical properties, such as the degree of exposure of the hydrophobic chains. Specifically, transmembrane helices gravitate towards loose packing regions of the membrane, where insertion is more favorable[4].

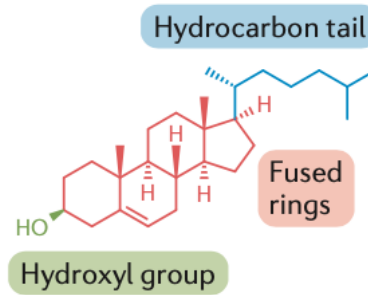
c Cholesterol

FIGURE 1.4: **Chemical structure of a cholesterol.** Non-polar lipid found in mammalian cells. Structure defined by a hydroxyl group, fused rings and a hydrocarbon tail. Specially important in affecting the viscosity of the lipid bilayer.[2]

The distribution of GPL's, sphingolipids and sterols across both membrane leaflets is not uniform, but rather asymmetric. Lipids such as phosphatidylserine(PS) are inclined to flip-flop between inner and outer leaflets as a result of changes in pH[5–7]. Under acidic conditions, PS headgroups are neutralized, and the lipid flips towards the inner leaflet of the membrane, hence increasing asymmetry[1–3]. This same behavior is also observed in other negatively charged lipids. Lipid asymmetry also contributes to the curvature of the membrane and can promote peptide insertion[8].

Cells membranes also function as protein recruiters, with headgroups initiating the lipid-protein interactions that lead to embedding or insertion of the protein or peptide into the membrane[9–12]. As mentioned above, proteins and peptides are susceptible to the physical properties of the membrane patch they are interacting with, including curvature, packing, type of headgroup, charge and thickness of the membrane[10, 13, 14]. An example of a protein factor affected by these properties is lateral diffusion. Proteins and peptides aim to bury their helical domains within the hydrophobic region of the membrane, hence they are prone to remain in areas of the membrane where lipid tails are long enough to cover them[10, 11, 15]. Most of these characteristics are affected by changes in the environment surrounding the cell, which is a common property of certain diseases such as cancer[16–18].

1.2 Characteristics of cancer cells

Cancer is the second leading cause of deaths in the US with over 1.7 million new cases per year[19]. It is caused by the uncontrolled growth of cells in the patient's body, and it can be localized to a single area or organ, or spread through various areas of the body, at which point it's considered metastatic. Current chemotherapy treatments aim to stop or slow down the proliferation of tumors by killing cancer cells, and there is no universal medication that can target all types of cancer. Furthermore, some of those structural segments can also be found in healthy cells, which increases the difficulty of specificity on targeting cancer cells exclusively, thus increasing side effects in the patient.

One characteristic that all cancer cells have in common is the fact that the micro-environment surrounding the cells have a lower pH than healthy cells[16, 17, 20]. This property is the result of the Warburg Effect[21, 22], a process by which the glucose intake in cells to produce ATP and lactate increases independently of whether there is oxygen present or not (**Fig. 1.5**). In normal cells, ATP is mostly produced via oxidative phosphorylation, a process in which glucose is broken down to produce pyruvate and carbon dioxide in the presence of oxygen. When cells lack oxygen, glucose can still be broken down via anaerobic glycolysis, producing ATP and lactate, however this occurs at a much lower rate. Cancer cells favor the production of lactate as a byproduct instead of carbon dioxide in a process called aerobic glycolysis. The lactate produced is then secreted to the outside of the cell, which in turn lowers the pH of the surrounding microenvironment.

pH is a chemical scale by which we measure whether a certain substance is acidic or basic. In other words, it allows scientist to determine if a substance is corrosive or abrasive, or if it's safe for contact or consumption. The acidity or alkalinity of a mixture is the determined by the following formula:

$$pH = -\log[H^+] \quad (1.1)$$

In this chemical scale, pH of 1 to around 6-6.5 are considered acidic, substances with pH of 6.5-7.5 are considered neutral, and substances with a pH of 7.5 or higher are considered alkaline. Healthy cells in the human body have a pH of 7.2, while cancer cells have a pH of around 6.8, and thus, it allows us to use it as a

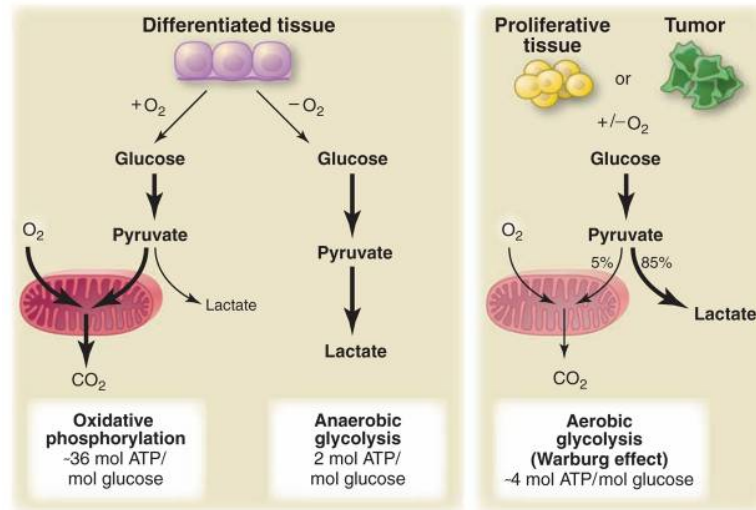


FIGURE 1.5: **Warburg effect.** *Left:* Oxidative phosphorylation and anaerobic glycolysis processes of healthy cells. *Right:* Aerobic glycolysis process of cancer cells.[22]

means to differentiate between healthy and cancer cells for targeted drug delivery and early imaging detection.

1.3 The pH Low Insertion Peptide

The pH Low Insertion Peptide (pHLIP) is a 36 residue peptide derived from the helix C of bacteriorhodopsin, and it's of special interest in the scientific community due to its ability to spontaneously fold and insert into the cell membrane under acidic conditions(**Fig. 1.6**). This capability is due to the presence of 6 acidic residues distributed along the peptide, and 1 alkaline residue in its N-terminal, summing up to an overall net charge of -5.

1.3.1 Origins and discovery

The pH Low Insertion Peptide (pHLIP) was discovered by the Engelman group at Yale university while they were performing studies on the folding mechanism of membrane proteins such as bacteriorhodopsin[24]. Their working hypothesis was that proteins with a significant percentage of secondary structure could spontaneously insert into a phospholipid bilayer, provided the free energy obtained from

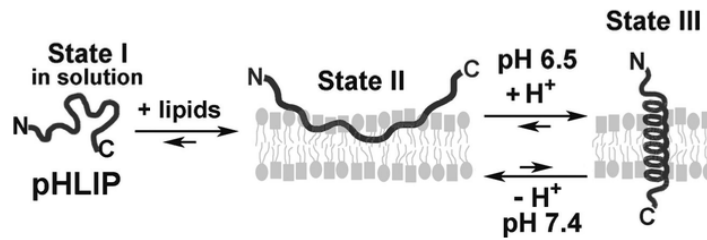


FIGURE 1.6: **Mechanism of folding and insertion of pHLIP.** pHLIP has three distinctive states: unstructured in solution (state I), embedded in the membrane (state II) both a $\text{pH} > 7$ and inserted as a transmembrane helix (state III) at $\text{pH} < 6.5$. [23]

such partition was large enough. Out of the seven peptides obtained from bacteriorhodopsin, only helix C showed weak association with the lipid vesicles used, indicating it could easily be recovered. Furthermore, gel filtration chromatography inferred that the peptide preferred an oligomeric conformation in solution. Using fluorescence spectroscopy, they were able to determine that, upon folding, the hydrophobic section of pHLIP spontaneously inserts into the phospholipid membrane at low pH. Circular Dichroism (CD) spectroscopy concluded that pHLIP depends on the presence of a phospholipid membrane and a low pH to undergo a conformational transition from coil in solution to transmembrane helix. This study catapulted the interest and subsequent studies of the peptide for its promising biomedical applications.

1.3.2 pHLIP's mechanism

Although the initial study proved that pHLIP spontaneously folds and inserts into a phospholipid lipid membrane under acidic conditions, the details of such process and how other factors, such as lipid composition, salt concentration or mutations, would affect the system were poorly understood. Thus, a race began towards understanding the fundamentals of pHLIP. The main two experimental techniques consistently used by scientists have been CD and fluorescence spectroscopy [25–28], due to their advantages in detecting conformational changes in the secondary structure and capture of insertion of the peptide via burial of the tryptophan residues in its N-terminus, respectively (**Fig 1.7**).

Other studies have incorporated solid state NMR (ssNMR) [29–31], small-angle neutron and X-ray Scattering (SANS and SAXS) [32, 33], and molecular dynamics

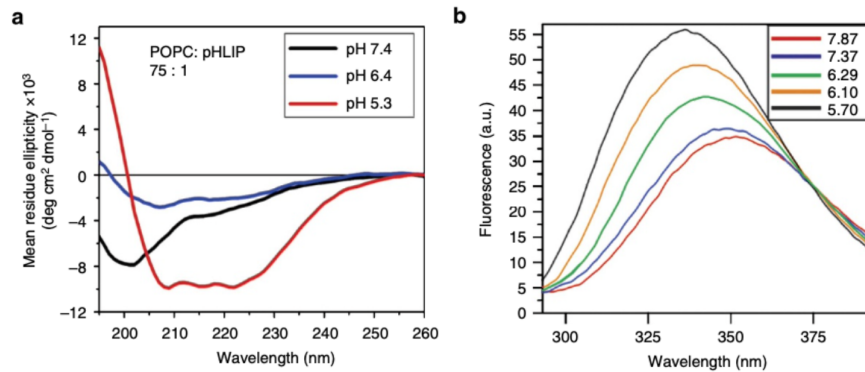


FIGURE 1.7: **Folding and insertion events through CD and fluorescence spectroscopy.** *Figure A:* CD spectroscopy of pHLIP at pH 7.4(*black*), 6.4(*blue*) and 5.3(*red*). Results show how pHLIP’s conformation changes from a coil conformation (*blue and black*) to helical at acidic pH (*red*). *Figure B:* Fluorescence spectroscopy of pHLIP as a function of pH. Blue shift is observed from pH 7.87 to 5.70, which indicates that pHLIP’s tryptophans have progressed from being in contact with the solvent to be inserted into the membrane.[29]

simulations[34, 35]. These new techniques have allowed us to understand how salt concentration and charge of headgroups affects pHLIP binding and embedding to the membrane [35, 36], differentiate between the pka’s of each acidic residue in pHLIP as they protonate[25, 26, 37] and even map out the possible entry and exit mechanisms of the peptide [30, 33, 37].

A recent kinetic study of pHLIP was performed using CD and fluorescence quenching to investigate single-tryptophan variants of the peptide at positions 6, 17 and 30[37]. The results show embedding of pHLIP into the bilayer, followed by increase in helical content due to protonation of acidic residues, which triggers insertion of the peptide. Interestingly, exit pathway seem to happen via destabilization of the peptide at the transmembrane position due to loss of helicity, and then exit (**Fig. 1.8**).

1.3.3 pHLIP cancer studies

As we established before, pHLIP is of high interest in the scientific community due to its potential for early detection and targeted drug delivery in cancer. In recent years, several *in vivo*, *in vitro* and computational studies were done to better understand how does pHLIP work in real cancer cells and their environment[38, 39]. Recent studies, such as the one done by Svoronos and Engelman[40], where they used a mathematical method they developed to model insertion process of

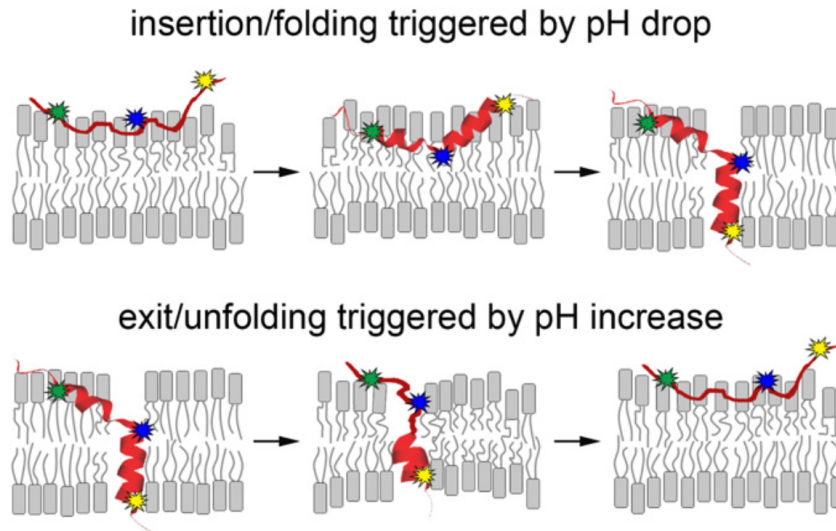


FIGURE 1.8: **Generalized model of insertion and exit mechanism of pHLIP.** Single-tryptophan pHLIP variants at positions 6 (*green*), 17 (*blue*) and 30 (*red*). Insertion of pHLIP via initial embedding, partial folding and finally, insertion to transmembrane conformation. Exit pathway involves destabilization of the transmembrane peptide followed by exit. [37]

the peptide and then use it to compare biodistributions of the wild-type pHLIP variant between healthy and tumor tissues via a pharmacokinetic model. They were able to identify crucial factors that affect tumor targeting and delivery of pHLIP such as enhanced permeability and retention (EPR) effect and variations of intracellular pH, two very well know factors that vary between tumors tissues; and pHLIP variants that are able to perform better than the wild-type pHLIP, thus improving our knowledge for the development of new pHLIP sequences that might enhance tumor targeting and efficient drug delivery.

Another research study concentrated on the effect of the variations of the intra- and inter-tumor pH on the delivery of magnetic nanoparticles (MNP's) with pHLIP[41]. They were able to show that pHLIP-modified MNP's accumulated more effectively on tumor cells with pH 6.4 than at pH 7.2, and that pHLIP-modified MNP's were retained longer by the tumor cells as compared to non-pHLIP MNP's.

Although these studies bring us closer towards using pH Low Insertion Peptides in clinical trials, there is still much to be understood, hence the focus of this research. In the next few chapters we will be covering how deprotonation of transmembrane pHLIP modifies the stability of the lipid-peptide system and the mapping of the initial steps towards exit of the peptide, the effects of pHLIP

insertion on membrane fluctuations and diffusion coefficients, and the relationship between salt concentration and conformational changes of pHLIP.

Bibliography

- [1] Geoffrey M. Copper. *The Cell: A Molecular Approach*. 2nd Edition. 2000. ISBN: 10: 0-87893-106-6.
- [2] Takeshi Harayama and Howard Riezman. “Understanding the diversity of membrane lipid composition”. en. In: *Nature Reviews Molecular Cell Biology* 19.5 (May 2018), pp. 281–296. ISSN: 1471-0072, 1471-0080. DOI: [10.1038/nrm.2017.138](https://doi.org/10.1038/nrm.2017.138). URL: <http://www.nature.com/articles/nrm.2017.138> (visited on 07/21/2021).
- [3] Gerrit van Meer, Dennis R. Voelker, and Gerald W. Feigenson. “Membrane lipids: where they are and how they behave”. en. In: *Nature Reviews Molecular Cell Biology* 9.2 (Feb. 2008), pp. 112–124. ISSN: 1471-0072, 1471-0080. DOI: [10.1038/nrm2330](https://doi.org/10.1038/nrm2330). URL: <http://www.nature.com/articles/nrm2330> (visited on 07/21/2021).
- [4] Yusuf A. Hannun and Lina M. Obeid. “Sphingolipids and their metabolism in physiology and disease”. en. In: *Nature Reviews Molecular Cell Biology* 19.3 (Mar. 2018), pp. 175–191. ISSN: 1471-0072, 1471-0080. DOI: [10.1038/nrm.2017.107](https://doi.org/10.1038/nrm.2017.107). URL: <http://www.nature.com/articles/nrm.2017.107> (visited on 07/29/2021).
- [5] W. F. Drew Bennett et al. “Molecular View of Cholesterol Flip-Flop and Chemical Potential in Different Membrane Environments”. en. In: *Journal of the American Chemical Society* 131.35 (Sept. 2009), pp. 12714–12720. ISSN: 0002-7863, 1520-5126. DOI: [10.1021/ja903529f](https://doi.org/10.1021/ja903529f). URL: <https://pubs.acs.org/doi/10.1021/ja903529f> (visited on 07/29/2021).
- [6] Nicolas Sapay, W. F. Drew Bennett, and D. Peter Tieleman. “Molecular Simulations of Lipid Flip-Flop in the Presence of Model Transmembrane

- Helices”. en. In: *Biochemistry* 49.35 (Sept. 2010), pp. 7665–7673. ISSN: 0006-2960, 1520-4995. DOI: [10.1021/bi100878q](https://doi.org/10.1021/bi100878q). URL: <https://pubs.acs.org/doi/10.1021/bi100878q> (visited on 07/29/2021).
- [7] Michael H. L. Nguyen et al. “Peptide-Induced Lipid Flip-Flop in Asymmetric Liposomes Measured by Small Angle Neutron Scattering”. en. In: *Langmuir* 35.36 (Sept. 2019), pp. 11735–11744. ISSN: 0743-7463, 1520-5827. DOI: [10.1021/acs.langmuir.9b01625](https://doi.org/10.1021/acs.langmuir.9b01625). URL: <https://pubs.acs.org/doi/10.1021/acs.langmuir.9b01625> (visited on 07/29/2021).
- [8] Haden L. Scott et al. “Phosphatidylserine Asymmetry Promotes the Membrane Insertion of a Transmembrane Helix”. en. In: *Biophysical Journal* 116.8 (Apr. 2019), pp. 1495–1506. ISSN: 00063495. DOI: [10.1016/j.bpj.2019.03.003](https://doi.org/10.1016/j.bpj.2019.03.003). URL: <https://linkinghub.elsevier.com/retrieve/pii/S0006349519301894> (visited on 03/18/2021).
- [9] Mathieu Pinot et al. “Polyunsaturated phospholipids facilitate membrane deformation and fission by endocytic proteins”. en. In: *Science* 345.6197 (Aug. 2014), pp. 693–697. ISSN: 0036-8075, 1095-9203. DOI: [10.1126/science.1255288](https://doi.org/10.1126/science.1255288). URL: <https://www.sciencemag.org/lookup/doi/10.1126/science.1255288> (visited on 07/29/2021).
- [10] Riya Raghupathy et al. “Transbilayer Lipid Interactions Mediate Nanoclustering of Lipid-Anchored Proteins”. en. In: *Cell* 161.3 (Apr. 2015), pp. 581–594. ISSN: 00928674. DOI: [10.1016/j.cell.2015.03.048](https://doi.org/10.1016/j.cell.2015.03.048). URL: <https://linkinghub.elsevier.com/retrieve/pii/S0092867415003682> (visited on 07/29/2021).
- [11] F.-X. Contreras et al. “Specificity of Intramembrane Protein-Lipid Interactions”. en. In: *Cold Spring Harbor Perspectives in Biology* 3.6 (June 2011), a004705–a004705. ISSN: 1943-0264. DOI: [10.1101/cshperspect.a004705](https://doi.org/10.1101/cshperspect.a004705). URL: <http://cshperspectives.cshlp.org/lookup/doi/10.1101/cshperspect.a004705> (visited on 07/29/2021).
- [12] Haden L. Scott et al. “The Negative Charge of the Membrane Has Opposite Effects on the Membrane Entry and Exit of pH-Low Insertion Peptide”. en. In: *Biochemistry* 54.9 (Mar. 2015), pp. 1709–1712. ISSN: 0006-2960, 1520-4995. DOI: [10.1021/acs.biochem.5b00069](https://doi.org/10.1021/acs.biochem.5b00069). URL: <https://pubs.acs.org/doi/10.1021/acs.biochem.5b00069> (visited on 03/18/2021).

- [13] Matthew B Stone et al. “Protein sorting by lipid phase-like domains supports emergent signaling function in B lymphocyte plasma membranes”. en. In: *eLife* 6 (Feb. 2017), e19891. ISSN: 2050-084X. DOI: [10.7554/eLife.19891](https://doi.org/10.7554/eLife.19891). URL: <https://elifesciences.org/articles/19891> (visited on 07/29/2021).
- [14] Alexander G. Karabadzhak et al. “Bilayer Thickness and Curvature Influence Binding and Insertion of a pHLIP Peptide”. en. In: *Biophysical Journal* 114.9 (May 2018), pp. 2107–2115. ISSN: 00063495. DOI: [10.1016/j.bpj.2018.03.036](https://doi.org/10.1016/j.bpj.2018.03.036). URL: <https://linkinghub.elsevier.com/retrieve/pii/S0006349518304582> (visited on 03/18/2021).
- [15] Taehoon Kim and Wonpil Im. “Revisiting Hydrophobic Mismatch with Free Energy Simulation Studies of Transmembrane Helix Tilt and Rotation”. en. In: *Biophysical Journal* 99.1 (July 2010), pp. 175–183. ISSN: 00063495. DOI: [10.1016/j.bpj.2010.04.015](https://doi.org/10.1016/j.bpj.2010.04.015). URL: <https://linkinghub.elsevier.com/retrieve/pii/S0006349510004789> (visited on 07/29/2021).
- [16] Pawel Swietach et al. “The chemistry, physiology and pathology of pH in cancer”. en. In: *Philosophical Transactions of the Royal Society B: Biological Sciences* 369.1638 (Mar. 2014), p. 20130099. ISSN: 0962-8436, 1471-2970. DOI: [10.1098/rstb.2013.0099](https://doi.org/10.1098/rstb.2013.0099). URL: <https://royalsocietypublishing.org/doi/10.1098/rstb.2013.0099> (visited on 03/18/2021).
- [17] Erez Persi et al. “Systems analysis of intracellular pH vulnerabilities for cancer therapy”. en. In: *Nature Communications* 9.1 (Dec. 2018), p. 2997. ISSN: 2041-1723. DOI: [10.1038/s41467-018-05261-x](https://doi.org/10.1038/s41467-018-05261-x). URL: <http://www.nature.com/articles/s41467-018-05261-x> (visited on 03/18/2021).
- [18] Francesca Perrotti et al. “Advances in Lipidomics for Cancer Biomarkers Discovery”. en. In: *International Journal of Molecular Sciences* 17.12 (Nov. 2016), p. 1992. ISSN: 1422-0067. DOI: [10.3390/ijms17121992](https://doi.org/10.3390/ijms17121992). URL: <http://www.mdpi.com/1422-0067/17/12/1992> (visited on 07/29/2021).
- [19] Rebecca L. Siegel et al. “Cancer Statistics, 2021”. en. In: *CA: A Cancer Journal for Clinicians* 71.1 (Jan. 2021), pp. 7–33. ISSN: 0007-9235, 1542-4863. DOI: [10.3322/caac.21654](https://doi.org/10.3322/caac.21654). URL: <https://onlinelibrary.wiley.com/doi/10.3322/caac.21654> (visited on 03/09/2021).

- [20] Xiao Luo et al. “Highly Sensitive Hill-Type Small-Molecule pH Probe That Recognizes the Reversed pH Gradient of Cancer Cells”. en. In: *Analytical Chemistry* 90.9 (May 2018), pp. 5803–5809. ISSN: 0003-2700, 1520-6882. DOI: [10.1021/acs.analchem.8b00218](https://doi.org/10.1021/acs.analchem.8b00218). URL: <https://pubs.acs.org/doi/10.1021/acs.analchem.8b00218> (visited on 03/18/2021).
- [21] O. Warburg. “On the Origin of Cancer Cells”. en. In: *Science* 123.3191 (Feb. 1956), pp. 309–314. ISSN: 0036-8075, 1095-9203. DOI: [10.1126/science.123.3191.309](https://doi.org/10.1126/science.123.3191.309). URL: <https://www.sciencemag.org/lookup/doi/10.1126/science.123.3191.309> (visited on 03/18/2021).
- [22] M. G. Vander Heiden, L. C. Cantley, and C. B. Thompson. “Understanding the Warburg Effect: The Metabolic Requirements of Cell Proliferation”. en. In: *Science* 324.5930 (May 2009), pp. 1029–1033. ISSN: 0036-8075, 1095-9203. DOI: [10.1126/science.1160809](https://doi.org/10.1126/science.1160809). URL: <https://www.sciencemag.org/lookup/doi/10.1126/science.1160809> (visited on 03/09/2021).
- [23] Joab O. Onyango et al. “Noncanonical Amino Acids to Improve the pH Response of pHLIP Insertion at Tumor Acidity”. en. In: *Angewandte Chemie International Edition* 54.12 (Mar. 2015), pp. 3658–3663. ISSN: 14337851. DOI: [10.1002/anie.201409770](https://doi.org/10.1002/anie.201409770). URL: <http://doi.wiley.com/10.1002/anie.201409770> (visited on 03/18/2021).
- [24] John F Hunt et al. “Spontaneous, pH-Dependent Membrane Insertion of a Transbilayer R-Helix”. en. In: (), p. 16.
- [25] Justin Fendos, Francisco N. Barrera, and Donald M. Engelman. “Aspartate Embedding Depth Affects pHLIP’s Insertion pK_a ”. en. In: *Biochemistry* 52.27 (July 2013), pp. 4595–4604. ISSN: 0006-2960, 1520-4995. DOI: [10.1021/bi400252k](https://doi.org/10.1021/bi400252k). URL: <https://pubs.acs.org/doi/10.1021/bi400252k> (visited on 03/18/2021).
- [26] Francisco N. Barrera et al. “Roles of Carboxyl Groups in the Transmembrane Insertion of Peptides”. en. In: *Journal of Molecular Biology* 413.2 (Oct. 2011), pp. 359–371. ISSN: 00222836. DOI: [10.1016/j.jmb.2011.08.010](https://doi.org/10.1016/j.jmb.2011.08.010). URL: <https://linkinghub.elsevier.com/retrieve/pii/S0022283611008771> (visited on 03/18/2021).
- [27] O. A. Andreev et al. “pH (low) insertion peptide (pHLIP) inserts across a lipid bilayer as a helix and exits by a different path”. en. In: *Proceedings of the National Academy of Sciences* 107.9 (Mar. 2010), pp. 4081–4086. ISSN:

- 0027-8424, 1091-6490. DOI: [10.1073/pnas.0914330107](https://doi.org/10.1073/pnas.0914330107). URL: <http://www.pnas.org/cgi/doi/10.1073/pnas.0914330107> (visited on 03/18/2021).
- [28] Damien Thévenin, Ming An, and Donald M. Engelman. “pHLIP-Mediated Translocation of Membrane-Impermeable Molecules into Cells”. en. In: *Chemistry & Biology* 16.7 (July 2009), pp. 754–762. ISSN: 10745521. DOI: [10.1016/j.chembiol.2009.06.006](https://doi.org/10.1016/j.chembiol.2009.06.006). URL: <https://linkinghub.elsevier.com/retrieve/pii/S107455210900204X> (visited on 03/18/2021).
- [29] Nicolas S. Shu et al. “Residue-specific structures and membrane locations of pH-low insertion peptide by solid-state nuclear magnetic resonance”. en. In: *Nature Communications* 6.1 (Nov. 2015), p. 7787. ISSN: 2041-1723. DOI: [10.1038/ncomms8787](https://doi.org/10.1038/ncomms8787). URL: <http://www.nature.com/articles/ncomms8787> (visited on 03/18/2021).
- [30] Sarah A. Otieno et al. “pH-dependent thermodynamic intermediates of pHLIP membrane insertion determined by solid-state NMR spectroscopy”. en. In: *Proceedings of the National Academy of Sciences* 115.48 (Nov. 2018), pp. 12194–12199. ISSN: 0027-8424, 1091-6490. DOI: [10.1073/pnas.1809190115](https://doi.org/10.1073/pnas.1809190115). URL: <http://www.pnas.org/lookup/doi/10.1073/pnas.1809190115> (visited on 03/18/2021).
- [31] Federica Rinaldi et al. “Decoration of Nanovesicles with pH (Low) Insertion Peptide (pHLIP) for Targeted Delivery”. en. In: *Nanoscale Research Letters* 13.1 (Dec. 2018), p. 391. ISSN: 1931-7573, 1556-276X. DOI: [10.1186/s11671-018-2807-8](https://doi.org/10.1186/s11671-018-2807-8). URL: <https://nanoscalereslett.springeropen.com/articles/10.1186/s11671-018-2807-8> (visited on 03/18/2021).
- [32] Theyencheri Narayanan et al. “pHLIP Peptide Interaction with a Membrane Monitored by SAXS”. en. In: *The Journal of Physical Chemistry B* 120.44 (Nov. 2016), pp. 11484–11491. ISSN: 1520-6106, 1520-5207. DOI: [10.1021/acs.jpcc.6b06643](https://doi.org/10.1021/acs.jpcc.6b06643). URL: <https://pubs.acs.org/doi/10.1021/acs.jpcc.6b06643> (visited on 03/18/2021).
- [33] Haden L. Scott et al. “On the Mechanism of Bilayer Separation by Extrusion, or Why Your LUVs Are Not Really Unilamellar”. en. In: *Biophysical Journal* 117.8 (Oct. 2019), pp. 1381–1386. ISSN: 00063495. DOI: [10.1016/j.bpj.2019.09.006](https://doi.org/10.1016/j.bpj.2019.09.006). URL: <https://linkinghub.elsevier.com/retrieve/pii/S0006349519307805> (visited on 08/02/2021).

- [34] Tomás F. D. Silva, Diogo Vila-Viçosa, and Miguel Machuqueiro. “Improved Protocol to Tackle the pH Effects on Membrane-Inserting Peptides”. en. In: *Journal of Chemical Theory and Computation* 17.7 (July 2021), pp. 3830–3840. ISSN: 1549-9618, 1549-9626. DOI: [10.1021/acs.jctc.1c00020](https://doi.org/10.1021/acs.jctc.1c00020). URL: <https://pubs.acs.org/doi/10.1021/acs.jctc.1c00020> (visited on 08/02/2021).
- [35] Chitrak Gupta, Yue Ren, and Blake Mertz. “Cooperative Nonbonded Forces Control Membrane Binding of the pH-Low Insertion Peptide pHLIP”. en. In: *Biophysical Journal* 115.12 (Dec. 2018), pp. 2403–2412. ISSN: 00063495. DOI: [10.1016/j.bpj.2018.11.002](https://doi.org/10.1016/j.bpj.2018.11.002). URL: <https://linkinghub.elsevier.com/retrieve/pii/S0006349518312219> (visited on 03/18/2021).
- [36] Victor Vasquez-Montes et al. “Divalent Cations and Lipid Composition Modulate Membrane Insertion and Cancer-Targeting Action of pHLIP”. en. In: *Journal of Molecular Biology* 431.24 (Nov. 2019), pp. 5004–5018. ISSN: 0022-2836. DOI: [10.1016/j.jmb.2019.10.016](https://doi.org/10.1016/j.jmb.2019.10.016).
- [37] Gregory Slaybaugh et al. “Kinetics of pHLIP peptide insertion into and exit from a membrane”. en. In: *Proceedings of the National Academy of Sciences* 117.22 (June 2020), pp. 12095–12100. ISSN: 0027-8424, 1091-6490. DOI: [10.1073/pnas.1917857117](https://doi.org/10.1073/pnas.1917857117). URL: <http://www.pnas.org/lookup/doi/10.1073/pnas.1917857117> (visited on 08/02/2021).
- [38] Alexander M. Demin et al. “Smart Design of a pH-Responsive System Based on pHLIP-Modified Magnetite Nanoparticles for Tumor MRI”. en. In: *ACS Applied Materials & Interfaces* (July 2021), acsami.1c07748. ISSN: 1944-8244, 1944-8252. DOI: [10.1021/acsami.1c07748](https://doi.org/10.1021/acsami.1c07748). URL: <https://pubs.acs.org/doi/10.1021/acsami.1c07748> (visited on 08/02/2021).
- [39] Luoping Zhai et al. “A Dual pH-Responsive DOX-Encapsulated Liposome Combined with Glucose Administration Enhanced Therapeutic Efficacy of Chemotherapy for Cancer”. en. In: *International Journal of Nanomedicine* Volume 16 (May 2021), pp. 3185–3199. ISSN: 1178-2013. DOI: [10.2147/IJN.S303874](https://doi.org/10.2147/IJN.S303874). URL: <https://www.dovepress.com/a-dual-ph-responsive-dox-encapsulated-liposome-combined-with-glucose-a-peer-reviewed-fulltext-article-IJN> (visited on 08/02/2021).

- [40] Alexander A. Svoronos and Donald M. Engelman. “Pharmacokinetic modeling reveals parameters that govern tumor targeting and delivery by a pH-Low Insertion Peptide (pHLIP)”. en. In: *Proceedings of the National Academy of Sciences* 118.1 (Jan. 2021), e2016605118. ISSN: 0027-8424, 1091-6490. DOI: [10.1073/pnas.2016605118](https://doi.org/10.1073/pnas.2016605118). URL: <http://www.pnas.org/lookup/doi/10.1073/pnas.2016605118> (visited on 08/02/2021).
- [41] Alexandra G. Pershina et al. “Variation in tumor pH affects pH-triggered delivery of peptide-modified magnetic nanoparticles”. en. In: *Nanomedicine: Nanotechnology, Biology and Medicine* 32 (Feb. 2021), p. 102317. ISSN: 15499634. DOI: [10.1016/j.nano.2020.102317](https://doi.org/10.1016/j.nano.2020.102317). URL: <https://linkinghub.elsevier.com/retrieve/pii/S1549963420301714> (visited on 08/02/2021).

Chapters/chapterI

Chapter 2

Methods

Proteins and membrane systems have been studied using a wide range of experimental techniques, however high resolution data normally requires static systems (x-ray) while the analysis of processes in real time normally requires high concentration samples (NMR)[1]. Molecular dynamics (MD) simulations is a computational technique that uses Newton's second law of motion to mimic real time processes of biological systems with atomic resolution. Thus MD is able to provide more detailed information of the system (**Fig. 2.1**).

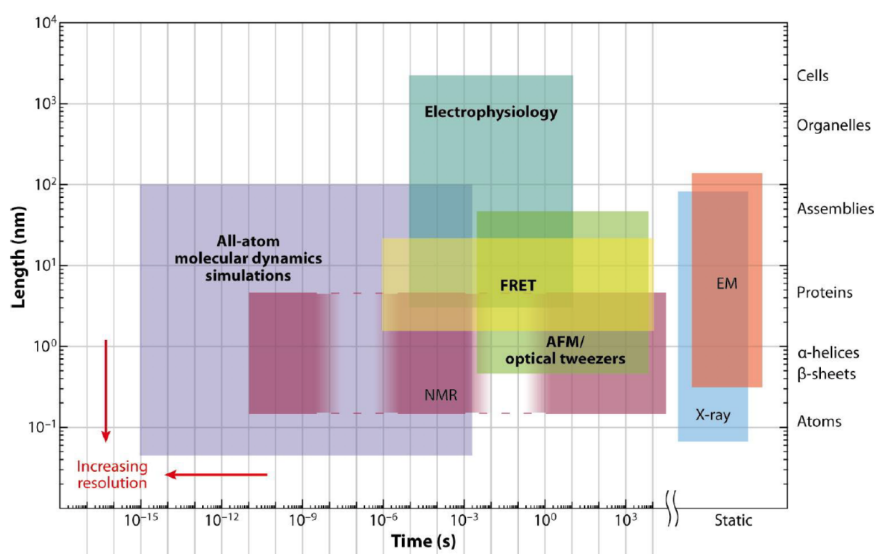


FIGURE 2.1: Molecular dynamics as a higher resolution technique. Graphical depiction of the resolution of current experimental versus molecular dynamics (MD) simulations. MD allows to research short biological processes at the atomic level, hence avoiding loss of detailed information of the system.[1]

In order to use MD simulations, we need the three-dimensional coordinates of each atom with respect to all other atoms in a protein which are normally obtained through x-ray crystallography[2, 3], NMR spectroscopy[4, 5] or cryo-electron spectroscopy[6, 7]. Other files needed are a topology file, which defines how each atom is bonded to one another, and the corresponding force fields, a series of mathematical models that depict the interaction between atoms using the following formula:

$$V_{total} = V_{bond} + V_{angle} + V_{dihedral} + V_{improper} + V_{LJ} + V_{coulomb} \quad (2.1)$$

Where V_{bond} and V_{angle} describe the contributions to the potential energy of the system by the harmonic oscillators corresponding to the stretching and bending movements between atoms connected by a bond; $V_{dihedral}$ and $V_{improper}$ are the contributions to the potential energy of the system corresponding to the clockwise torsional rotations between 2 planes, each formed by 3 bonded atoms, i.e: sinusoidal oscillations; V_{LJ} corresponds to the intermolecular pairwise potential between 2 atoms or molecules. Specifically, it account for the attractive and repulsive interactions between atoms as a function of the distance between them, and its described with the following equation:

$$V_{LJ}(r) = 4\varepsilon\left[\left(\frac{\sigma}{r}\right)^{12} - \left(\frac{\sigma}{r}\right)^6\right] \quad (2.2)$$

Where $(\sigma/r)^{12}$ accounts for the repulsive interactions and $(\sigma/r)^6$ accounts for the attractive interactions between 2 atoms.

Finally, $V_{coulomb}$ corresponding to the potential energy of the electrostatic interaction between 2 charged atoms, i.e: Coulomb potential:

$$F = \frac{k * Q_1 * Q_2}{d^2} \quad (2.3)$$

The MD software uses the potential values obtained for each atom to calculate the new positions by solving Newton's second law of motions[8]:

$$x(t + \Delta t) = x(t) + \Delta t[v(t) + \Delta t f(t)/2m] \quad (2.4)$$

Where $x(t+\Delta t)$ is the position calculated, $x(t)$ is the previous position, Δt is the timestep, $v(t)$ is the velocity of each atom, $f(t)$ is the force and m is the mass of the atom.

The new positions are calculated each timestep, generating a time-dependent pathway.

Analysis of a system is very much dependent on what aspects one wants to look at. Some of the most common ones are:

- 1) Root Mean Square Displacement (RMSD) calculates the difference in the coordinates of the backbone of a protein from a reference as a function of time. This reference can be the crystal structure used, the coordinates from the first step, or the coordinates of a specified frame[9, 10].
- 2) Area per lipid calculates the area in the x-y dimension of each lipid by getting the x-y dimensions of the box and dividing it by the number of lipids per leaflet[11, 12].
- 3) Lipid deuterium order parameter quantifies the order of the carbon-hydrogen backbone of lipid tails. Normally parallel to area per lipid, it allows us to quantify if the tails of a lipid are tightly packed or if they are adopting other conformations due to loose packing[13, 14].
- 4) Mean-square displacement, much like RMSD, calculates the difference in position of an atom or molecule from its reference structure[15, 16].
- 5) Principal Component Analysis (PCA) allows for a reduction of dimensionality of the system in order to be able to obtain the most characteristic conformations of the peptide[17].

For more information on the methodology of molecular dynamics simulations, please refer to our book chapter.[18]

Bibliography

- [1] Ron O. Dror et al. “Biomolecular Simulation: A Computational Microscope for Molecular Biology”. In: *Annual Review of Biophysics* 41.1 (June 2012). Publisher: Annual Reviews, pp. 429–452. ISSN: 1936-122X. DOI: [10.1146/annurev-biophys-042910-155245](https://doi.org/10.1146/annurev-biophys-042910-155245). URL: <https://doi.org/10.1146/annurev-biophys-042910-155245> (visited on 08/03/2021).
- [2] M. S. Smyth and J. H. J. Martin. “x-ray crystallography”. In: *Journal of Clinical Pathology: Molecular Pathology* 53 (2000), pp. 8–14.
- [3] Wladek Minor, Zbigniew Dauter, and Mariusz Jaskolski. “The young person’s guide to the PDB”. en. In: (2017), p. 15.
- [4] A. Cavalli et al. “Protein structure determination from NMR chemical shifts”. en. In: *Proceedings of the National Academy of Sciences* 104.23 (June 2007), pp. 9615–9620. ISSN: 0027-8424, 1091-6490. DOI: [10.1073/pnas.0610313104](https://doi.org/10.1073/pnas.0610313104). URL: <http://www.pnas.org/cgi/doi/10.1073/pnas.0610313104> (visited on 08/03/2021).
- [5] Nicholas J. Fowler, Adnan Sljoka, and Mike P. Williamson. “A method for validating the accuracy of NMR protein structures”. en. In: *Nature Communications* 11.1 (Dec. 2020), p. 6321. ISSN: 2041-1723. DOI: [10.1038/s41467-020-20177-1](https://doi.org/10.1038/s41467-020-20177-1). URL: <http://www.nature.com/articles/s41467-020-20177-1> (visited on 08/03/2021).
- [6] Emeka Nwanochie and Vladimir N. Uversky. “Structure Determination by Single-Particle Cryo-Electron Microscopy: Only the Sky (and Intrinsic Disorder) is the Limit”. en. In: *International Journal of Molecular Sciences* 20.17 (Aug. 2019), p. 4186. ISSN: 1422-0067. DOI: [10.3390/ijms20174186](https://doi.org/10.3390/ijms20174186). URL: <https://www.mdpi.com/1422-0067/20/17/4186> (visited on 08/03/2021).

- [7] Wah Chiu et al. “Evolution of standardization and dissemination of cryo-EM structures and data jointly by the community, PDB, and EMDB”. en. In: *Journal of Biological Chemistry* 296 (Jan. 2021), p. 100560. ISSN: 00219258. DOI: [10.1016/j.jbc.2021.100560](https://doi.org/10.1016/j.jbc.2021.100560). URL: <https://linkinghub.elsevier.com/retrieve/pii/S0021925821003380> (visited on 08/03/2021).
- [8] Isaac Newton. *Philosophiæ Naturalis Principia Mathematica (Mathematical Principles of Natural Philosophy)*. New latin. 1st edition. 1687.
- [9] Karen Sargsyan, Cédric Grauffel, and Carmay Lim. “How Molecular Size Impacts RMSD Applications in Molecular Dynamics Simulations”. In: *Journal of Chemical Theory and Computation* 13.4 (Apr. 2017). Publisher: American Chemical Society, pp. 1518–1524. ISSN: 1549-9618. DOI: [10.1021/acs.jctc.7b00028](https://doi.org/10.1021/acs.jctc.7b00028). URL: <https://doi.org/10.1021/acs.jctc.7b00028>.
- [10] Irina Kufareva and Ruben Abagyan. “Methods of protein structure comparison”. eng. In: *Methods in molecular biology (Clifton, N.J.)* 857 (2012), pp. 231–257. ISSN: 1940-6029. DOI: [10.1007/978-1-61779-588-6_10](https://doi.org/10.1007/978-1-61779-588-6_10). URL: <https://pubmed.ncbi.nlm.nih.gov/22323224>.
- [11] Avigdor Leftin et al. “Area per lipid and cholesterol interactions in membranes from separated local-field (13)C NMR spectroscopy”. eng. In: *Biophysical journal* 107.10 (Nov. 2014). Publisher: The Biophysical Society, pp. 2274–2286. ISSN: 1542-0086. DOI: [10.1016/j.bpj.2014.07.044](https://doi.org/10.1016/j.bpj.2014.07.044). URL: <https://pubmed.ncbi.nlm.nih.gov/25418296>.
- [12] Jacob J Kinnun et al. “Elastic deformation and area per lipid of membranes: atomistic view from solid-state deuterium NMR spectroscopy”. eng. In: *Biochimica et biophysica acta* 1848.1 Pt B (Jan. 2015). Edition: 2014/06/16, pp. 246–259. ISSN: 0006-3002. DOI: [10.1016/j.bbamem.2014.06.004](https://doi.org/10.1016/j.bbamem.2014.06.004). URL: <https://pubmed.ncbi.nlm.nih.gov/24946141>.
- [13] Thomas J. Piggot et al. “On the Calculation of Acyl Chain Order Parameters from Lipid Simulations”. In: *Journal of Chemical Theory and Computation* 13.11 (Nov. 2017). Publisher: American Chemical Society, pp. 5683–5696. ISSN: 1549-9618. DOI: [10.1021/acs.jctc.7b00643](https://doi.org/10.1021/acs.jctc.7b00643). URL: <https://doi.org/10.1021/acs.jctc.7b00643>.
- [14] Louic S. Vermeer et al. “Acyl chain order parameter profiles in phospholipid bilayers: computation from molecular dynamics simulations and comparison with 2H NMR experiments”. en. In: *European Biophysics Journal* 36.8 (Nov. 2007), pp. 919–931. ISSN: 0175-7571, 1432-1017. DOI: [10.1007/s00249-007-](https://doi.org/10.1007/s00249-007-)

- 0192-9. URL: <http://link.springer.com/10.1007/s00249-007-0192-9> (visited on 09/19/2021).
- [15] Gary Dunderdale et al. “Importance of Particle Tracking and Calculating the Mean-Squared Displacement in Distinguishing Nanopropulsion from Other Processes”. In: *Langmuir* 28.30 (July 2012). Publisher: American Chemical Society, pp. 10997–11006. ISSN: 0743-7463. DOI: [10.1021/la301370y](https://doi.org/10.1021/la301370y). URL: <https://doi.org/10.1021/la301370y>.
- [16] Dominique Ernst and Jürgen Köhler. “Measuring a diffusion coefficient by single-particle tracking: statistical analysis of experimental mean squared displacement curves”. In: *Physical Chemistry Chemical Physics* 15.3 (2013). Publisher: The Royal Society of Chemistry, pp. 845–849. ISSN: 1463-9076. DOI: [10.1039/C2CP43433D](https://doi.org/10.1039/C2CP43433D). URL: <http://dx.doi.org/10.1039/C2CP43433D>.
- [17] Ian T. Jolliffe and Jorge Cadima. “Principal component analysis: a review and recent developments”. In: *Philosophical Transactions of the Royal Society A: Mathematical, Physical and Engineering Sciences* 374.2065 (Apr. 2016). Publisher: Royal Society, p. 20150202. DOI: [10.1098/rsta.2015.0202](https://doi.org/10.1098/rsta.2015.0202). URL: <https://doi.org/10.1098/rsta.2015.0202> (visited on 09/19/2021).
- [18] N. Frazee et al. “In Silico Prediction of the Binding, Folding, Insertion, and Overall Stability of Membrane-Active Peptides.” In: *Moreira I.S., Machuqueiro M., Mourão J. (eds) Computational Design of Membrane Proteins*. Vol. 2315. Methods in Molecular Biology. New York, NY: Humana, July 2021. ISBN: 978-1-07-161467-9.

Chapter 3

Using Simulation to Understand the Role of Titration on the Stability of a Peptide–Lipid Bilayer Complex

3.1 Abstract

The pH-Low Insertion Peptide (pHLIP) is an anionic membrane-active peptide with promising potential for applications in imaging of cancer tumors and targeted delivery of chemotherapeutics. The key advantage of pHLIP lies in its acid sensitivity: in acidic cellular environments, pHLIP can insert unidirectionally into the plasma membrane. Partitioning-folding coupling is triggered by titration of the acidic residues in pHLIP, transforming pHLIP from a hydrophilic to a hydrophobic peptide. Despite this knowledge, the reverse pathway that leads to exit of the peptide from the plasma membrane is poorly understood. Our hypothesis is that sequential deprotonation of pHLIP is a prerequisite for exit of the peptide from the plasma membrane. We carried out molecular dynamics (MD) simulations to characterize the effect that deprotonation of the acidic residues of pHLIP has on the stability of the peptide when inserted into a model lipid bilayer of 1-palmitoyl-2-oleoyl-*sn*-3-phosphocholine (POPC). Initiation of the exit mechanism is facilitated by a complex relationship between the peptide, bulk solvent, and the membrane environment. As the N-terminal acidic residues of pHLIP are

deprotonated, localized loss of helicity drives unfolding of the peptide and more pronounced interactions with the bilayer at the lipid-water interface. Deprotonation of the C-terminal acidic residues (D25, D31, D33, and E34) leads to further loss of secondary structure distal from the C-terminus, as well as formation of a water channel that stabilizes the orientation of pHLIP parallel to the membrane normal. Together, these results help explain how stabilization of intermediates between the surface-bound and inserted states of pHLIP occur and provide insights into rational design of pHLIP variants with modified abilities of insertion.

3.2 Introduction

The pH-Low Insertion Peptide (pHLIP) is a membrane-active peptide that in recent years has shown much promise in clinical applications to treat cancer.[1, 2] pHLIP was originally derived from transmembrane helix C of bacteriorhodopsin and was discovered during a mechanistic study on folding of membrane proteins [3]. The peptide exists in a coiled conformation in solution (state I). Upon encountering a membrane surface, it spontaneously binds (state II). Folding and insertion is triggered by protonation of the acidic residues in pHLIP (E3, D14, D25, D31, D33, and E34), with insertion occurring unidirectionally (state III) (**Fig. 3.1**). Initial studies posited that protonation of D14 and D25, the acidic residues in the transembrane segment of pHLIP, were the driving factors in the acid-sensitivity of the peptide [3–5]. Subsequent studies have shown that folding and insertion of pHLIP is much more nuanced, with protonation occurring in a non-sequential and non-binary manner [6, 7].

In particular, it has been difficult to harmonize experimental and computational studies to produce a consensus on particular aspects of the binding, folding, and insertion mechanism of pHLIP. Fluorescence and circular dichroism (CD) spectroscopic studies have been used extensively to establish that binding of pHLIP is most effective in PC-only lipid systems, and that anionic lipid headgroups can lead to shallower binding of pHLIP [4, 8–11]. Site-specific fluorescence labeling revealed that particular segments of pHLIP exhibit a characteristic pK_a of insertion [7], lending support to a multi-step model of insertion that was initially suggested by stopped-flow kinetics studies on the insertion and exit mechanisms of pHLIP [5]. To date, solid-state NMR has provided an exquisite level of detail on the insertion mechanism of pHLIP; the peptide can coexist in a surface-bound and transmembrane inserted state at slightly acidic pH [12], indicating that several conformational intermediates exist in the insertion pathway. The next study from Qiang, An, and coworkers established that protonation of aspartic acids in the state II \rightarrow state III transition was not sequential and did not depend solely on D14 and D25; rather, D31 and D33 were protonated first, followed by D25 and D14 [6]. Fluorescence quenching experiments also showed that the membrane environment underwent a significant degree of perturbation at intermediate pH values, with penetration of water molecules into the hydrophobic interior [6]. Most recently, Qiang, An, and coworkers were able to correlate thermodynamic intermediate states with protonation of specific residues in pHLIP, confirming that

protonation of D31 and D33 are the trigger for partitioning into the bilayer as the initial step in insertion as well as driving conformational changes in the N-terminal half of the peptide [13]. Equilibrium molecular dynamics (MD) simulations have been effective in providing detailed descriptions of pHLIP in solution [14] and binding of pHLIP [15, 16], showing that pHLIP can undergo partial folding in solution and the surface-bound state without protonation of key acidic residues. To date, the most notable characterization of the inserted state of pHLIP has been a constant pH MD study on pHLIP and the L16H variant [17]. There it was shown that deprotonation of D14 was the determining factor in destabilization of positioning of pHLIP within the bilayer, shifting the peptide to a more surface-bound position.

Although the mechanism of folding and insertion of pHLIP is now more fully characterized, the molecular interactions that govern the reverse pathway (unfolding and exit) are poorly understood. Acquisition of this detailed knowledge has implications in relating the behavior of pHLIP to biomedically relevant phenomena, such as residence time of pHLIP in tumor tissue. Determination of the effect of deprotonation of specific acidic residues in pHLIP on the stability of the inserted state is significant to this understanding: we know that the insertion and exit pathways are thermodynamically equivalent [13], but kinetics studies indicate that these pathways are independent from one another [5]. We hypothesize that deprotonation of the N-terminal acidic residues are a prerequisite for unfolding of pHLIP, while deprotonation of C-terminal residues are key to anchoring pHLIP in state III. Furthermore, we wanted to probe the role of internal hydration of the bilayer in state III, despite evidence that pHLIP does not create a pore in the inserted state [4]. To test these hypotheses, we carried out equilibrium molecular dynamics (MD) simulations of pHLIP in state III, sequentially deprotonating the acidic residues from the N- to the C-terminus. Despite the fact that sequential deprotonation of pHLIP may not reflect the exact order of deprotonation in the state III \rightarrow state II transition, it nonetheless provides a comparative basis between the different acidic residues in pHLIP. Interestingly, we found that although deprotonation of N-terminal acidic residues are important to initial unfolding of the peptide, the protonation state of the C-terminal acidic residues hold the key to stabilization of the proteolipid complex.

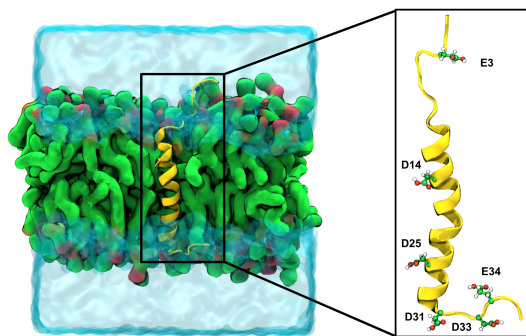


FIGURE 3.1: **Overview of systems studied.** *Left:* Snapshot of pHLIP (yellow) folded and inserted into a POPC bilayer (surface, green and red). *Inset:* Close-up of pHLIP highlighting the acidic residues that are either protonated or deprotonated in this study.

3.3 Computational Methods

3.3.1 System setup

Coordinates for pHLIP (amino acid sequence GGEQNPIYWARYADWLFTTPLL-LLDLALLVDADEGT) were obtained from bacteriorhodopsin (PDB 1FBB) by selecting residues 72 to 107 and mutating residue 105 from Gln to Glu. pHLIP was inserted as a transmembrane helix into a 1-palmitoyl-2-oleoyl-*sn*-3-phosphocholine (POPC) bilayer at a 150:1 lipid:peptide ratio, with 50 waters per lipid and 100 mM NaCl, using the replacement method in the charmm-gui web server [18]. Each system was designed with sequential deprotonation of the acidic residues in pHLIP from the N-terminus to the C-terminus of the peptide (**Table 3.1**). Although this progression of protonation states and system setup is not completely consistent with what we do know about the insertion of pHLIP [6, 7, 13, 17], it allows for a simplified comparison between the individual acidic residues in pHLIP (without the benefit of an enhanced sampling technique such as constant pH MD) as well as extension to timescales that facilitate equilibration of the bilayer surrounding the peptide [19, 20].

3.3.2 MD simulations

All systems generated from charmm-gui were equilibrated for 50 ns with a 2 fs timestep in the NPT ensemble ($P = 1$ atm, $T = 310$ K) using the Langevin thermostat and Nose-Hoover barostat in NAMD 2.13 [21]. The charmm36 force

label	deprotonated residues	net charge of pHLIP
none	none	+1
N _t -E3	E3	0
N _t -D14	E3, D14	-1
N _t -D25	E3, D14, D25	-2
N _t -D31	E3, D14, D25, D31	-3
N _t -D33	E3, D14, D25, D31, D33	-4
N _t -C _t	E3, D14, D25, D31, D33, E34	-5

TABLE 3.1: List of protonation states of pHLIP in this study.

fields for lipids and proteins, and the TIP3P model for water [22–24] were used. Standard cutoffs for non-bonded forces consistent with charmm force fields (10 Å switching distance and 12 Å cutoff) were used. After equilibration, coordinates from the last frame of the trajectory were converted to the AMBER force field topology (ff14SB, OPC and lipid17 [25–27]) to be used in production runs. Minimization and equilibration of the Amber-based system was carried out for 1 ns with a 2 fs timestep in the *NPT* ensemble ($T = 310$ K, $P = 1$ atm) using the Langevin thermostat and Monte Carlo barostat with semi-anisotropic pressure coupling to maintain the aspect ratio of the xy -plane of the lipid bilayer, all in the sander MD engine in AMBER18 [28]. An 8 Å cutoff for non-bonded forces was used, consistent with Amber force fields. Production runs utilized the same settings as minimization and equilibration, this time utilizing the GPU version of pmemd in AMBER18 [28, 29]. Stabilization of general positioning of pHLIP in the bilayer was monitored by measuring the z-position of D14 and D25 for each of the respective protonation states (**Fig. S1**). Simulations were run in triplicate for an aggregate time of 15 μ s per protonation state.

3.3.3 Analysis

Analysis was performed using VMD [30], cpptraj in AmberTools [28], LOOS [31], and in-house scripts. VMD and gnuplot [32] were used to render all snapshots and plot data.

3.4 Results and Discussion

Deprotonation of acidic residues can lead to either localized or distal loss in helicity

To analyze our hypothesis that deprotonation of pHLIP in state III leads to destabilization of the proteolipid complex, we examined the relationship of deprotonation to helicity of pHLIP. As we increased the degree of deprotonation of acidic residues, we observed a localized loss of helicity (**Fig. 3.2A**). However, deprotonation of the C-terminal acidic residues (in particular, D25, D31, and E34) has a more distal effect, decreasing helicity from residues 9-15. This behavior could be related to the fact that deprotonation of the C-terminal acidic residues (D31, D33, E34, and the carboxy terminus) is the most likely protonation state of the inserted TM conformation of pHLIP [13, 17]. In general, helicity decreases with an increase in deprotonation, specifically in residues 9-13 in the N-terminus and residues 17-29 in the C-terminus. This loss of helicity indicates a decrease in the stability of the peptide in the membrane as a function of the degree of deprotonation. Although we don't observe a direct effect between the deprotonated residue and localized changes in helicity, the overall helicity of pHLIP clearly shows a direct correlation between protonation and helicity. Helicity decreases from nearly half of the peptide in a folded helical state when all acidic residues are protonated to less than 30% helicity when all acidic residues are deprotonated (**Fig. 3.2B** and **Fig. S2**).

Unfolding of the helical segment of pHLIP leads to global changes in the peptide as well. Radius of gyration (r_g) can be used as a general indicator of this helix-to-coil transition. As pHLIP is deprotonated, r_g increases, indicating that the entire peptide is unfolding while still embedded in the bilayer (**Fig. 3.3**). Interestingly, upon deprotonation of all acidic residues, r_g decreases, consistent with partial recapture of helicity in the C-terminal half of the transmembrane segment. This indicates the potential for cooperativity between deprotonation of D31, D33, and E34 and refolding of the C-terminal segment of residues that is exposed to bulk solvent in the cytoplasm.

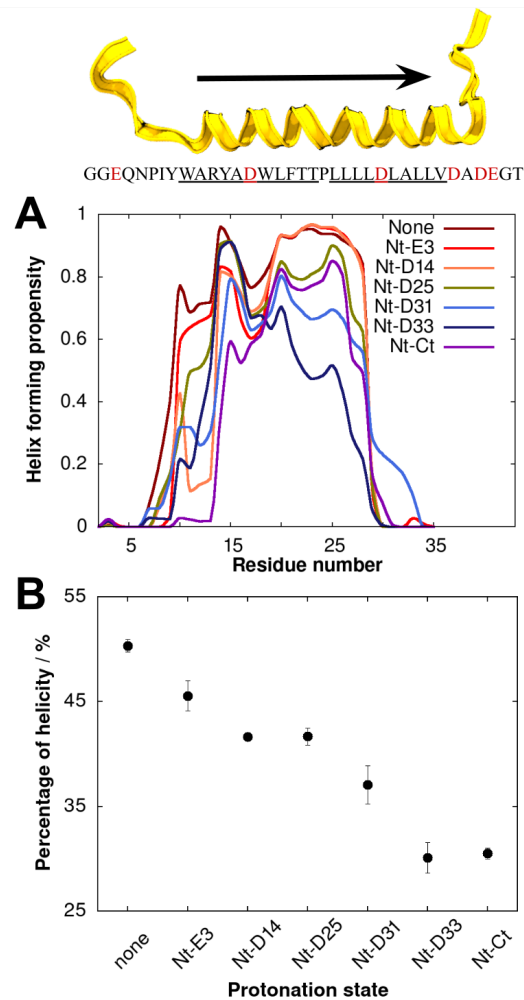


FIGURE 3.2: **Sequential deprotonation of pHLIP leads to localized and global changes in helicity.** *Top:* Representative conformation of pHLIP in the fully folded state. Primary amino acid sequence of pHLIP, with putative transmembrane segment underlined. **A)** Per-residue helicity of pHLIP as a function of protonation state. **B)** Total helical content of pHLIP as a function of protonation state.

3.4.1 pHLIP repositions in the bilayer in distinct ways to compensate for deprotonation

Upon identifying that deprotonation of acidic residues triggers unfolding in pHLIP, we turned our attention to the role that the bilayer plays in this mechanism. A complex relationship exists between the two components that maintains bilayer stability while also facilitating unfolding of pHLIP. The helical tilt angle gradually decreases with sequential deprotonation of pHLIP, proceeding from a maximum of 32° to 21° in the fully deprotonated state **Fig. 3.4A**. This shift is actually manifested in contrasting motions within pHLIP: upon deprotonation of the first

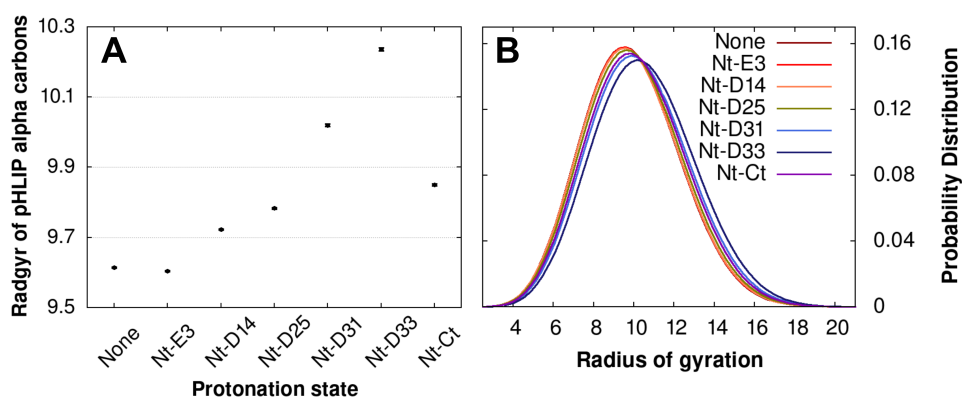


FIGURE 3.3: **Deprotonation of acidic residues triggers expansion of pHLIP.** **A)** Average radius of gyration (r_g) of the TM segment of pHLIP as a function of deprotonation of acidic residues. **B)** distribution of r_g of the TM segment of pHLIP as a function of deprotonation of acidic residues.

C-terminal acidic residue (D25), a sharp increase occurs in the tilt angle of the N-terminal half of pHLIP, initiating movement of this segment of the peptide to a position more parallel to the lateral plane of the lipid bilayer (**Fig. 3.4B**). However, the tilt angle of the C-terminal half of pHLIP notably decreases, also upon deprotonation of D25 (**Fig. 3.4C**). The compensatory motions of the two TM segments are captured by the hinge angle centered around the kink at P20, where we observe a slight increase in the angle – as the N-terminal segment becomes more parallel to the bilayer surface and the C-terminal segment becomes more parallel to the bilayer normal, pHLIP becomes slightly more linear (**Fig. 3.4D**).

Closer examination of the interactions between pHLIP and the bilayer reveal that individual residues and groups of residues play a specific role in destabilization of the proteolipid complex. First, a clear demarcation exists in the positioning of the TM helix upon deprotonation of any C-terminal acidic residues (**Fig. 3.5**). Second, deprotonation of C-terminal acidic residues (D25, D31, D33, and E34) leads to protrusion of the C-terminus from the bilayer. This effectively switches these residues from nonpolar to hydrophilic side chains, stabilizing their position with respect to the interior of the bilayer. Third, an increase in deprotonation also leads to partitioning of the N-terminal segment of pHLIP (residues 1-8) into the headgroup region of the upper leaflet. This behavior could potentially stabilize the N-terminal position of pHLIP, compensating for the increased movement of the C-terminal half of the peptide as D25, D31, D33, and E34 are deprotonated.

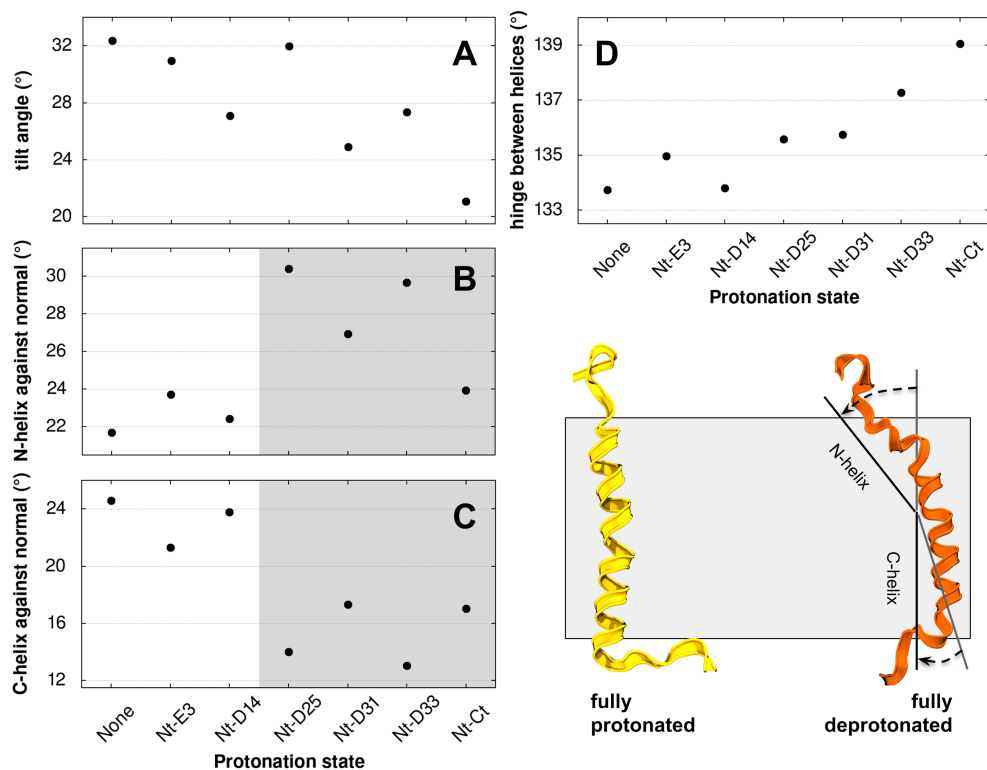


FIGURE 3.4: **Hydrophobic effect leads to compensating motions of N- and C-terminal halves of pHLIP TM helix as acidic residues are progressively deprotonated.** A) Helix tilt angle with respect to the membrane normal, as defined by the vector from residues 8-30 in pHLIP. B) Helix tilt angle with respect to the membrane normal, as defined by the vector from residues 8-19 in pHLIP. C) Helix tilt angle with respect to the membrane normal, as defined by the vector from residues 21-30 in pHLIP. D) Hinge angle as measured between the vectors formed by the N-terminal (residues 10 to 19) and C-terminal (residues 21 to 30) halves of the transmembrane (TM) helix of pHLIP. *Lower right:* schematic showing the corresponding change in tilt angle of each TM segment of pHLIP as it is fully deprotonated.

3.4.2 Localized destabilization of the bilayer is closely coupled to deprotonation of pHLIP and hydration of the hydrophobic interior

The cooperative motions of pHLIP that occur as a function of deprotonation take place in concert with destabilization of the lipid bilayer. The radial distribution function (RDF) of water with respect to pHLIP reveals a stark contrast upon deprotonation of the C-terminal acidic residues: beginning with D25, a sharp increase in the RDF occurs, indicating an influx of waters into the hydrophobic interior of the bilayer (**Fig. 3.6A** and **S3A**). If we count the frequency with which a water molecule enters the interior of the membrane, a similar trend emerges:

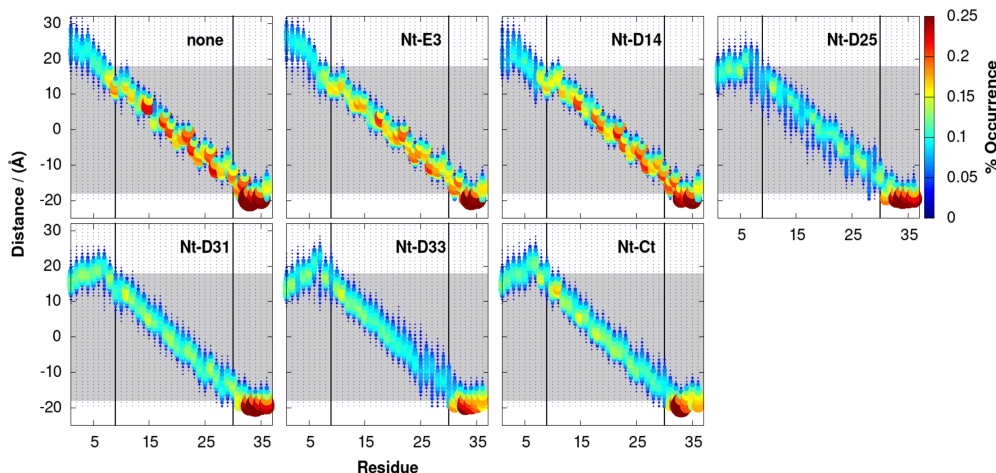


FIGURE 3.5: **Deprotonation has subtle localized and global effects on positioning of pHLIP in state III.** Per-residue distance distribution of pHLIP with respect to the midplane of the POPC bilayer (zero corresponds to the projection onto the z-axis of the center of mass of the bilayer). Heat bar indicates the probability of per-residue distance. Thick black vertical lines indicate the boundaries of the TM segment of pHLIP.

upon deprotonation of D25, a sharp spike (almost three orders of magnitude) is observed in the diffusion of water into the bilayer interior (**Fig. 3.6B**). The residency time of waters in the bilayer also reflects the shift in the diffusive behavior of waters as the bilayer becomes destabilized, showing that when the C-terminal residues of pHLIP are deprotonated, the majority of waters spend a short time (< 20 ns) in the hydrophobic region of the bilayer, indicating fast exchange of water molecules with bulk solvent. In contrast, when fewer residues are deprotonated, waters can spend > 40 ns in the bilayer, indicating a snorkeling effect that is stabilized by interactions with pHLIP (**Fig. 3.6C**). Finally, deprotonation of pHLIP also leads to global disruption of the bilayer, where we observe that the entire lipid patch has a noticeably lower molecular order parameter (MOP) upon deprotonation of D25, well beyond the second and third shell of lipids (**Fig. 3.6D**). Visualization of the water density in our simulations paints a similar picture. As the N-terminal acidic residues are deprotonated, there is a slight increase in the influx of water molecules from bulk extracellular solvent, but it is not until D25 is deprotonated that the peptide-bilayer interface is disrupted to the point that water molecules can snorkel into the bilayer interior, forming a continuous pore connecting bulk solvent from the exterior and interior of the cell (**Fig. 3.7**).

All other measurements of the bilayer paint a similar picture: deprotonation of D25 and subsequent C-terminal acidic residues are the key to facilitating migration

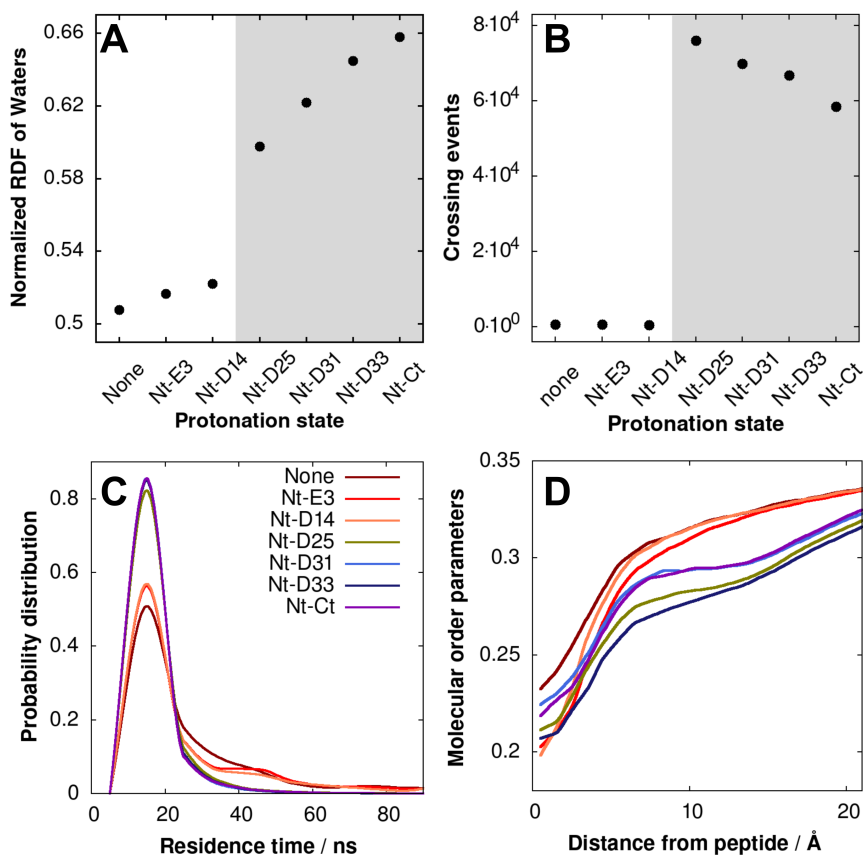


FIGURE 3.6: **Destabilization of hydrophobic interior of bilayer is coupled to deprotonation of pHLIP in state III.** **A)** Maximum value of the first shell of the radial distribution function (RDF) of water with respect to pHLIP. **B)** Explicit count of the number of times a water molecule diffuses into the membrane interior, shown as the number of crossing events. **C)** Probability distribution of the time a given water molecule spends in the hydrophobic region of the bilayer. **D)** Molecular order parameter (MOP) of pHLIP.

of pHLIP towards the outer leaflet of the membrane. There is a clear transition from more ordered to less ordered acyl chains upon deprotonation of D25 (**Figs. S3B** and **S3C**). This disorder in the interior of the bilayer manifests itself in a noticeable increase in area per lipid (**Fig. S3D**) and corresponding decrease in bilayer thickness (**Fig. S3E**). Although pHLIP remains in a TM state in all of our simulations, the decrease in bilayer thickness corresponding to deprotonation of D25 is more pronounced in the upper leaflet than the lower leaflet (**Figs. S3F** and **S3G**). In addition to equilibrium biophysical properties of the bilayer, we observe that insertion of pHLIP significantly alters the lateral diffusion of lipids and their motions along the bilayer normal in the fully inserted state. The lateral diffusion of lipids is noticeably slower when pHLIP is fully protonated (**Fig. S4A**), as well as reducing the mean squared displacement (MSD) of PC headgroups in half (**Fig.**

S4B). Overall, this indicates that pHLIP in the fully inserted state has both a localized and distal effect of ordering the membrane.

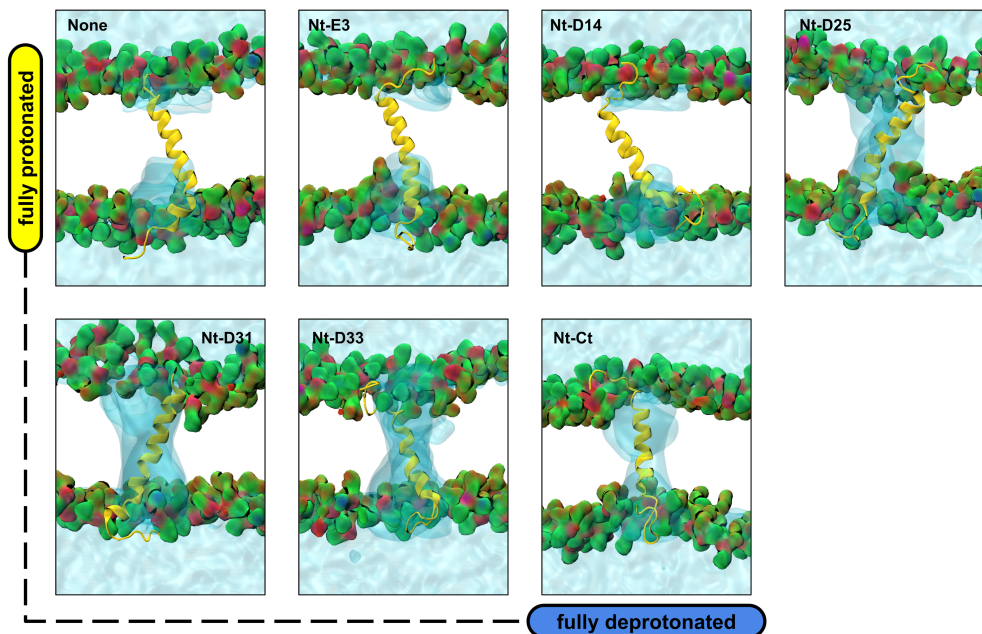


FIGURE 3.7: **Deprotonation of acidic residues leads to penetration of water molecules into interior of the bilayer.** Volumetric representation of average water density for each protonation state in pHLIP. Average structure of pHLIP is used to show the gradual invasion of waters as pHLIP is sequentially deprotonated. *Red and green surface*: headgroups of upper and lower leaflets of POPC bilayer; *blue surface*: water; *yellow cartoon*: pHLIP.

3.4.3 Implications of results on understanding of pHLIP in state III

Although the use of equilibrium MD simulations does not allow us to model the reversible protonation and deprotonation events that drive the transition of pHLIP from the folded, inserted state to the unfolded, surface-bound state, it does provide valuable insights into how deprotonation of acidic residues leads to destabilization of pHLIP in state III. We observed both localized and distal effects on the helicity of pHLIP when deprotonating acidic residues. It is clear that unfolding of the N-terminal half of pHLIP is a prerequisite for exit, but multiple factors can tune this process. This particular result is not unexpected, as a recent constant pH MD study on pHLIP in state III revealed that the N-terminal half of pHLIP migrates to the bilayer-water interface at neutral pH [17]. Calculation of the pK_a of acidic residues revealed that D14 was the trigger for this migration, and although they

were unable to resolve the pK_a of D25, it is expected that deprotonation of D25 also contributed to this surface-bound state, in agreement with our results. What is noticeably different in our simulations is the restoration of helicity in the C-terminal half of pHLIP upon deprotonation of all acidic residues, including E34. A possible explanation for this localized increase in folding lies in the N-terminal segment of pHLIP: we observed a decrease in the overall and C-terminal tilt angles of pHLIP (i.e., less surface-bound and more inserted). This shift in the orientation of the peptide helps offset the migration of deprotonated E34 towards bulk solvent on the cytoplasmic side of the bilayer. The presence of R11 sandwiched between aromatic residues (Y8, W9, Y12, and W15) helps facilitate this shift: previous studies on model peptides and pHLIP showed that the location of an arginine residue slightly off-center in the transmembrane segment, in close proximity to aromatic residues, allows the arginine sidechain to snorkel towards the bilayer surface and interact with bulk solvent [33]. The transmembrane orientation can also interchange with a surface-bound orientation that is presumably stabilized by partitioning of aromatic sidechains into the headgroup region of the membrane [15, 33], which is consistent with the transition between states II and III in pHLIP.

What appears to occur during deprotonation of pHLIP within the bilayer is a cooperative effect between R11 and the deprotonated acidic residues. These two groups act in concert to stabilize a localized deformation in the membrane. The guanidinium group of arginine is able to stabilize single-span peptides at the bilayer-water interface by forming a bidentate hydrogen bond with the phosphate moiety of the PC headgroup; this interaction is what leads to the snorkeling of the sidechain towards extracellular solvent [34]. In the context of membrane protein folding via the translocon, a shift of 1.2 Å of the arginine residue towards the bilayer-water interface lowers the free energy of membrane integration by 0.4 kcal/mol [35].

Likewise, deprotonation of acidic residues help trigger the state III \rightarrow state II transition of pHLIP. One way in which this is accomplished is by extending the penetration of waters into the interior of the bilayer. Temperature-accelerated MD (TAMD) simulations have been able to demonstrate that negatively-charged acidic residues recruit waters into the membrane in order to decrease the energy penalty for translocation of transmembrane loops across the membrane [36]. Our results are consistent with this study, showing a sharp increase in hydration of the bilayer interior upon sequential deprotonation of D25, D31, D33, and E34. Beginning with

D25, there is a transition in the behavior of water molecules interacting with the bilayer – the majority of water molecules freely diffuse between bulk solvent and the bilayer, leading to a localized deformation of the proteolipid complex. This observation is also supported by time-resolved Fourier transform infrared (FTIR) spectroscopic and MD studies on pHLIP in state III, where it was determined that the C-terminal residues of pHLIP were more solvent-exposed in state III [37, 38]. The hypothesis that the C-terminus of pHLIP extends out of the inner plasma membrane and into cytoplasmic solvent [6, 17], which would require the C-terminal acidic residues (D31, D33, and E34) to be deprotonated, is also in agreement with this observation. In addition to water penetration, divalent cations can play a role in stabilizing these intermediates; physiological concentrations of calcium were shown to increase the pK_a of insertion well above neutral pH [39]. It was hypothesized that Ca^{2+} ions act to coordinate between deprotonated acidic residues in pHLIP and lipid headgroups, stabilizing intermediates between states II and III and lowering the energy barrier for folding and insertion. In essence, the positioning of the N-terminal half of pHLIP to a more surface-bound orientation stabilizes the rest of the peptide during the exit process [40].

The physicochemical properties of the membrane can have a noticeable effect on binding and insertion of pHLIP [10, 11, 41, 42], making it critical to obtain a detailed understanding of the relationship between pHLIP and the membrane environment. A key characteristic of pHLIP is that it acts as a monomer without forming a pore [4]. However, it is clear from solid-state NMR and fluorescence experiments that pHLIP perturbs the bilayer environment during insertion to the point that there is a significant influx of water into the bilayer [6], and presumably would do the same during exit. Our simulations provide ample evidence that this is indeed the case: a clear transition in the proteolipid complex occurs upon deprotonation of D25 and subsequent C-terminal acidic residues. This transition is localized with respect to invasion of water molecules into the bilayer interior, but is also propagated to the bulk region of the bilayer. Ordering of the bilayer chains is restored approximately 12-15 Å from pHLIP for all combinations of the N-terminal deprotonations, but this recovery does not occur with deprotonation of the C-terminal residues. The majority of perturbation to the bilayer appears to occur in the extracellular leaflet, where the N-terminal half of pHLIP undergoes considerable movement and transitions from a helical to a coiled conformation. This leads to a subsequent increase in area per lipid and decrease in membrane thickness. More interesting is the effect of pHLIP on the diffusion of the bilayer;

when pHLIP is fully inserted and protonated, lateral diffusion of the POPC lipids is decreased by a factor of two and fluctuations of the headgroups along the membrane normal are nearly half of their value compared to when pHLIP is fully deprotonated. This ordering of the lipid bilayer via insertion of pHLIP does not exist for heterogeneous bilayers containing cholesterol (unpublished results), indicating that pHLIP has a similar effect to cholesterol or sphingomyelin in inducing localized ordering of the membrane [19, 43].

Conventional fluorescence and CD spectroscopy techniques led to the initial suggestion that pHLIP can reversibly interconvert between states I, II, and III upon a transition from a neutral pH to an acidic, membrane-bound environment [3, 4]. Subsequent studies have shown that this mechanism is much more nuanced. Kinetics studies indicated that multiple substates exist, with distinct pathways for insertion and exit [5, 8, 44]. Solid-state NMR and fluorescence spectroscopy revealed that each of the acidic residues in pHLIP possess a unique pK_a , with titration occurring in a non-linear fashion [6, 7], as well as revealing that pHLIP exists in multiple states at slightly acidic pH [6, 13]. In addition to these mechanistic studies, it has become clear that the function of pHLIP can be influenced by both the membrane environment and peptide composition. Non-PC lipids can prevent partitioning of pHLIP to form a stable membrane-bound complex [9–11]; physiological salt concentrations can decrease the propensity for pHLIP to insert into a membrane [16]; even shifting the location of acidic residues in pHLIP or substituting acidic residues with more potent non-natural amino acids can enhance the effectiveness of insertion [8, 45]. How do our results provide additional insights into this seemingly simple, yet complex mechanism?

It is clear that each half of the transmembrane segment of pHLIP stabilizes the inserted state of the peptide in their own unique manner. From our previous [14, 15] and current studies, we know that R11 and the surrounding aromatic residues (Y8, W9, Y12, and W15) play a critical role in stabilizing the partitioned and inserted states of pHLIP. As discussed above, arginine can play a key role in stabilizing interactions of a peptide with the bilayer proximal to the headgroups of phospholipids, and the presence of the aromatic residues adds to this stabilizing effect. Similar to what was observed by Machuqueiro and coworkers [17], deprotonation of the N-terminal acidic residues leads to interconversion between inserted and surface-bound states. With respect to the C-terminal half of the transmembrane segment, the long stretch of nonpolar residues from position 21-30 anchors

pHLIP within the membrane. Interestingly, deprotonation of the C-terminal acidic residues has an opposing effect: it stabilizes the C-terminus of pHLIP by making it more favorable for D31, D33, and E34 to remain exposed to bulk solvent from the cytoplasm while also accelerating the rate of unfolding of the N-terminal half of pHLIP. This mechanism is strikingly similar to the exit pathway that was suggested by Reshetnyak and coworkers in their first kinetics study of pHLIP [5].

3.5 Conclusion

Our results provide a detailed picture into the early stages of exit of pHLIP from a lipid bilayer. This aspect of the pHLIP mechanism has often been overlooked, but is a key element to fundamental understanding of pHLIP and development of biomedical applications such as diagnostic imaging of tumors, which depend on intimate knowledge of residence times within tissues. As stated above, the function of pHLIP can be influenced by numerous factors; comprehensive understanding of the effects of these factors will require creative approaches, both experimental and computational. This initial study into the exit mechanism of pHLIP will serve as a solid foundation for comparison to other membrane environments and use of enhanced sampling techniques, which are currently underway in our lab. Ultimately we expect that this will inform researchers in development of pHLIP variants and conjugates with imaging agents or small molecule drugs.

Bibliography

- [1] Nerissa Therese Viola-Villegas et al. “Understanding the Pharmacological Properties of a Metabolic PET Tracer in Prostate Cancer”. en. In: *Proceedings of the National Academy of Sciences* 111.20 (May 2014), pp. 7254–7259. ISSN: 0027-8424, 1091-6490. DOI: [10.1073/pnas.1405240111](https://doi.org/10.1073/pnas.1405240111).
- [2] Kelly E. Burns, Matthew K. Robinson, and Damien Thévenin. “Inhibition of Cancer Cell Proliferation and Breast Tumor Targeting of pHLIP–Monomethyl Auristatin E Conjugates”. In: *Molecular Pharmaceutics* 12.4 (Apr. 2015), pp. 1250–1258. ISSN: 1543-8384. DOI: [10.1021/mp500779k](https://doi.org/10.1021/mp500779k).
- [3] John F. Hunt et al. “Spontaneous, pH-Dependent Membrane Insertion of a Transbilayer α -Helix”. In: *Biochemistry* 36.49 (Dec. 1997), pp. 15177–15192. ISSN: 0006-2960. DOI: [10.1021/bi970147b](https://doi.org/10.1021/bi970147b).
- [4] Yana K. Reshetnyak et al. “A Monomeric Membrane Peptide That Lives in Three Worlds: In Solution, Attached to, and Inserted across Lipid Bilayers”. English. In: *Biophysical Journal* 93.7 (Jan. 2007), pp. 2363–2372. ISSN: 0006-3495. DOI: [10.1529/biophysj.107.109967](https://doi.org/10.1529/biophysj.107.109967).
- [5] Oleg A. Andreev et al. “pH (Low) Insertion Peptide (pHLIP) Inserts across a Lipid Bilayer as a Helix and Exits by a Different Path”. en. In: *Proceedings of the National Academy of Sciences* 107.9 (Feb. 2010), pp. 4081–4086. ISSN: 0027-8424, 1091-6490. DOI: [10.1073/pnas.0914330107](https://doi.org/10.1073/pnas.0914330107).
- [6] Samuel Z. Hanz et al. “Protonation-Driven Membrane Insertion of a pH-Low Insertion Peptide”. ENG. In: *Angewandte Chemie (International Ed. in English)* 55.40 (Sept. 2016), pp. 12376–12381. ISSN: 1521-3773. DOI: [10.1002/anie.201605203](https://doi.org/10.1002/anie.201605203).

- [7] Haden L. Scott, Justin M. Westerfield, and Francisco N. Barrera. “Determination of the Membrane Translocation pK of the pH-Low Insertion Peptide”. English. In: *Biophysical Journal* 113.4 (Aug. 2017), pp. 869–879. ISSN: 0006-3495. DOI: [10.1016/j.bpj.2017.06.065](https://doi.org/10.1016/j.bpj.2017.06.065).
- [8] Alexander G. Karabadzhak et al. “Modulation of the pHLIP Transmembrane Helix Insertion Pathway”. English. In: *Biophysical Journal* 102.8 (Apr. 2012), pp. 1846–1855. ISSN: 0006-3495. DOI: [10.1016/j.bpj.2012.03.021](https://doi.org/10.1016/j.bpj.2012.03.021).
- [9] Haden L. Scott et al. “The Negative Charge of the Membrane Has Opposite Effects on the Membrane Entry and Exit of pH-Low Insertion Peptide”. English. In: *Biochemistry* 54.9 (Mar. 2015), pp. 1709–1712. ISSN: 1520-4995. DOI: [10.1021/acs.biochem.5b00069](https://doi.org/10.1021/acs.biochem.5b00069).
- [10] Alexander Kyrychenko et al. “Lipid Headgroups Modulate Membrane Insertion of pHLIP Peptide”. English. In: *Biophysical Journal* 108.4 (Feb. 2015), pp. 791–794. ISSN: 0006-3495. DOI: [10.1016/j.bpj.2015.01.002](https://doi.org/10.1016/j.bpj.2015.01.002).
- [11] Victor Vasquez-Montes et al. “Comparison of Lipid-Dependent Bilayer Insertion of pHLIP and Its P20G Variant”. In: *Biochimica et Biophysica Acta (BBA) - Biomembranes* 1860.2 (Feb. 2018), pp. 534–543. ISSN: 0005-2736. DOI: [10.1016/j.bbamem.2017.11.006](https://doi.org/10.1016/j.bbamem.2017.11.006).
- [12] Nicolas S. Shu et al. “Residue-Specific Structures and Membrane Locations of pH-Low Insertion Peptide by Solid-State Nuclear Magnetic Resonance”. English. In: *Nature Communications* 6 (July 2015), p. 7787. DOI: [10.1038/ncomms8787](https://doi.org/10.1038/ncomms8787).
- [13] Sarah A. Otieno et al. “pH-Dependent Thermodynamic Intermediates of pHLIP Membrane Insertion Determined by Solid-State NMR Spectroscopy”. In: *Proceedings of the National Academy of Sciences* 115.48 (Nov. 2018), pp. 12194–12199. DOI: [10.1073/pnas.1809190115](https://doi.org/10.1073/pnas.1809190115).
- [14] Chittrak Gupta and Blake Mertz. “Protonation Enhances the Inherent Helix-Forming Propensity of pHLIP”. In: *ACS Omega* 2.11 (Nov. 2017), pp. 8536–8542. ISSN: 2470-1343. DOI: [10.1021/acsomega.7b01371](https://doi.org/10.1021/acsomega.7b01371).
- [15] Chittrak Gupta, Yue Ren, and Blake Mertz. “Cooperative Nonbonded Forces Control Membrane Binding of the pH-Low Insertion Peptide pHLIP”. English. In: *Biophysical Journal* 115.12 (Dec. 2018), pp. 2403–2412. ISSN: 0006-3495. DOI: [10.1016/j.bpj.2018.11.002](https://doi.org/10.1016/j.bpj.2018.11.002).

- [16] Justin Westerfield et al. “Ions Modulate Key Interactions between pHLIP and Lipid Membranes”. In: *Biophysical Journal* 117.5 (Sept. 2019), pp. 920–929. ISSN: 0006-3495. DOI: [10.1016/j.bpj.2019.07.034](https://doi.org/10.1016/j.bpj.2019.07.034).
- [17] Diogo Vila-Viçosa et al. “Membrane-Induced pKa Shifts in Wt-pHLIP and Its L16H Variant”. In: *Journal of Chemical Theory and Computation* (May 2018). ISSN: 1549-9618. DOI: [10.1021/acs.jctc.8b00102](https://doi.org/10.1021/acs.jctc.8b00102).
- [18] Sunhwan Jo et al. “CHARMM-GUI: A Web-Based Graphical User Interface for CHARMM”. eng. In: *Journal of Computational Chemistry* 29.11 (Aug. 2008), pp. 1859–1865. ISSN: 1096-987X. DOI: [10.1002/jcc.20945](https://doi.org/10.1002/jcc.20945).
- [19] Alexander J. Sodt et al. “The Molecular Structure of the Liquid-Ordered Phase of Lipid Bilayers”. In: *Journal of the American Chemical Society* 136.2 (Jan. 2014), pp. 725–732. ISSN: 0002-7863. DOI: [10.1021/ja4105667](https://doi.org/10.1021/ja4105667).
- [20] Almudena Pino-Angeles and Themis Lazaridis. “Effects of Peptide Charge, Orientation, and Concentration on Melittin Transmembrane Pores”. English. In: *Biophysical Journal* 114.12 (June 2018), pp. 2865–2874. ISSN: 0006-3495. DOI: [10.1016/j.bpj.2018.05.006](https://doi.org/10.1016/j.bpj.2018.05.006).
- [21] Marcelo C. R. Melo et al. “NAMD Goes Quantum: An Integrative Suite for Hybrid Simulations”. en. In: *Nature Methods* 15.5 (May 2018), pp. 351–354. ISSN: 1548-7105. DOI: [10.1038/nmeth.4638](https://doi.org/10.1038/nmeth.4638).
- [22] Jeffery B. Klauda et al. “Update of the CHARMM All-Atom Additive Force Field for Lipids: Validation on Six Lipid Types”. In: *Journal of Physical Chemistry B* 114.23 (2010), pp. 7830–7843.
- [23] Robert B. Best et al. “Optimization of the Additive CHARMM All-Atom Protein Force Field Targeting Improved Sampling of the Backbone ϕ , ψ and Side-Chain $X1$ and $X2$ Dihedral Angles”. In: *Journal of Chemical Theory and Computation* 8.9 (Sept. 2012), pp. 3257–3273. ISSN: 1549-9618. DOI: [10.1021/ct300400x](https://doi.org/10.1021/ct300400x).
- [24] William L. Jorgensen et al. “Comparison of Simple Potential Functions for Simulating Liquid Water”. In: *The Journal of Chemical Physics* 79.2 (July 1983), pp. 926–935. ISSN: 0021-9606. DOI: [10.1063/1.445869](https://doi.org/10.1063/1.445869).
- [25] Saeed Izadi, Ramu Anandakrishnan, and Alexey V. Onufriev. “Building Water Models: A Different Approach”. In: *The Journal of Physical Chemistry Letters* 5.21 (Nov. 2014), pp. 3863–3871. ISSN: 1948-7185. DOI: [10.1021/jz501780a](https://doi.org/10.1021/jz501780a).

- [26] Callum J. Dickson et al. “Lipid14: The Amber Lipid Force Field”. eng. In: *Journal of Chemical Theory and Computation* 10.2 (Feb. 2014), pp. 865–879. ISSN: 1549-9626. DOI: [10.1021/ct4010307](https://doi.org/10.1021/ct4010307).
- [27] James A. Maier et al. “ff14SB: Improving the Accuracy of Protein Side Chain and Backbone Parameters from ff99SB”. eng. In: *Journal of Chemical Theory and Computation* 11.8 (Aug. 2015), pp. 3696–3713. ISSN: 1549-9626. DOI: [10.1021/acs.jctc.5b00255](https://doi.org/10.1021/acs.jctc.5b00255).
- [28] D.A. Case et al. *Amber18*. University of California, San Francisco. 2019.
- [29] Andreas W. Götz et al. “Routine Microsecond Molecular Dynamics Simulations with AMBER on GPUs. 1. Generalized Born”. In: *Journal of Chemical Theory and Computation* 8.5 (May 2012), pp. 1542–1555. ISSN: 1549-9618. DOI: [10.1021/ct200909j](https://doi.org/10.1021/ct200909j).
- [30] W. Humphrey, A. Dalke, and K. Schulten. “VMD: Visual Molecular Dynamics”. eng. In: *Journal of Molecular Graphics* 14.1 (Feb. 1996), pp. 33–38. ISSN: 0263-7855.
- [31] Tod D. Romo, Nicholas Leioatts, and Alan Grossfield. “Lightweight Object Oriented Structure Analysis: Tools for Building Tools to Analyze Molecular Dynamics Simulations”. en. In: *Journal of Computational Chemistry* 35.32 (Dec. 2014), pp. 2305–2318. ISSN: 1096-987X. DOI: [10.1002/jcc.23753](https://doi.org/10.1002/jcc.23753).
- [32] Thomas Williams and Colin Kelley. *Gnuplot 5.2: An Interactive Plotting Program*. 2020.
- [33] Vitaly V. Vostrikov et al. “Changes in Transmembrane Helix Alignment by Arginine Residues Revealed by Solid-State NMR Experiments and Coarse-Grained MD Simulations”. In: *Journal of the American Chemical Society* 132.16 (Apr. 2010), pp. 5803–5811. ISSN: 0002-7863. DOI: [10.1021/ja100598e](https://doi.org/10.1021/ja100598e).
- [34] Sudha Dorairaj and Toby W. Allen. “On the Thermodynamic Stability of a Charged Arginine Side Chain in a Transmembrane Helix”. en. In: *Proceedings of the National Academy of Sciences* 104.12 (Mar. 2007), pp. 4943–4948. ISSN: 0027-8424, 1091-6490. DOI: [10.1073/pnas.0610470104](https://doi.org/10.1073/pnas.0610470104).
- [35] Karin Öjemalm et al. “Energetics of Side-Chain Snorkeling in Transmembrane Helices Probed by Nonproteinogenic Amino Acids”. en. In: *Proceedings of the National Academy of Sciences* (Sept. 2016), p. 201606776. ISSN: 0027-8424, 1091-6490. DOI: [10.1073/pnas.1606776113](https://doi.org/10.1073/pnas.1606776113).

- [36] Samarthaben J. Patel and Reid C. Van Lehn. “Characterizing the Molecular Mechanisms for Flipping Charged Peptide Flanking Loops across a Lipid Bilayer”. In: *The Journal of Physical Chemistry B* 122.45 (Nov. 2018), pp. 10337–10348. ISSN: 1520-6106. DOI: [10.1021/acs.jpccb.8b06613](https://doi.org/10.1021/acs.jpccb.8b06613).
- [37] Jennifer C. Flanagan and Carlos R. Baiz. “Site-Specific Peptide Probes Detect Buried Water in a Lipid Membrane”. en. In: *Biophysical Journal* 116.9 (May 2019), pp. 1692–1700. ISSN: 00063495. DOI: [10.1016/j.bpj.2019.03.002](https://doi.org/10.1016/j.bpj.2019.03.002).
- [38] Jennifer C. Flanagan, Alfredo E. Cardenas, and Carlos R. Baiz. “Ultrafast Spectroscopy of Lipid–Water Interfaces: Transmembrane Crowding Drives H-Bond Dynamics”. In: *The Journal of Physical Chemistry Letters* (May 2020), pp. 4093–4098. DOI: [10.1021/acs.jpcllett.0c00783](https://doi.org/10.1021/acs.jpcllett.0c00783).
- [39] Victor Vasquez-Montes et al. “Divalent Cations and Lipid Composition Modulate Membrane Insertion and Cancer-Targeting Action of pHLIP”. en. In: *Journal of Molecular Biology* 431.24 (Nov. 2019), pp. 5004–5018. ISSN: 0022-2836. DOI: [10.1016/j.jmb.2019.10.016](https://doi.org/10.1016/j.jmb.2019.10.016).
- [40] Eric V. Schow et al. “Arginine in Membranes: The Connection Between Molecular Dynamics Simulations and Translocon-Mediated Insertion Experiments”. en. In: *The Journal of Membrane Biology* 239.1 (Jan. 2011), pp. 35–48. ISSN: 1432-1424. DOI: [10.1007/s00232-010-9330-x](https://doi.org/10.1007/s00232-010-9330-x).
- [41] Alexander G. Karabadzhak et al. “Bilayer Thickness and Curvature Influence Binding and Insertion of a pHLIP Peptide”. eng. In: *Biophysical Journal* 114.9 (May 2018), pp. 2107–2115. ISSN: 1542-0086. DOI: [10.1016/j.bpj.2018.03.036](https://doi.org/10.1016/j.bpj.2018.03.036).
- [42] Haden L. Scott et al. “Phosphatidylserine Asymmetry Promotes the Membrane Insertion of a Transmembrane Helix”. In: *Biophysical Journal* 116.8 (Apr. 2019), pp. 1495–1506. ISSN: 0006-3495. DOI: [10.1016/j.bpj.2019.03.003](https://doi.org/10.1016/j.bpj.2019.03.003).
- [43] Alexander J. Sodt, Richard W. Pastor, and Edward Lyman. “Hexagonal Substructure and Hydrogen Bonding in Liquid-Ordered Phases Containing Palmitoyl Sphingomyelin”. In: *Biophysical Journal* 109.5 (Sept. 2015), pp. 948–955. ISSN: 0006-3495. DOI: [10.1016/j.bpj.2015.07.036](https://doi.org/10.1016/j.bpj.2015.07.036).

- [44] Gregory Slaybaugh et al. “Kinetics of pHLIP Peptide Insertion into and Exit from a Membrane”. en. In: *Proceedings of the National Academy of Sciences* 117.22 (May 2020), pp. 12095–12100. ISSN: 0027-8424, 1091-6490. DOI: [10.1073/pnas.1917857117](https://doi.org/10.1073/pnas.1917857117).
- [45] Joab O. Onyango et al. “Noncanonical Amino Acids to Improve the pH Response of pHLIP Insertion at Tumor Acidity”. eng. In: *Angewandte Chemie (International Ed. in English)* 54.12 (Mar. 2015), pp. 3658–3663. ISSN: 1521-3773. DOI: [10.1002/anie.201409770](https://doi.org/10.1002/anie.201409770).

Chapters/stateIII

Chapter 4

The Transmembrane Helix of pHLIP Slows Down Membrane Thickness Fluctuations and Translational Diffusion

Disclaimer: The following study was a collaboration with various scientists. The author of this dissertation contributed the all-atoms molecular dynamics simulations data only.

4.1 Abstract

Cellular membranes interact with surface-associated and transmembrane proteins that are responsible for a range of biological functions, which are facilitated through dynamical interactions with the host lipid membrane. Despite the recognized importance of protein-membrane interactions, the question as to how proteins affect membrane dynamics, in particular collective fluctuations, remains largely unanswered. Here, we used neutron spin echo (NSE) spectroscopy to selectively access membrane bending and thickness fluctuation modes to determine the dynamic response of a lipid bilayer interacting with the pH-low insertion peptide (pHLIP). A salient feature of the peptide is that it transitions from a surface-associated (SA) state, at neutral pH, to a transmembrane (TM) helix under acidic conditions.

Our results indicate that pHLIP's SA state does not affect membrane bending or thickness fluctuations. Importantly, however, when in the TM state, pHLIP slows down membrane thickness fluctuations without affecting bending dynamics, indicating that TM insertion alters the membrane viscosity but not its rigidity. These observations are consistent with molecular dynamics simulations and solid-state NMR data showing that pHLIP promotes distortions in lipid tail conformations, which result in an increase in membrane viscosity and a reduction in lateral lipid diffusion. The findings potentially suggest a new mechanism for modulation of biological function, whereby TM protein insertion drives a redistribution of lipid tail conformations that lead to a slowdown in thickness fluctuations. Thus, these results have far-reaching implications in how we understand membrane signaling and in potential therapeutic applications of pHLIP.

4.2 Introduction

Cell membranes orchestrate multiple key functions through a delicate interplay between membrane proteins and their host lipid matrix[1–3]. Numerous studies over the past few decades have elegantly illustrated the intimate link between the structure and function of membrane proteins and the physico-chemical properties of the lipid environment in which they reside[4]. Examples range from the role of membrane curvature in the photochemical function of rhodopsin or the gating behavior of mechanosensitive channels[5–7], to the effect of membrane thickness on the enzymatic activity of membrane proteins[4, 8, 9]. Such studies, often accompanied by theoretical or computational modeling, have significantly contributed to our understanding of how the structural parameters of lipid membranes, such as bilayer thickness and curvature, can influence the function of membrane-associated proteins[10, 11]. However, major gaps still exist in our understanding as to how membrane proteins could, in turn, alter the properties of their host membranes, and importantly, how the different states of the protein impact lipid dynamics. Since functional modes in lipid-protein complexes occur over multiple length- and timescales, understanding the intricate cooperativity between membrane proteins and lipid membranes requires knowledge of how different classes of proteins influence hierarchical membrane dynamics, from individual lipid motions up to collective membrane fluctuations.

Membrane proteins account for approximately half the mass of mammalian plasma membranes[12, 13]. They are grouped into two broad categories, namely surface-associated (SA) and transmembrane (TM) proteins, both of which are crucial to the cell's viability and function. Among the peptides or proteins that can adopt both SA and TM states is the pH-low insertion peptide (pHLIP). At neutral pH, pHLIP adsorbs to the membrane surface, but when the environmental pH decreases, pHLIP transforms into a TM α -helix[14, 15]. The amino acid sequence of pHLIP includes seven acidic groups whose protonation triggers membrane insertion, allowing for controllable conformational changes[16]. Its pH-responsiveness also allows the peptide to target aggressive solid tumors, which typically possess an acidic extracellular medium[17]. Indeed, pHLIP is a promising candidate for selective cancer therapeutics, as it is able to translocate cargo, such as radionuclides, toxins, and antisense molecules into the cytoplasm of cancer cells[18, 19].

However, to exploit its full potential in cancer applications, it is important to understand its dynamical interactions with host membranes, both in its SA and TM states.

Among the rich dynamics of lipid membranes, collective membrane fluctuations have been implicated in various protein functions, including the ability of proteins to bind to or insert in membranes[20, 21]. These fluctuations primarily manifest in two dynamic modes, i.e. bending and thickness fluctuations. Specifically, bending fluctuations are controlled by the mechanical properties of the membrane, generally described by the bending rigidity modulus, and have been extensively studied both experimentally and theoretically[22, 23]. On the other hand, fluctuations around the average membrane thickness are less explored but have been linked to a number of vital membrane phenomena, including passive permeation, pore formation, and ion channel gating[20, 24]. Although membrane thickness fluctuations have long been theoretically predicted[25], they only became experimentally accessible with the advent of neutron spin echo (NSE) spectroscopy[25–28]. Unlike other spectroscopy methods, NSE can simultaneously access the length- (a few nm) and timescales (~ 100 ns) over which membrane thickness fluctuations occur[24, 29, 30]. Concurrent developments in membrane fluctuation theory has enabled the interpretation of thickness fluctuations in relation to membrane viscoelastic properties, further emphasizing the importance of this dynamic mode in biological function[31]. These developments have now opened new avenues to explore how complex membrane dynamics respond to protein association and conformational changes. Notably, the timescale of membrane thickness fluctuations happens to coincide with that of protein folding events[27, 32], suggesting a type of dynamical synergy between proteins and their host lipid membranes.

In this work, we used complementary physical characterization techniques to study how SA and TM pHLIP affect membrane structure and dynamics. We used NSE to directly probe the effect of pHLIP on the membrane’s bending and thickness fluctuations. Measurements were performed on lipid vesicles composed of 1,2-dioleoyl-*sn*-glycero-3-phosphocholine (DOPC), 1,2-dioleoyl-*sn*-glycero-3-phosphoserine (DOPS), and cholesterol (Chol)[33], at a mixing ratio (76/4/20) that is comparable to previous pHLIP studies[34]. Coarse-grained molecular dynamics (MD) simulations[35] of full lipid vesicles corroborated the NSE results showing that TM pHLIP reduces

the membrane thickness fluctuation rate. Membrane structural information in the absence and presence of pHLIP, was obtained by small-angle neutron and X-ray scattering (SANS and SAXS). Complementary solid-state NMR measurements and all-atom MD simulations provided molecular details pertaining to the interactions of TM pHLIP with membrane lipids. We propose that combined, these observations point to a potential means by which synergistic protein-membrane dynamics may regulate membrane functions.

4.3 Results

4.3.1 Effect of pHLIP on bilayer dynamics in its SA and TM states.

Experiments were carried out on large unilamellar vesicles composed of DOPC/-DOPS/Chol at a molar ratio of 76/4/20 and a lipid:peptide (L:P) molar ratio of 150:1. The anionic lipid, DOPS, was used to ensure vesicle unilamellarity[36, 37], as determined by SAXS (**Fig. S1**). At pH 8, pHLIP adsorbs to the vesicle surface in a largely unstructured conformation (**Fig. S2**)[38]. However, a drop in pH triggers pHLIP to insert into the membrane, with a pH midpoint of 4.90 ± 0.08 (pK_{FI} , obtained using Eq. S1). At pH 4, well into the acidic baseline of the transition, pHLIP transforms into a TM helix (**Fig. S2**)[16, 39].

After determining the pH values where the peptide adopted stable SA and TM states, NSE experiments were performed to probe the effect of peptide conformations on membrane dynamics. **Fig. S3A** shows typical NSE intermediate scattering functions, $S(q, t)/S(q, 0)$, where q is the wavevector transfer and t is the Fourier time. Fits of the intermediate scattering functions, using the elastic-sheet fluctuation model $S(q, t)/S(q, 0) = \exp[-(\Gamma t)^{2/3}]$, yielded the relaxation rates, Γ , at different q -values (or inverse length scales)[40]. The relaxation rates, $\Gamma(q)$, of *protiated* vesicles in deuterated buffer showed the typical q^3 -dependence (**Fig. S3B**, blue data points), a signature of bending fluctuations as predicted by Zilman and Granek[40]. Using refinements proposed by Watson and Brown[41], the Zilman-Granek theory for bending relaxations can be expressed as:

$$\Gamma_{bend}(q) = 0.0069 \frac{k_B T}{\eta_{D2O}} \sqrt{\frac{k_B T}{\kappa}} q^3, (Eq.1)$$

where κ is the membrane bending modulus, κ_B is the Boltzmann constant, T is the temperature, and η_{D_2O} is the viscosity of D_2O . In this treatment, the location of the neutral surface is assumed to be at the hydrophobic-hydrophilic interface[28, 42]. Control experiments on peptide-free lipid vesicles showed that the change in pH had almost no effect on the membrane bending modulus, κ (Table 1), consistent with previous studies on other model membranes[43]. Similarly, we observed that the presence of pHLIP did not cause significant changes in κ , neither in its SA (pH 8) or TM (pH 4) states, as all κ values were within the margin of experimental error (Table 1 and Fig. S4)[43].

Table 1. Dynamic membrane parameters obtained from the analysis of NSE and all-atom MD simulations.

pH	pHLIP	Bending	Thickness		Area	Viscosity	Diffusion
		Modulus	Fluctuations	Compressibility		Constant	
		κ ($\kappa_B T$)	Γ_{TF} (ns^{-1} 10^{-3})	Δd_m (\AA)	K_A (N/m)	μ (nPa·s·m)	D (10^{-5} cm ² /s)
8	-	30.34 ± 2.47	7.3 ± 0.9	3.5 ± 0.6	0.262 ± 0.021	31.92 ± 3.49	
4	-	29.22 ± 1.33	7.3 ± 1.7	3.4 ± 0.8	0.261 ± 0.021	32.02 ± 4.14	1.28 ± 0.72
8	+	26.88 ± 1.81	6.5 ± 2.3	3.4 ± 1.0	0.232 ± 0.018	30.51 ± 3.52	
4	+	32.90 ± 2.75	1.7 ± 0.6	3.8 ± 1.5	0.284 ± 0.031	105.89 ± 54.79	0.59 ± 0.06

NSE parameters are the bending modulus, κ , time-scale of the thickness fluctuation, Γ_{TF} , amplitude of the thickness fluctuation, Δd_m , area compressibility modulus, K_A , and membrane viscosity, μ . Error bars represent ± 1 standard deviation (S.D.) of the fitting parameters.

On the other hand, NSE measurements performed on *chain-perdeuterated* membrane analogs, using DOPC- d_{66} and Chol- d_{40} , showed a clear deviation from the q^3 dependence in Γ at $q \sim 0.08 \text{ \AA}^{-1}$, a value which corresponds to the membrane thickness (Fig. S3B). Specifically, the observed excess dynamics are attributed to thickness fluctuations (Fig. S3, red data points)[26–28] and are well described by a Lorentz function (second term in Eq. 2), such that the overall relaxation rate can be expressed as:

$$\frac{\Gamma(q)}{q^3} = \frac{\Gamma_{bend}(q)}{q^3} + \frac{\Gamma_{TF}}{q_0^3} \frac{1}{1+(q-q_0)^2\zeta^2}, \quad (Eq.2)$$

where Γ_{TF} is the relaxation rate of membrane thickness fluctuations, q_0 is the peak position of the Lorentzian, and $1/\zeta$ is the half width at half maximum (HWHM)

determined by the thickness fluctuation amplitude, Δd_m , such that $\Delta d_m \approx \frac{2D_c}{\zeta q_0}$, where $2D_c$ is the bilayer hydrocarbon thickness. Using these expressions, NSE data of bilayers in the presence and absence of pHLIP were analyzed to determine both Γ_{TF} and Δd_m (**Fig. 4.1B** and **Table 1**). Control experiments of lipid-only samples showed that pH alone had no effect on membrane thickness fluctuations (**Fig. S6** and **Table 1**), with Γ_{TF} and Δd_m values being comparable to those reported previously (**Table 1**)[26–28]. Specifically, Δd_m was found to account for $\sim 10\%$ of the membrane thickness, in all cases. In the presence of pHLIP, we found that SA pHLIP (pH 8) did not result in any major changes to Γ_{TF} , whereas for TM pHLIP Γ_{TF} experienced a fourfold decrease (**Fig. 4.1D** and **Table 1**). Notably, no changes to Δd_m were observed in either conformation of pHLIP (**Fig. S5** and **Table 1**), indicating that the suppression in thickness fluctuations as a result of TM pHLIP is due to a slowdown in the fluctuation rate rather than a decrease in the fluctuation amplitude. These observations, therefore, reveal a specific peptide-induced effect on the rate of membrane thickness fluctuations that is dependent on pHLIP’s conformation.

Synergistic coarse-grained molecular dynamics (CG-MD) simulations were performed on large unilamellar lipid vesicles with transmembrane peptide-like inclusions (**Fig. S7**). This approach allowed us to simulate the membrane fluctuation signals, in the absence and presence of transmembrane peptides, as measured by NSE[35]. The static scattering function, $S(q)$, of the simulated vesicles was calculated from the density-density correlation function by taking the discrete Fourier transform of the density distribution of all lipid beads, such that $S(q) = 1/N \langle \rho_{\vec{q}} \rho_{-\vec{q}} \rangle$. Membrane fluctuation signals were calculated from the simulations as $S(q, t)/S(q, 0) = 1/N \langle \rho_{\vec{q}}(\Delta t) \rho_{-\vec{q}} \rangle$, which represents the time autocorrelation of the scattering function, $S(q)$ after an elapsed time Δt . This is analogous to the intermediate dynamic scattering function measured by NSE. Analysis of the temporal decays in $S(q, t)/S(q, 0)$, following the procedure developed in a previous work[35], yielded the relaxation rates of membrane thickness fluctuations. As seen in **Fig. 4.1C**, the simulated vesicle with TM peptides showed a remarkable suppression in the membrane thickness fluctuation signal relative to the lipid-only vesicle. These simulation results directly correlate those obtained by NSE experiments and suggest a “pinning mechanism” by which transmembrane peptide-like inclusions restrict the rate of fluctuations in membrane thickness.

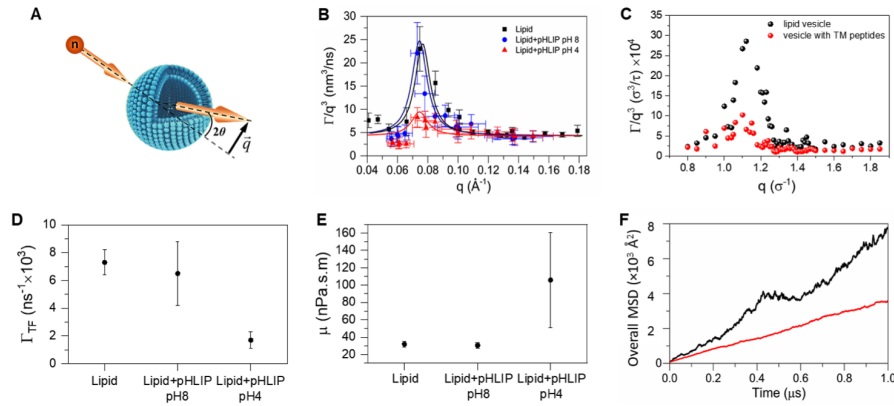


FIGURE 4.1: TM pHLIP slows down the rate of membrane thickness fluctuations and increases membrane viscosity. (A) NSE schematic, where lipid vesicles scatter neutrons with a scattering angle 2θ and wavevector transfer \vec{q} . (B) NSE data, showing the normalized relaxation rate, $\frac{\Gamma}{q^3}$, as a function of q for tail perdeuterated membranes. Data are shown in the absence (black) and presence of pHLIP in its SA (blue, pH 8) or TM (red, pH 4) states. Peak height is associated with the rate of thickness fluctuations, while peak width describes the fluctuation amplitude. Lines are fits to the data using Eq. 2. (C) CG-MD simulation of membrane Fluctuation signals as detected by NSE, for vesicles without (black) and with (red) TM peptide incorporated. The suppression of thickness Fluctuations with TM pHLIP, compared to peptide-free membranes, is manifested in differences in the $\frac{\Gamma}{q^3}$ vs. q plots. (D) The rates of thickness fluctuations, extracted from fits to the data in (B), show remarkable suppression in the presence of TM pHLIP relative to the peptide-free membrane, and no changes with SA pHLIP. (E) Membrane viscosity changes exhibit a similar trend, as only TM pHLIP increases viscosity. (F) Atomistic MD simulations show a decrease in the mean-squared displacement (MSD) of the lipid headgroups in the presence (red) of pHLIP compared to lipid-only membranes (black). Error bars represent ± 1 S.D.

To relate membrane fluctuations to other biologically relevant properties, we used the polymer-brush model, which describes the area compressibility modulus as $K_A = \beta\kappa/(2D_c)^2$ [44], where β is a constant that defines the degree of coupling between the bilayer leaflets (herein set to $\beta = 24$)[44] and $2D_c$ is the mechanical thickness of the membrane, which in the case of DOPC-Chol membranes, is modified according to references[33, 45]. In the q -range where thickness fluctuation modes dominate, the relaxation rates are dictated by the membrane viscosity, μ , such that $\Gamma_{TF} \approx K_A/\mu$ [31, 42, 46]. Put together, these biophysical membrane parameters yield a modified expression of Eq. 2 that allows for the direct determination of membrane viscosity (see Eq. S5 in Supporting Information). Based on this mathematical framework, the minimal changes in the measured bending rigidities (Fig. S4) indicate that K_A values of membranes with SA or TM pHLIP are similar (Fig. S8). The constant thickness fluctuation rate, Γ_{TF} , obtained

with SA pHLIP indicates that the surface association of the peptide did not affect membrane viscosity (μ). In contrast, TM pHLIP caused a large increase in μ beyond the errors of the fitted parameters (**Fig. 4.1E** and **Table 1**).

To understand the molecular mechanism by which TM-PHLIP modulates membrane thickness fluctuations, we utilized an all-atom MD approach with a more realistic representation of the peptide and lipid molecules. We first determined the effect of pHLIP on lipid dynamics, as mean square displacement (MSD) of DOPC headgroups. We then used the MSD data to calculate the lipid diffusion constant, whereby we observed that TM pHLIP depressed lipid mobility (**Fig. 4.1F** and **Table 1**). The observed decrease in the diffusion constant is in agreement with our current NSE conclusions, namely that TM pHLIP increases membrane viscosity. MSD analysis included both in-plane lipid diffusion, as well as movement along the membrane normal. When the MSD was determined normal to the membrane, we observed similar values in the absence ($20.3 \times 10^3 \text{ \AA}^{-2}$) and presence ($20.8 \times 10^3 \text{ \AA}^{-2}$) of TM pHLIP. This observation indicates that the effect of pHLIP on lipid mobility is limited to in-plane motions. These observations support both NSE and CG-MD results showing that pHLIP does not alter the amplitude of the thickness fluctuations.

Interestingly, the changes in lipid diffusion inferred from NSE analysis and observed directly in atomistic MD simulations are not reflected in fluorescent probe measurements of molecular lipid dynamics. For those measurements, we used fluorescent 1,6-diphenyl-1,3,5-hexatriene (DPH) and 9-(2,2-dicyanovinyl)julolidine (DCVJ), two rotationally sensitive probes commonly used to measure membrane fluidity and viscosity, respectively[47, 48]. We found that neither SA pHLIP nor TM pHLIP affected the rotational diffusion of the probes (see Supporting Information). How the differences between the measurement modes can explain these results are examined in the Discussion section.

4.3.2 Average bilayer thickness is not affected by pHLIP.

The interaction between membrane proteins and their lipidic environment is primarily driven by their need to sequester their hydrophobic amino acids into the

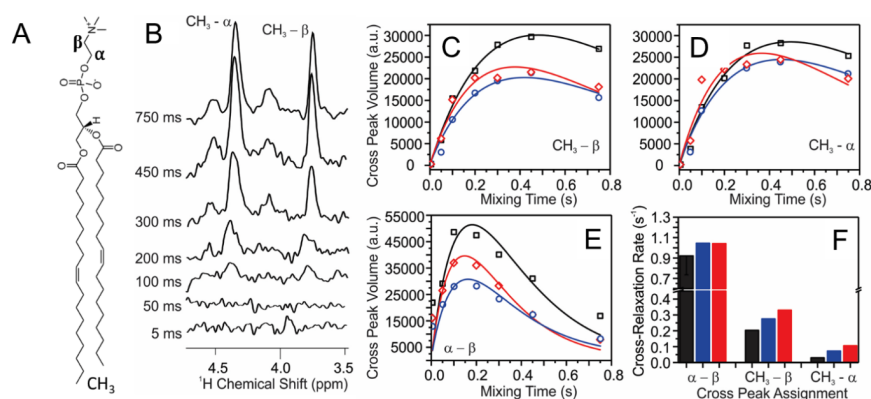


FIGURE 4.2: **Solid-state NMR cross-relation rates and the effect of pHLIP.** (A) Schematic of a DOPC lipid molecule showing the PC headgroup α and β carbons, and the two terminal CH_3 groups. (B) 1D slices at different mixing times showing the build-up of cross-relaxation peaks between acyl chain terminal methyl group protons and the PC headgroup α and β carbons in vesicles of DOPC/DOPS/Chol with containing pHLIP at pH 8. (C-E) Experimental peak volumes (symbols) and simulated build-up curves (lines) for three sets of cross peaks: (C) $\text{CH}_3 - \beta$ H, (D) $\text{CH}_3 - \alpha$ H, and (E) $\alpha - \beta$. Legend: Black + Squares, lipid only; Blue + Circles: pHLIP pH 8; Red + Diamonds, pHLIP pH 4. (F) Best-fit cross-relaxation rates for individual H spin-pairs (i.e. $\alpha - \beta$, $\text{CH}_3 - \alpha$ and $\text{CH}_3 - \beta$). Colors/markers are the same as in plots C-F.

bilayer's hydrophobic acyl chain region[49]. To examine this in more detail, we performed SANS and SAXS experiments to determine if pHLIP affected bilayer structural properties. With SANS, deuterium labeling was used to maximize the neutron contrast between the protonated lipid headgroups and the deuterated acyl chain region of the membrane – this was achieved through the use of DOPC- d_{66} and Chol- d_{40} [49]. Joint analysis of the SANS and SAXS data[50–52] resulted in the following structural parameters (**Table S1**): (i) area per lipid (A_L); (ii) total bilayer thickness (Luzzati thickness) (D_B); (iii) hydrophobic thickness ($2D_c$); and (iv) phosphate-to-phosphate distance (D_{HH}) (Figs. S9, S10, S11, and S12). Of particular interest was the bilayer's hydrophobic thickness which could be altered in the case of hydrophobic mismatch between the lipid membrane and TM pHLIP. Our results indicate that the addition of pHLIP did not alter the average bilayer structure (**Table S1, Fig. S11**), including the average membrane hydrophobic thickness, as confirmed by the all-atom MD simulations (**Fig. S13**). This is consistent with the relatively constant Δd_m values obtained from our NSE experiments and coarse-grained MD simulations. These results also agree with a previous study on the effect of pHLIP on bilayers of 1-palmitoyl-2-oleoyl-*sn*-glycero-3-phosphocholine (POPC)[53] that showed that neither pHLIP adsorption

nor insertion altered membrane structure, even at elevated peptide concentrations. Based on recently measured scaling relationships[54], the negligible effect of pHLIP on A_L supports the NSE conclusion that K_A is not affected by the different states of pHLIP (**Table 1**), corroborating that the decrease in the rate of thickness fluctuations ($\Gamma_{TF} \approx K_A/\mu$) observed with TM pHLIP is the result of increased membrane viscosity.

4.3.3 TM pHLIP increases lipid acyl chain snorkeling.

In fluid membranes, acyl chain dynamics allow for the interaction between the lipid’s acyl chain terminal methyl group (CH_3) and polar headgroups (i.e., “snorkeling”) and can be measured by solid state NMR (ssNMR)[55]. We hypothesized that if TM pHLIP promotes lipid tail snorkeling, this would lead to increased molecular friction within the bilayer, causing an increase in membrane viscosity and a slowdown of thickness fluctuations. To measure headgroup-terminal methyl group interactions, we performed two-dimensional (2D) ^1H - ^1H NOESY ssNMR experiments and determined the cross-relaxation rate between the terminal CH_3 hydrogens and the choline α and β carbons at pH 8 and pH 4. As a positive control, we measured the cross-relaxation rate between the neighboring α and β choline hydrogens. **Fig. 4.2** shows that TM pHLIP increases the cross-relaxation rate between the headgroup choline and terminal CH_3 of the acyl chains – i.e., the terminal CH_3 of the acyl chain snorkels to explore the lipid headgroup region.

Additional analysis of the atomistic MD simulations in the presence of TM pHLIP was performed to seek further evidence of lipid tail snorkeling (**Fig. 4.3**). To this end we measured the distance between the C_α of the lipid headgroup and the terminal CH_3 group (**Fig. 4.3**). In the absence of pHLIP, we observed that most CH_3 groups were located at the midplane of the bilayer, As expected[56], we observed that most lipid acyl chains were extended and located at the midplane of the bilayer in the absence of pHLIP. Only 11% of lipids exhibited an exaggerated kink at the acyl chain double bond, resulting in a CH_3 - C_α distance of $leg\ 8\ \text{\AA}$, which is compatible with the notion of snorkeling (**Fig. 4.3A**, inset, black line). However, in the presence of TM pHLIP the distance distribution shifted towards lower values. Specifically, for the lipid molecules found within a $10\ \text{\AA}$ radius of pHLIP, we observed an increase of $\sim 70\%$ in short-range CH_3 - C_α ($leg\ 8\ \text{\AA}$) interactions and

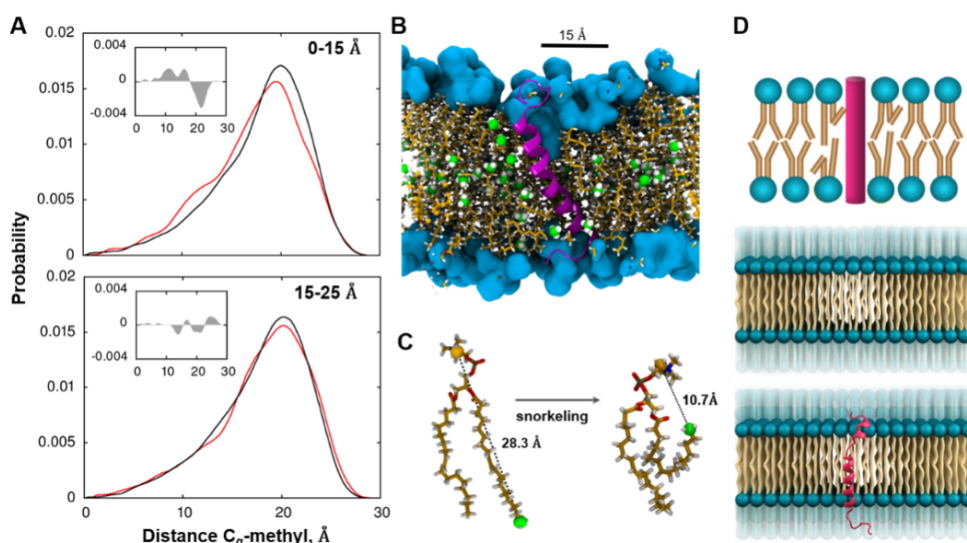


FIGURE 4.3: **TM pHLIP increases snorkeling of lipid tails to the water-bilayer interface.** (A) Probability distribution of the distance between the CH₃ groups of oleoyl chains and the plane formed by the C_α of the choline headgroups. Black lines show data from neat bilayers, and red lines consider only lipids within 15 Å of pHLIP (*top*), or between 15 and 25 Å from the helix (*bottom*). *Insets* show the subtraction between red and black lines. (B) Representative snapshots of a DOPC/DOPC/Chol bilayer containing TM pHLIP. Phospholipid headgroups are shown in blue, and tails in yellow. CH₃ groups are shown as green spheres. Cholesterol molecules are shown in a ball and stick representation. (C) A representative DOPC molecule with fully extended acyl chains can snorkel reducing the distance to the choline headgroup in the presence of TM pHLIP. C_α (yellow) and CH₃ (green) are shown in spheres and are used for distance measurements. (D) Schematic of the effect of snorkeling on the DOPC oleoyl chain, depicting a structural change that enables nearby acyl chains to explore a larger conformation space and experience more entanglement. This manifest itself in increased membrane viscosity and slower thickness fluctuations compared to neat membranes.

a pronounced increase in the probability density at ~ 4 Å (arrow in **Fig. 4.3A**), indicating a conformational preference of DOPC molecules, in pHLIP's proximity, to be in the “snorkeling” configuration. This is distinct from dynamic snorkeling events, where acyl chains continuously explore the conformational space between the bilayer center and the headgroup region, which generally results in a gradual change in the probability distribution (black line in **Fig. S3A**) rather than a localized distribution peak as the one we see in the presence of pHLIP (red line in **Fig. S3A**). Interestingly, the simulations show that the localized influence of pHLIP continues when the cumulative distribution function is calculated within a larger region around pHLIP (15 Å radius), but noticeably decreases beyond this range (**Fig. 4.3B**). However, even far from pHLIP, there is a slight increase in

population of very close (*leg* 4 Å) CH₃-C_α interactions (**Fig. 4.3B**, right inset), indicating that the TM state of pHLIP exerts proximal and distal effects on its membrane environment (**Fig. 4.3C**).

4.4 Discussion

To better understand biological membranes, it is necessary to elucidate how hierarchical dynamics in lipids and membrane proteins manifest themselves, not only in isolation, but also when operating in synergy. In this study we adopted a hierarchical approach to probe a range of dynamics in membranes with pHLIP, as a model peptide with tunable membrane-associated states. Our approach combined fluorescence spectroscopy, atomistic MD simulations, and ssNMR to probe local lipid dynamics, and NSE spectroscopy and CG-MD simulations to probe collective membrane dynamics (i.e. bending and thickness fluctuations). Recent developments in NSE data analysis[28] and newly developed theories[31] have made it possible to relate collective fluctuations to biophysical membrane properties, including membrane viscosity (μ). This has created a unique opportunity to bridge the gap between collective membrane fluctuations and molecular diffusive motions probed by fluorescence spectroscopy and atomistic MD simulations. Combining such measurements have enabled us to carry out direct observations on the conformational effects of pHLIP for a wide range of membrane dynamics that span molecular rotations, lateral diffusion, and collective fluctuations. Moreover, the application of all-atom MD simulations provided complementary mechanistic information on how these different physical phenomena might be related to acyl chain configuration.

The current work complements previous biophysical studies on pHLIP that have largely focused on understanding how membrane characteristics may influence the efficacy of pHLIP for targeted cancer therapy[18, 57, 58]. As pointed out, pHLIP adsorbs to the membrane surface at neutral pH, but inserts into the membrane at acidic pH[59]. Membrane insertion of pHLIP is defined by its pK of insertion[14, 34, 60], which depends on lipid composition. For instance, the presence of negatively charged lipids, specifically phosphatidylserine (PS), decreases pK [39, 61] as does the presence of cholesterol in the bilayer[34]. In this study, we find that the inclusion of both PS and Chol in phosphatidylcholine membranes decreases the

pK to its lowest value yet observed for pHLIP, i.e., $pK = 4.90 \pm 0.08$ (**Fig. S2**), suggesting that a membrane’s chemical properties may have an additive effect on pK of insertion.

4.4.1 pHLIP suppresses membrane thickness fluctuations by increasing lipid viscosity.

To access thickness fluctuations and associated membrane parameters, chain-perdeuterated analogues of DOPC and cholesterol were synthesized, as described in Supporting Information. Control experiments using pure lipid vesicles showed that pH had no effect on membrane thickness fluctuations in the absence of pHLIP (**Fig. S6**). In addition, NSE measurements on protiated vesicles showed that pHLIP did not alter, to any extent, the membrane bending modulus (**Fig. S4** and **Table 1**). These results are consistent with recent MD simulations showing that peripheral proteins had no effect on membrane bending rigidity and that TM proteins, in amounts similar to those used here (pHLIP occupying less than 10% of the membrane area), had a minimal effect on the bending rigidity of the host membrane [63](#). However, it has also been shown that at higher peptide densities (L:P of 50:1), the TM peptide, GWALP23, increases the bending modulus of membranes[\[62\]](#).

In contrast, TM pHLIP suppressed the rate of membrane thickness fluctuations, as observed both by NSE and CG-MD simulations (**Fig. 4.1B-C**). In NSE experiments, the null response of the neat membrane to changes in pH implies that the slowdown of membrane thickness fluctuations is the result of TM pHLIP (**Fig. 4.1B**). SANS/SAXS data, and atomistic MD simulations, indicated no changes in membrane structure due to pHLIP (**Table S1**), suggesting that the observed reduction in thickness fluctuations is not the result of hydrophobic mismatch between the bilayer hydrophobic core and pHLIP[\[49, 63–66\]](#), but rather due to a slowdown in the fluctuation rate[\[31\]](#). Since membrane bending rigidity, and accordingly, area compressibility, showed little to no change upon the addition of pHLIP, the decrease in the thickness fluctuation rate, Γ_{TF} , indicates an “effective” increase in the membrane viscosity, μ , caused by TM pHLIP. In comparison, SA pHLIP did not affect either Γ_{TF} or μ (**Fig. 4.1** and **Table 1**), indicating that changes to these

two parameters result from the interaction of TM pHLIP with the lipid acyl chains.

It is important to point out that although the increase in membrane viscosity is fully supported by our analysis of the NSE data, the magnitude of the increased viscosity requires further assessment. The reported fits to the NSE data assumed that the two bilayer leaflets are coupled according to the polymer-brush model and that the transition of pHLIP to its TM state does not change the interleaflet coupling. In the polymer brush model, the two bilayer leaflets are loosely coupled with a coupling constant $\beta = 24$ that is proportional to the coupling strength between the leaflets. However, variations in the coupling constant have been previously observed[67, 68]. If we consider this possibility and assume an extreme coupling scenario in which TM pHLIP causes the two leaflets to be fully coupled (i.e., $\beta = 12$), this would result in a two-fold increase in membrane viscosity relative to pHLIP-free membranes. One, however would reasonably expect a scenario where TM pHLIP results in an intermediate β value between the polymer brush model and a fully coupled bilayer. Although this would require additional experimental studies (that are beyond the scope of this work), this notion is consistent with the results from ssNMR and atomistic MD simulations that will be discussed below.

4.4.2 TM pHLIP reduces lipid translational diffusion more than rotational diffusion.

Molecular motions in lipid membranes are comprised of lateral lipid diffusion within the plane of the membrane and rotational motions of lipid molecules about their axes, among others. Using DPH and DCVJ probes that are sensitive to rotational motions, we were able to measure changes in rotational lipid diffusion in the two membrane-associated states of pHLIP. We found that neither SA pHLIP nor TM pHLIP affected the rotational diffusion of the probes (**Fig. S14**). Importantly, the contrast between NSE and fluorescence results can be rationalized by taking into account the fundamental differences between rotational and translational lipid diffusion; i.e., the range of energy dissipation of their individual effects[69, 70]. For example, differences between translational and rotational diffusion have been previously reported in studies of membranes containing proteins and cholesterol[71–74]. In a 2D environment, the velocity field generated by rotation falls off as $1/r$, where r is the distance between two particles[69]. However, the

velocity field generated by translation decreases as $\log r$, indicating translational diffusion membrane effects are farther reaching than rotational diffusion effects, which are more local[69]. Since both fluorescent probes and pHLIP were used in relatively small amounts, the separation between the probes (DPH or DCVJ) and pHLIP may preclude the possibility of the molecular probes sensing the local influence of pHLIP on membrane viscosity – due to the rapid loss of energy propagation of rotational diffusion. Note that in the case of NSE, neutrons detect an ensemble average of all lipid motions within the time-resolution window, thus bridging the gap between the effect that pHLIP has on molecular motions and collective lipid membrane fluctuations.

These observations are in agreement with a recent study by Qiang, An and co-workers that reported the effects of pHLIP on POPC diffusion using ^{31}P ss-NMR[75]. Specifically, they probed pHLIP-induced dynamics in POPC vesicles and observed a reduction of the microsecond correlation time at acidic pH, compared to membranes at pH 7.4. Their results showed that on the microsecond timescale, the main contribution to motion is the lateral diffusion of lipids, which was slowed down in the presence of TM pHLIP. However, no changes were observed in the nanosecond correlation times that are associated with lipid uniaxial rotation and head group wobbling. Their results are thus consistent with our conclusions that TM pHLIP affects translational lipid diffusion to a greater extent than rotational diffusive motions. Of significance, our atomistic MD simulations show a >50% decrease in lateral diffusion of lipids for TM pHLIP systems compared to lipid-only systems on the microsecond timescale (**Fig. 4.1F**).

4.4.3 Lipid tails exhibit more snorkeling in the presence of TM pHLIP.

To better understand the molecular mechanism by which pHLIP increases membrane viscosity and slows down membrane thickness fluctuations, we used proton 2D ^1H - ^1H NOESY ssNMR spectroscopy. For example, ssNMR has been previously used to gain mechanistic information about the insertion of pHLIP into POPC membranes[76, 77]. A feature of fluid bilayers that is often overlooked is their acyl chain terminal methyl groups snorkeling to the membrane surface and their interaction with the lipid headgroups. Indeed, White and co-workers observed that

10% to 20% of the DOPC acyl chain methyl groups are kinked in such a way that they can be found in the vicinity of the choline headgroups. This is also evident from the atomistic MD simulations which show a distribution of $\text{CH}_3\text{-C}_\alpha$ distances (black line, **Fig. 4.3A**), as one would expect for *dynamic* snorkeling events. In comparison, the simulations with TM pHLIP showed a shift in the distribution to smaller distances indicating longer residence of the CH_3 groups near the lipid headgroups. More importantly, our probability distribution shows a peak at $\sim 4 \text{ \AA}$ indicating a statistical increase in the number of acyl chains that explore the lipid headgroup region (red line, **Fig. 4.3A**, consistent with ssNMR results (**Fig. 4.2**). This result implies a change in the conformational entropy of the lipid molecules in the vicinity of pHLIP, which increases the free space available to nearby lipids and enables their chains to explore a larger conformation space – consequently resulting in higher in-plane friction due to increased acyl chain entanglement and/or leaflet coupling.

Lipid tail snorkeling can thus explain why TM pHLIP reduces lateral lipid mobility (**Fig. 4.1C**), as irregularly shaped lipids can get "tangled", leading to increased friction[78, 79], in a way that is analogous to irregularly-shaped epithelial cells exhibiting reduced 2D mobility[80]. Additionally, lipid tails from the opposite monolayer can fill the space left by a snorkeled tail, increasing interleaflet coupling (**Fig. 4.3E**). Any combination of these two effects would cause an increase in membrane viscosity, which can result in a dampening of the thickness fluctuation rate.

4.5 Conclusion

We have shown that TM pHLIP suppresses the rate of thickness fluctuations through an "effective" increase of membrane viscosity, while surface-associated pHLIP had no such effect. SANS and SAXS measurements indicated that the effect on thickness fluctuations is not caused by changes to the average membrane thickness. We therefore propose that increased membrane viscosity is rather the result of altered acyl chain conformations, which restricts lateral lipid diffusion, causing an effective increase in membrane viscosity.

The current study also shows that a TM pHLIP can alter the rate of membrane thickness fluctuations. While pHLIP contains more polar residues than the average TM domain, multiple examples exist of proteins with TM regions enriched in polar, and even multiple charged residues (for example, the T cell receptor-CD3 complex[81]). Our results may also be instructive with regard to how rapidly fluctuating membranes can impact protein motions that occur on similar timescales[27, 32]. We therefore hypothesize the intriguing possibility that suppressing membrane thickness fluctuations may serve as a mechanism by which a membrane protein can affect nearby proteins without the need for protein-protein contact (effect at a distance). Slower membrane fluctuations may hinder protein motions, such as domain movements that might otherwise be facilitated by a more rapidly fluctuating membrane or prevent transient hydrophobic mismatch. Suppressing thickness fluctuations may additionally limit the occurrence of pore formation to allow the membrane to function as a semi-permeable barrier[20]. However, more studies are needed to unequivocally show that membrane thickness fluctuations are one mode of action in modulating protein activity.

Bibliography

- [1] Rob Phillips et al. “Emerging roles for lipids in shaping membrane-protein function”. en. In: *Nature* 459.7245 (May 2009), pp. 379–385. ISSN: 0028-0836, 1476-4687. DOI: [10.1038/nature08147](https://doi.org/10.1038/nature08147). URL: <http://www.nature.com/articles/nature08147> (visited on 08/02/2021).
- [2] Morten Ø. Jensen and Ole G. Mouritsen. “Lipids do influence protein function—the hydrophobic matching hypothesis revisited”. en. In: *Biochimica et Biophysica Acta (BBA) - Biomembranes* 1666.1-2 (Nov. 2004), pp. 205–226. ISSN: 00052736. DOI: [10.1016/j.bbamem.2004.06.009](https://doi.org/10.1016/j.bbamem.2004.06.009). URL: <https://linkinghub.elsevier.com/retrieve/pii/S0005273604001634> (visited on 08/02/2021).
- [3] E Perozo et al. “Physical principles underlying the transduction of bilayer deformation forces during mechanosensitive channel gating.” In: *Nat Struct Biol* 9 (Sept. 2002), pp. 696–703. DOI: [10.1038/nsb827](https://doi.org/10.1038/nsb827).
- [4] Michael F. Brown. “Soft Matter in Lipid–Protein Interactions”. In: *Annual Review of Biophysics* 46.1 (May 2017), pp. 379–410. DOI: <https://doi.org/10.1146/annurev-biophys-070816-033843>.
- [5] Sergei I. Sukharev et al. “Energetic and Spatial Parameters for Gating of the Bacterial Large Conductance Mechanosensitive Channel, MscL”. en. In: *Journal of General Physiology* 113.4 (Apr. 1999), pp. 525–540. ISSN: 0022-1295, 1540-7748. DOI: [10.1085/jgp.113.4.525](https://doi.org/10.1085/jgp.113.4.525). URL: <https://rupress.org/jgp/article/113/4/525/11040/Energetic-and-Spatial-Parameters-for-Gating-of-the> (visited on 08/02/2021).
- [6] Tristan Ursell et al. “Cooperative Gating and Spatial Organization of Membrane Proteins through Elastic Interactions”. en. In: *PLoS Computational Biology* 3.5 (May 2007). Ed. by Andrej Sali, e81. ISSN: 1553-7358. DOI:

- 10.1371/journal.pcbi.0030081. URL: <https://dx.plos.org/10.1371/journal.pcbi.0030081> (visited on 08/02/2021).
- [7] Michael F. Brown. “Modulation of rhodopsin function by properties of the membrane bilayer”. In: *Chemistry and Physics of Lipids* 73.1-2 (Sept. 1994), pp. 159–180. DOI: [https://doi.org/10.1016/0009-3084\(94\)90180-5](https://doi.org/10.1016/0009-3084(94)90180-5).
- [8] C. Hidalgo, D.D. Thomas, and N. Ikemoto. “Effect of the lipid environment on protein motion and enzymatic activity of sarcoplasmic reticulum calcium ATPase.” en. In: *Journal of Biological Chemistry* 253.19 (Oct. 1978), pp. 6879–6887. ISSN: 00219258. DOI: [10.1016/S0021-9258\(17\)38002-X](https://doi.org/10.1016/S0021-9258(17)38002-X). URL: <https://linkinghub.elsevier.com/retrieve/pii/S002192581738002X> (visited on 08/02/2021).
- [9] Olaf S. Andersen and Roger E. Koeppe. “Bilayer Thickness and Membrane Protein Function: An Energetic Perspective”. In: *Annual Review of Biophysics and Biomolecular Structure* 36.1 (June 2007), pp. 107–130. DOI: <https://doi.org/10.1146/annurev.biophys.36.040306.132643>.
- [10] E Lindahl and M Sansom. “Membrane proteins: molecular dynamics simulations”. en. In: *Current Opinion in Structural Biology* 18.4 (Aug. 2008), pp. 425–431. ISSN: 0959440X. DOI: [10.1016/j.sbi.2008.02.003](https://doi.org/10.1016/j.sbi.2008.02.003). URL: <https://linkinghub.elsevier.com/retrieve/pii/S0959440X08000304> (visited on 08/02/2021).
- [11] Jens A. Lundbæk et al. “Lipid bilayer regulation of membrane protein function: gramicidin channels as molecular force probes”. en. In: *Journal of The Royal Society Interface* 7.44 (Mar. 2010), pp. 373–395. ISSN: 1742-5689, 1742-5662. DOI: [10.1098/rsif.2009.0443](https://doi.org/10.1098/rsif.2009.0443). URL: <https://royalsocietypublishing.org/doi/10.1098/rsif.2009.0443> (visited on 08/02/2021).
- [12] G. Guidotti. “Membrane Proteins”. In: *Annual Review of Biochemistry* 41.1 (July 1972), pp. 731–752. DOI: <https://doi.org/10.1146/annurev.bi.41.070172.003503>.
- [13] A. D. Dupuy and D. M. Engelman. “Protein area occupancy at the center of the red blood cell membrane”. en. In: *Proceedings of the National Academy of Sciences* 105.8 (Feb. 2008), pp. 2848–2852. ISSN: 0027-8424, 1091-6490. DOI: [10.1073/pnas.0712379105](https://doi.org/10.1073/pnas.0712379105). URL: <http://www.pnas.org/cgi/doi/10.1073/pnas.0712379105> (visited on 08/02/2021).

- [14] Yana K. Reshetnyak et al. “A Monomeric Membrane Peptide that Lives in Three Worlds: In Solution, Attached to, and Inserted across Lipid Bilayers”. en. In: *Biophysical Journal* 93.7 (Oct. 2007), pp. 2363–2372. ISSN: 00063495. DOI: [10.1529/biophysj.107.109967](https://doi.org/10.1529/biophysj.107.109967). URL: <https://linkinghub.elsevier.com/retrieve/pii/S0006349507714911> (visited on 08/02/2021).
- [15] John C. Deacon, Donald M. Engelman, and Francisco N. Barrera. “Targeting acidity in diseased tissues: Mechanism and applications of the membrane-inserting peptide, pHLIP”. en. In: *Archives of Biochemistry and Biophysics* 565 (Jan. 2015), pp. 40–48. ISSN: 00039861. DOI: [10.1016/j.abb.2014.11.002](https://doi.org/10.1016/j.abb.2014.11.002). URL: <https://linkinghub.elsevier.com/retrieve/pii/S0003986114003841> (visited on 08/02/2021).
- [16] Haden L. Scott, Justin M. Westerfield, and Francisco N. Barrera. “Determination of the Membrane Translocation pK of the pH-Low Insertion Peptide”. en. In: *Biophysical Journal* 113.4 (Aug. 2017), pp. 869–879. ISSN: 00063495. DOI: [10.1016/j.bpj.2017.06.065](https://doi.org/10.1016/j.bpj.2017.06.065). URL: <https://linkinghub.elsevier.com/retrieve/pii/S0006349517307531> (visited on 08/02/2021).
- [17] Veronica Estrella et al. “Acidity Generated by the Tumor Microenvironment Drives Local Invasion”. en. In: *Cancer Research* 73.5 (Mar. 2013), pp. 1524–1535. ISSN: 0008-5472, 1538-7445. DOI: [10.1158/0008-5472.CAN-12-2796](https://doi.org/10.1158/0008-5472.CAN-12-2796). URL: <http://cancerres.aacrjournals.org/lookup/doi/10.1158/0008-5472.CAN-12-2796> (visited on 08/02/2021).
- [18] Christopher J. Cheng et al. “MicroRNA silencing for cancer therapy targeted to the tumour microenvironment”. en. In: *Nature* 518.7537 (Feb. 2015), pp. 107–110. ISSN: 0028-0836, 1476-4687. DOI: [10.1038/nature13905](https://doi.org/10.1038/nature13905). URL: <http://www.nature.com/articles/nature13905> (visited on 08/02/2021).
- [19] M. An et al. “pH-(low)-insertion-peptide (pHLIP) translocation of membrane impermeable phalloidin toxin inhibits cancer cell proliferation”. en. In: *Proceedings of the National Academy of Sciences* 107.47 (Nov. 2010), pp. 20246–20250. ISSN: 0027-8424, 1091-6490. DOI: [10.1073/pnas.1014403107](https://doi.org/10.1073/pnas.1014403107). URL: <http://www.pnas.org/cgi/doi/10.1073/pnas.1014403107> (visited on 08/02/2021).
- [20] Liviu Movileanu et al. “Transbilayer Pores Induced by Thickness Fluctuations”. In: *Bulletin of Mathematical Biology* 68 (Apr. 2006), pp. 1231–1255. DOI: <https://doi.org/10.1007/s11538-006-9069-9>.

- [21] Maikel C Rheinstädter. “Collective molecular dynamics in proteins and membranes (Review)”. In: *Biointerphases* 3.2 (June 2008), FB83. DOI: [10.1116/1.3007992](https://doi.org/10.1116/1.3007992).
- [22] Patricia Bassereau, Benoit Sorre, and Aurore Lévy. “Bending lipid membranes: Experiments after W. Helfrich’s model”. en. In: *Advances in Colloid and Interface Science* 208 (June 2014), pp. 47–57. ISSN: 00018686. DOI: [10.1016/j.cis.2014.02.002](https://doi.org/10.1016/j.cis.2014.02.002). URL: <https://linkinghub.elsevier.com/retrieve/pii/S0001868614000360> (visited on 08/02/2021).
- [23] W Helfrich. “Elastic Properties of Lipid Bilayers: Theory and Possible Experiments”. en. In: *Zeitschrift für Naturforschung C* 28.11-12 (Dec. 1973), pp. 693–703. ISSN: 1865-7125, 0939-5075. DOI: [10.1515/znc-1973-11-1209](https://doi.org/10.1515/znc-1973-11-1209). URL: <https://www.degruyter.com/document/doi/10.1515/znc-1973-11-1209/html> (visited on 08/02/2021).
- [24] Michihiro Nagao. “Observation of local thickness fluctuations in surfactant membranes using neutron spin echo”. In: *Phys. Rev. E* 80.3 Pt1 (), p. 031606.
- [25] S.B. Hladky and D.W. Gruen. “Thickness fluctuations in black lipid membranes”. en. In: *Biophysical Journal* 38.3 (June 1982), pp. 251–258. ISSN: 00063495. DOI: [10.1016/S0006-3495\(82\)84556-6](https://doi.org/10.1016/S0006-3495(82)84556-6). URL: <https://linkinghub.elsevier.com/retrieve/pii/S0006349582845566> (visited on 08/02/2021).
- [26] Andrea C. Woodka et al. “Lipid Bilayers and Membrane Dynamics: Insight into Thickness Fluctuations”. In: *Phys. Rev. Letters* 109 (July 2012), p. 058102.
- [27] Rana Ashkar et al. “Tuning Membrane Thickness Fluctuations in Model Lipid Bilayers”. en. In: *Biophysical Journal* 109.1 (July 2015), pp. 106–112. ISSN: 00063495. DOI: [10.1016/j.bpj.2015.05.033](https://doi.org/10.1016/j.bpj.2015.05.033). URL: <https://linkinghub.elsevier.com/retrieve/pii/S0006349515005457> (visited on 08/02/2021).
- [28] Michihiro Nagao et al. “Probing Elastic and Viscous Properties of Phospholipid Bilayers Using Neutron Spin Echo Spectroscopy”. en. In: *The Journal of Physical Chemistry Letters* 8.19 (Oct. 2017), pp. 4679–4684. ISSN: 1948-7185. DOI: [10.1021/acs.jpcllett.7b01830](https://doi.org/10.1021/acs.jpcllett.7b01830). URL: <https://pubs.acs.org/doi/10.1021/acs.jpcllett.7b01830> (visited on 08/02/2021).

- [29] F Mezei. “Neutron spin echo: A new concept in polarized thermal neutron techniques”. In: *Zeitschrift für a Hadrons and nuclei* 255 (1972), pp. 146–160. DOI: <https://doi.org/10.1007/BF01394523>.
- [30] Rana Ashkar et al. “Neutron scattering in the biological sciences: progress and prospects.” In: *Acta Crystallographica Section* 74.12 (2018), pp. 1129–1168.
- [31] R. J. Bingham, S. W. Smye, and P. D. Olmsted. “Dynamics of an asymmetric bilayer lipid membrane in a viscous solvent”. en. In: *EPL (Europhysics Letters)* 111.1 (July 2015), p. 18004. ISSN: 0295-5075, 1286-4854. DOI: [10.1209/0295-5075/111/18004](https://doi.org/10.1209/0295-5075/111/18004). URL: <https://iopscience.iop.org/article/10.1209/0295-5075/111/18004> (visited on 08/02/2021).
- [32] Zheng Yi, Michihiro Nagao, and Dobrin P Bossev. “Bending elasticity of saturated and monounsaturated phospholipid membranes studied by the neutron spin echo technique”. en. In: *Journal of Physics: Condensed Matter* 21.15 (Apr. 2009), p. 155104. ISSN: 0953-8984, 1361-648X. DOI: [10.1088/0953-8984/21/15/155104](https://doi.org/10.1088/0953-8984/21/15/155104). URL: <https://iopscience.iop.org/article/10.1088/0953-8984/21/15/155104> (visited on 08/02/2021).
- [33] Saptarshi Chakraborty et al. “How cholesterol stiffens unsaturated lipid membranes”. en. In: *Proceedings of the National Academy of Sciences* 117.36 (Sept. 2020), pp. 21896–21905. ISSN: 0027-8424, 1091-6490. DOI: [10.1073/pnas.2004807117](https://doi.org/10.1073/pnas.2004807117). URL: <http://www.pnas.org/lookup/doi/10.1073/pnas.2004807117> (visited on 08/02/2021).
- [34] F. N. Barrera, J. Fendos, and D. M. Engelman. “Membrane physical properties influence transmembrane helix formation”. en. In: *Proceedings of the National Academy of Sciences* 109.36 (Sept. 2012), pp. 14422–14427. ISSN: 0027-8424, 1091-6490. DOI: [10.1073/pnas.1212665109](https://doi.org/10.1073/pnas.1212665109). URL: <http://www.pnas.org/cgi/doi/10.1073/pnas.1212665109> (visited on 08/02/2021).
- [35] Jan-Michael Y. Carrillo et al. “A Computational Approach for Modeling Neutron Scattering Data from Lipid Bilayers”. en. In: *Journal of Chemical Theory and Computation* 13.2 (Feb. 2017), pp. 916–925. ISSN: 1549-9618, 1549-9626. DOI: [10.1021/acs.jctc.6b00968](https://doi.org/10.1021/acs.jctc.6b00968). URL: <https://pubs.acs.org/doi/10.1021/acs.jctc.6b00968> (visited on 08/02/2021).

- [36] Norbert Kučerka et al. “Curvature Effect on the Structure of Phospholipid Bilayers”. en. In: *Langmuir* 23.3 (Jan. 2007), pp. 1292–1299. ISSN: 0743-7463, 1520-5827. DOI: [10.1021/la062455t](https://doi.org/10.1021/la062455t). URL: <https://pubs.acs.org/doi/10.1021/la062455t> (visited on 08/02/2021).
- [37] Haden L. Scott et al. “On the Mechanism of Bilayer Separation by Extrusion, or Why Your LUVs Are Not Really Unilamellar”. en. In: *Biophysical Journal* 117.8 (Oct. 2019), pp. 1381–1386. ISSN: 00063495. DOI: [10.1016/j.bpj.2019.09.006](https://doi.org/10.1016/j.bpj.2019.09.006). URL: <https://linkinghub.elsevier.com/retrieve/pii/S0006349519307805> (visited on 08/02/2021).
- [38] Francisco N. Barrera et al. “Roles of Carboxyl Groups in the Transmembrane Insertion of Peptides”. en. In: *Journal of Molecular Biology* 413.2 (Oct. 2011), pp. 359–371. ISSN: 00222836. DOI: [10.1016/j.jmb.2011.08.010](https://doi.org/10.1016/j.jmb.2011.08.010). URL: <https://linkinghub.elsevier.com/retrieve/pii/S0022283611008771> (visited on 03/18/2021).
- [39] Haden L. Scott et al. “The Negative Charge of the Membrane Has Opposite Effects on the Membrane Entry and Exit of pH-Low Insertion Peptide”. en. In: *Biochemistry* 54.9 (Mar. 2015), pp. 1709–1712. ISSN: 0006-2960, 1520-4995. DOI: [10.1021/acs.biochem.5b00069](https://doi.org/10.1021/acs.biochem.5b00069). URL: <https://pubs.acs.org/doi/10.1021/acs.biochem.5b00069> (visited on 03/18/2021).
- [40] AG Zilman and R Granek. “Undulations and Dynamic Structure Factor of Membranes”. In: *Phys. Rev. Letters* 77.23 (Dec. 1996), pp. 4788–4791. DOI: [10.1103/PhysRevLett.77.4788](https://doi.org/10.1103/PhysRevLett.77.4788).
- [41] Max C. Watson and Frank L.H. Brown. “Interpreting Membrane Scattering Experiments at the Mesoscale: The Contribution of Dissipation within the Bilayer”. en. In: *Biophysical Journal* 98.6 (Mar. 2010), pp. L9–L11. ISSN: 00063495. DOI: [10.1016/j.bpj.2009.11.026](https://doi.org/10.1016/j.bpj.2009.11.026). URL: <https://linkinghub.elsevier.com/retrieve/pii/S000634950901755X> (visited on 08/02/2021).
- [42] E.G. Kelley, P.D. Butler, and M Nagao. *Collective Dynamics in Model Biological Membranes Measured by Neutron Spin Echo Spectroscopy*. In Characterization of Biological Membranes. Boston, MA: Walter de Gruyter, Inc., Boston, MA, 2019.

- [43] Mohan Babu Boggara, Antonio Faraone, and Ramanan Krishnamoorti. “Effect of pH and Ibuprofen on the Phospholipid Bilayer Bending Modulus”. en. In: *The Journal of Physical Chemistry B* 114.24 (June 2010), pp. 8061–8066. ISSN: 1520-6106, 1520-5207. DOI: [10.1021/jp100494n](https://doi.org/10.1021/jp100494n). URL: <https://pubs.acs.org/doi/10.1021/jp100494n> (visited on 08/02/2021).
- [44] W. Rawicz et al. “Effect of Chain Length and Unsaturation on Elasticity of Lipid Bilayers”. en. In: *Biophysical Journal* 79.1 (July 2000), pp. 328–339. ISSN: 00063495. DOI: [10.1016/S0006-3495\(00\)76295-3](https://doi.org/10.1016/S0006-3495(00)76295-3). URL: <https://linkinghub.elsevier.com/retrieve/pii/S0006349500762953> (visited on 08/02/2021).
- [45] Milka Doktorova et al. “A New Computational Method for Membrane Compressibility: Bilayer Mechanical Thickness Revisited”. en. In: *Biophysical Journal* 116.3 (Feb. 2019), pp. 487–502. ISSN: 00063495. DOI: [10.1016/j.bpj.2018.12.016](https://doi.org/10.1016/j.bpj.2018.12.016). URL: <https://linkinghub.elsevier.com/retrieve/pii/S0006349518345302> (visited on 08/02/2021).
- [46] U Seifert and S. A Langer. “Viscous Modes of Fluid Bilayer Membranes”. en. In: *Europhysics Letters (EPL)* 23.1 (July 1993), pp. 71–76. ISSN: 0295-5075, 1286-4854. DOI: [10.1209/0295-5075/23/1/012](https://doi.org/10.1209/0295-5075/23/1/012). URL: <https://iopscience.iop.org/article/10.1209/0295-5075/23/1/012> (visited on 08/02/2021).
- [47] Chun En Kung and Jutta K. Reed. “Microviscosity measurements of phospholipid bilayers using fluorescent dyes that undergo torsional relaxation”. en. In: *Biochemistry* 25.20 (Oct. 1986), pp. 6114–6121. ISSN: 0006-2960, 1520-4995. DOI: [10.1021/bi00368a042](https://doi.org/10.1021/bi00368a042). URL: <https://pubs.acs.org/doi/abs/10.1021/bi00368a042> (visited on 08/02/2021).
- [48] J. R. Lakowicz. *Principles of Fluorescence Spectroscopy*. 2nd. New York: Kluwer Academic/Plenum, 1999.
- [49] O.G. Mouritsen and M. Bloom. “Mattress model of lipid-protein interactions in membranes”. en. In: *Biophysical Journal* 46.2 (Aug. 1984), pp. 141–153. ISSN: 00063495. DOI: [10.1016/S0006-3495\(84\)84007-2](https://doi.org/10.1016/S0006-3495(84)84007-2). URL: <https://linkinghub.elsevier.com/retrieve/pii/S0006349584840072> (visited on 08/02/2021).
- [50] Frederick A. Herberle et al. “Model-based approaches for the determination of lipid bilayer structure from small-angle neutron and X-ray scattering data”. In: *European Biophysics Journal* 41 (2012), pp. 875–890.

- [51] Norbert Kučerka et al. “Lipid Bilayer Structure Determined by the Simultaneous Analysis of Neutron and X-Ray Scattering Data”. en. In: *Biophysical Journal* 95.5 (Sept. 2008), pp. 2356–2367. ISSN: 00063495. DOI: [10.1529/biophysj.108.132662](https://doi.org/10.1529/biophysj.108.132662). URL: <https://linkinghub.elsevier.com/retrieve/pii/S0006349508783838> (visited on 08/02/2021).
- [52] Norbert Kučerka, Mu-Ping Nieh, and John Katsaras. “Fluid phase lipid areas and bilayer thicknesses of commonly used phosphatidylcholines as a function of temperature”. en. In: *Biochimica et Biophysica Acta (BBA) - Biomembranes* 1808.11 (Nov. 2011), pp. 2761–2771. ISSN: 00052736. DOI: [10.1016/j.bbamem.2011.07.022](https://doi.org/10.1016/j.bbamem.2011.07.022). URL: <https://linkinghub.elsevier.com/retrieve/pii/S0005273611002276> (visited on 08/02/2021).
- [53] Theyencheri Narayanan et al. “pHLIP Peptide Interaction with a Membrane Monitored by SAXS”. en. In: *The Journal of Physical Chemistry B* 120.44 (Nov. 2016), pp. 11484–11491. ISSN: 1520-6106, 1520-5207. DOI: [10.1021/acs.jpccb.6b06643](https://doi.org/10.1021/acs.jpccb.6b06643). URL: <https://pubs.acs.org/doi/10.1021/acs.jpccb.6b06643> (visited on 03/18/2021).
- [54] Elizabeth G. Kelley et al. “Scaling relationships for the elastic moduli and viscosity of mixed lipid membranes”. en. In: *Proceedings of the National Academy of Sciences* 117.38 (Sept. 2020), pp. 23365–23373. ISSN: 0027-8424, 1091-6490. DOI: [10.1073/pnas.2008789117](https://doi.org/10.1073/pnas.2008789117). URL: <http://www.pnas.org/lookup/doi/10.1073/pnas.2008789117> (visited on 08/02/2021).
- [55] Daniel Huster, Klaus Arnold, and Klaus Gawrisch. “Investigation of Lipid Organization in Biological Membranes by Two-Dimensional Nuclear Overhauser Enhancement Spectroscopy”. en. In: *The Journal of Physical Chemistry B* 103.1 (Jan. 1999), pp. 243–251. ISSN: 1520-6106, 1520-5207. DOI: [10.1021/jp983428h](https://doi.org/10.1021/jp983428h). URL: <https://pubs.acs.org/doi/10.1021/jp983428h> (visited on 08/02/2021).
- [56] M. Mihailescu et al. “Acyl-chain methyl distributions of liquid-ordered and -disordered membranes.” In: *Biophysical Journal* 100.6 (2011), pp. 1455–1462.
- [57] O. A. Andreev et al. “Mechanism and uses of a membrane peptide that targets tumors and other acidic tissues in vivo”. en. In: *Proceedings of the National Academy of Sciences* 104.19 (May 2007), pp. 7893–7898. ISSN: 0027-8424, 1091-6490. DOI: [10.1073/pnas.0702439104](https://doi.org/10.1073/pnas.0702439104). URL: <http://www.pnas.org/cgi/doi/10.1073/pnas.0702439104> (visited on 08/02/2021).

- [58] Oleg A. Andreev, Donald M. Engelman, and Yana K. Reshetnyak. “pH-sensitive membrane peptides (pHLIPs) as a novel class of delivery agents”. en. In: *Molecular Membrane Biology* 27.7 (Oct. 2010), pp. 341–352. ISSN: 0968-7688, 1464-5203. DOI: [10.3109/09687688.2010.509285](https://doi.org/10.3109/09687688.2010.509285). URL: <http://www.tandfonline.com/doi/full/10.3109/09687688.2010.509285> (visited on 08/02/2021).
- [59] Justin Westerfield et al. “Ions Modulate Key Interactions between pHLIP and Lipid Membranes”. en. In: *Biophysical Journal* 117.5 (Sept. 2019), pp. 920–929. ISSN: 00063495. DOI: [10.1016/j.bpj.2019.07.034](https://doi.org/10.1016/j.bpj.2019.07.034). URL: <https://linkinghub.elsevier.com/retrieve/pii/S000634951930623X> (visited on 08/02/2021).
- [60] John F. Hunt et al. “Spontaneous, pH-Dependent Membrane Insertion of a Transbilayer α -Helix”. In: *Biochemistry* 36.49 (Dec. 1997), pp. 15177–15192. ISSN: 0006-2960. DOI: [10.1021/bi970147b](https://doi.org/10.1021/bi970147b).
- [61] Haden L. Scott et al. “Phosphatidylserine Asymmetry Promotes the Membrane Insertion of a Transmembrane Helix”. en. In: *Biophysical Journal* 116.8 (Apr. 2019), pp. 1495–1506. ISSN: 00063495. DOI: [10.1016/j.bpj.2019.03.003](https://doi.org/10.1016/j.bpj.2019.03.003). URL: <https://linkinghub.elsevier.com/retrieve/pii/S0006349519301894> (visited on 03/18/2021).
- [62] Rebecca D. Utery et al. “Membrane Bending Moduli of Coexisting Liquid Phases Containing Transmembrane Peptide”. en. In: *Biophysical Journal* 114.9 (May 2018), pp. 2152–2164. ISSN: 00063495. DOI: [10.1016/j.bpj.2018.03.026](https://doi.org/10.1016/j.bpj.2018.03.026). URL: <https://linkinghub.elsevier.com/retrieve/pii/S0006349518303953> (visited on 08/04/2021).
- [63] Andrea Holt and J. Antoinette Killian. “Orientation and dynamics of transmembrane peptides: the power of simple models”. en. In: *European Biophysics Journal* 39.4 (Mar. 2010), pp. 609–621. ISSN: 0175-7571, 1432-1017. DOI: [10.1007/s00249-009-0567-1](https://doi.org/10.1007/s00249-009-0567-1). URL: <http://link.springer.com/10.1007/s00249-009-0567-1> (visited on 08/02/2021).
- [64] Maurits R. R. de Planque et al. “Influence of Lipid/Peptide Hydrophobic Mismatch on the Thickness of Diacylphosphatidylcholine Bilayers. A 2H NMR and ESR Study Using Designed Transmembrane R-Helical Peptides and Gramicidin A”. In: *Biochemistry* 37 (1998), pp. 9333–9345.
- [65] Osman Kahraman et al. “Bilayer-thickness-mediated interactions between integral membrane proteins”. In: *Phys. Rev. E* 93.4 (Apr. 2016), p. 042410.

- [66] J Antoinette Killian and Thomas KM Nyholm. “Peptides in lipid bilayers: the power of simple models”. en. In: *Current Opinion in Structural Biology* 16.4 (Aug. 2006), pp. 473–479. ISSN: 0959440X. DOI: [10.1016/j.sbi.2006.06.007](https://doi.org/10.1016/j.sbi.2006.06.007). URL: <https://linkinghub.elsevier.com/retrieve/pii/S0959440X06001114> (visited on 08/02/2021).
- [67] P Shchelokovskyy, S Tristram-Nagle, and R Dimova. “Effect of the HIV-1 fusion peptide on the mechanical properties and leaflet coupling of lipid bilayers”. en. In: *New Journal of Physics* 13.2 (Feb. 2011), p. 025004. ISSN: 1367-2630. DOI: [10.1088/1367-2630/13/2/025004](https://doi.org/10.1088/1367-2630/13/2/025004). URL: <https://iopscience.iop.org/article/10.1088/1367-2630/13/2/025004> (visited on 08/02/2021).
- [68] Hatsuho Usuda et al. “Interleaflet coupling of n-alkane incorporated bilayers.” In: *Physical Chemistry Chemical Physics* 22 (2020), pp. 5418–5426.
- [69] P. G. Saffman and M. Delbruck. “Brownian motion in biological membranes.” en. In: *Proceedings of the National Academy of Sciences* 72.8 (Aug. 1975), pp. 3111–3113. ISSN: 0027-8424, 1091-6490. DOI: [10.1073/pnas.72.8.3111](https://doi.org/10.1073/pnas.72.8.3111). URL: <http://www.pnas.org/cgi/doi/10.1073/pnas.72.8.3111> (visited on 08/02/2021).
- [70] P. G. Saffman. “Brownian motion in thin sheets of viscous fluid”. In: *Journal of Fluid Mechanics* 73.4 (Feb. 1976), pp. 593–602. DOI: <https://doi.org/10.1017/S0022112076001511>.
- [71] Tristan T. Hormel et al. “Measuring Lipid Membrane Viscosity Using Rotational and Translational Probe Diffusion”. In: *Phys. Rev. Letters* 112 (May 2014), p. 188101.
- [72] Andrey Filippov, Greger Orädd, and Göran Lindblom. “The Effect of Cholesterol on the Lateral Diffusion of Phospholipids in Oriented Bilayers”. en. In: *Biophysical Journal* 84.5 (May 2003), pp. 3079–3086. ISSN: 00063495. DOI: [10.1016/S0006-3495\(03\)70033-2](https://doi.org/10.1016/S0006-3495(03)70033-2). URL: <https://linkinghub.elsevier.com/retrieve/pii/S0006349503700332> (visited on 08/02/2021).
- [73] Katrin K. Halling et al. “Cholesterol Interactions with Fluid-Phase Phospholipids: Effect on the Lateral Organization of the Bilayer”. en. In: *Biophysical Journal* 95.8 (Oct. 2008), pp. 3861–3871. ISSN: 00063495. DOI: [10.1529/biophysj.108.133744](https://doi.org/10.1529/biophysj.108.133744). URL: <https://linkinghub.elsevier.com/retrieve/pii/S0006349508785254> (visited on 08/02/2021).

- [74] Omar Bakht, Priyadarshini Pathak, and Erwin London. “Effect of the Structure of Lipids Favoring Disordered Domain Formation on the Stability of Cholesterol-Containing Ordered Domains (Lipid Rafts): Identification of Multiple Raft-Stabilization Mechanisms”. en. In: *Biophysical Journal* 93.12 (Dec. 2007), pp. 4307–4318. ISSN: 00063495. DOI: [10.1529/biophysj.107.114967](https://doi.org/10.1529/biophysj.107.114967). URL: <https://linkinghub.elsevier.com/retrieve/pii/S0006349507716831> (visited on 08/02/2021).
- [75] Sarah A. Otieno et al. “pH-dependent thermodynamic intermediates of pHLIP membrane insertion determined by solid-state NMR spectroscopy”. en. In: *Proceedings of the National Academy of Sciences* 115.48 (Nov. 2018), pp. 12194–12199. ISSN: 0027-8424, 1091-6490. DOI: [10.1073/pnas.1809190115](https://doi.org/10.1073/pnas.1809190115). URL: <http://www.pnas.org/lookup/doi/10.1073/pnas.1809190115> (visited on 03/18/2021).
- [76] Samuel Z. Hanz et al. “Protonation-Driven Membrane Insertion of a pH-Low Insertion Peptide”. ENG. In: *Angewandte Chemie (International Ed. in English)* 55.40 (Sept. 2016), pp. 12376–12381. ISSN: 1521-3773. DOI: [10.1002/anie.201605203](https://doi.org/10.1002/anie.201605203).
- [77] Nicolas S. Shu et al. “Residue-specific structures and membrane locations of pH-low insertion peptide by solid-state nuclear magnetic resonance”. en. In: *Nature Communications* 6.1 (Nov. 2015), p. 7787. ISSN: 2041-1723. DOI: [10.1038/ncomms8787](https://doi.org/10.1038/ncomms8787). URL: <http://www.nature.com/articles/ncomms8787> (visited on 03/18/2021).
- [78] Jirasak Wong-ekkabut et al. “Effect of Lipid Peroxidation on the Properties of Lipid Bilayers: A Molecular Dynamics Study”. en. In: *Biophysical Journal* 93.12 (Dec. 2007), pp. 4225–4236. ISSN: 00063495. DOI: [10.1529/biophysj.107.112565](https://doi.org/10.1529/biophysj.107.112565). URL: <https://linkinghub.elsevier.com/retrieve/pii/S0006349507716752> (visited on 08/02/2021).
- [79] Hari S. Muddana et al. “Atomistic simulation of lipid and DiI dynamics in membrane bilayers under tension”. en. In: *Phys. Chem. Chem. Phys.* 13.4 (2011), pp. 1368–1378. ISSN: 1463-9076, 1463-9084. DOI: [10.1039/C0CP00430H](https://doi.org/10.1039/C0CP00430H). URL: <http://xlink.rsc.org/?DOI=C0CP00430H> (visited on 08/02/2021).

- [80] Jin-Ah Park et al. “Unjamming and cell shape in the asthmatic airway epithelium”. en. In: *Nature Materials* 14.10 (Oct. 2015), pp. 1040–1048. ISSN: 1476-1122, 1476-4660. DOI: [10.1038/nmat4357](https://doi.org/10.1038/nmat4357). URL: <http://www.nature.com/articles/nmat4357> (visited on 08/02/2021).
- [81] De Dong et al. “Structural basis of assembly of the human T cell receptor–CD3 complex”. en. In: *Nature* 573.7775 (Sept. 2019), pp. 546–552. ISSN: 0028-0836, 1476-4687. DOI: [10.1038/s41586-019-1537-0](https://doi.org/10.1038/s41586-019-1537-0). URL: <http://www.nature.com/articles/s41586-019-1537-0> (visited on 08/02/2021).

Chapters/chapterIV

Chapter 5

Understanding the effects of salt concentration on state I of pHLIP

5.1 Abstract

The pH Low Insertion Peptide (pHLIP) is a membrane-active peptide that has gained interest in recent years due to its potential for biological applications. pHLIP can be found in 3 distinctive states: coiled in solution (state I), bound to membrane surface (state II) and inserted into a lipid bilayer as a transmembrane helix under acidic conditions (state III). While the mechanism of insertion and exit of the peptide have been thoroughly studied, the biophysical properties that govern state I of the peptide remain unclear. In this study, we make use of molecular dynamics (MD) simulations to mimic protonated and deprotonated pHLIP in state I at NaCl concentration ranging between 0 and 150 mM. Our results show that changes in NaCl only affect deprotonated pHLIP while leaving protonated counterpart unaffected. Specifically, rise in NaCl increases helicity of N-terminus of deprotonated pHLIP and expands the motion range of the peptide at high concentrations, while maintaining protonated pHLIP mostly coiled and clustered. Finally, calculation of native contacts of the peptide show increased number of contacts found for deprotonated systems and longer contact times, as compared to protonated. We hope that our results will aid the search for new approaches towards the study of this state of pHLIP and bring us a step closer towards utilizing it for clinical applications.

5.2 Introduction

Membrane-active peptides (MAPs) are a family of peptides characterized by their ability to fold and insert into lipid bilayers[1–3]. These attributes make them of interest due to their potential for biomedical applications[4–6]. MAPs behave like intrinsically disordered proteins, typically aggregating in solution at above micromolar concentrations[4, 7].

The pH Low Insertion Peptide (pHLIP) is a membrane-active peptide that has shown potential in biomedical applications for diseases characterized by acidosis[8, 9]. pHLIP has been of special interest for early detection and targeted drug delivery in cancer[10, 11], due to its ability to spontaneously fold and insert into a lipid bilayer under acidic conditions[12, 13]. pHLIP exists in three states: as an unstructured peptide in solution (state I), bound to the membrane surface at neutral pH (state II) and inserted as a transmembrane helix at low pH, via protonation of its acidic residues[13, 14]. Although the general mechanism of pHLIP has been characterized, the specific intramolecular interactions that dictate pHLIP’s behavior in solution remain poorly understood. *In vivo* and *in vitro* studies are hindered by aggregation properties of the peptide at concentrations above 8 μ M[15], which is below the effective threshold of the peptide for clinical applications. Circular dichroism (CD) spectroscopy has shown that pHLIP remains mostly unstructured in solution[14], however, computational studies have shown that pHLIP transiently samples secondary structural conformations[16–18]. Without fundamental understanding of pHLIP’s behavior in solution, clinical applications of pHLIP remain hindered, hence the need for further studies.

In this project, we used of equilibrium molecular dynamics (MD) simulations to characterize the effects of salt concentration on fully protonated and fully deprotonated pHLIP (**Fig.5.1 table 5.1**). By changing the concentration of salt and protonation state, we were able to observe the direct effect it has on the peptide. Our results show that the effect of salt concentration is directly linked to the protonation state of pHLIP. Specifically, we observe differences in the behavior between fully protonated and fully deprotonated pHLIP when both system have the same salt concentration, while pHLIP remains mostly insensitive towards changes in salt concentration when compared within the same protonation state.

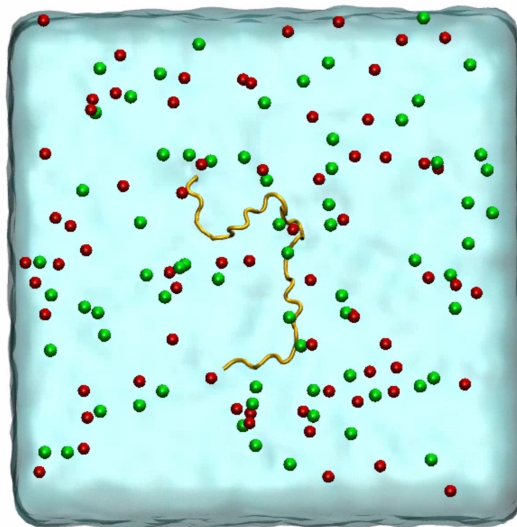


FIGURE 5.1: **pHLIP in state I**. pHLIP is represented as coil (*yellow*), surrounded by Na⁺ (*red*) and Cl⁻ (*green*) ions, and solvated in a water box.

5.3 Computational Methods

Bacteriorhodopsin (PDB 1FBB) was used to obtain initial coordinates of pHLIP (GGEQNPIYWARYADWLFTTPLLDDLALLVDADEGT) via selection of residues 72 to 107 in combination with mutation of residue 105 from Gln to Glu using the Visual Molecular Dynamics (VMD) software[19]. pHLIP was solvated at NaCl concentrations ranging from 0 mM to 150 mM via tleap, a module in AmberTools that uses initial coordinate files and AMBER force fields[20–23] to generate topology and coordinate files for the system(**Table 5.1**).

label	protonated residues	NaCl concentration /mM
dpt_0mM	none	0
dpt_20mM	none	20
dpt_50mM	none	50
dpt_100mM	none	100
dpt_150mM	none	150
prt_0mM	E3, D14, D25, D31, D33, E34	0
prt_20mM	E3, D14, D25, D31, D33, E34	20
prt_50mM	E3, D14, D25, D31, D33, E34	50
prt_100mM	E3, D14, D25, D31, D33, E34	100
prt_150mM	E3, D14, D25, D31, D33, E34	150

TABLE 5.1: List of states of pHLIP and salt concentrations in this study.

5.3.1 MD simulations

Systems were minimized and heated to 310 K for 40 ps at 2 fs timestep using Langevin dynamics thermostat to control temperature and isotropic pressure coupling, using the sander version of AMBER[23]. Following heating, the sets were equilibrated twice: 100 ps at 2 fs timestep and NVT ensemble ($T = 310$ K, constant volume), in order to let system adjust and set ideal periodic boundaries; and a further 100 ps at 2 fs timestep and NPT ensemble ($T = 310$ K, $P = 1$ atm) to let the water adjust to optimal density. Both equilibrations were performed using the sander version of AMBER. Production runs for each NaCl concentration were performed in triplet in the GPU version of pmemd in AMBER18[23, 24], for an aggregate time of 3 μ s each, with a 2 fs timestep and using the semi-isotropic pressure coupling. All runs has a 8 Å cutoff for non-bonded forces, as prescribed for Amber force fields.

5.3.2 Analysis

Analysis was performed using cpptraj in AmberTools[23], LOOS[25], pymol[26] and in-house scripts. Matplotlib[27] and gnuplot[28] were used to plot data.

5.4 Results and Discussion

5.4.1 Salt concentration affects helicity of N-terminus.

Previous studies have shown that pHLIP can sample a wide range of structures, from maintaining coiled conformation[29, 30]. to adopting structures with various percentages of helical content[16, 17, 31]. Particularly, the pHLIP variant P20G is known for having higher percentage of helical conformation in solution when compared to wild-type(WT) pHLIP, an attribute that increases pKa of insertion of the peptide, thus speeding up the process[32]. Helical content of the peptide in solution influences the insertion kinetics[33, 34], and thus the need for further investigation.

With this in mind, we performed helical content analysis of deprotonated and protonated WT-pHLIP at NaCl concentrations ranging from 0-150 mM to assess

how it affects the secondary structure of the peptide. To do this, we used the Ramachandran tool from LOOS[25], which determines the secondary structure of the peptide by calculating the angles formed between every 3 consecutive residues (Fig 5.2).

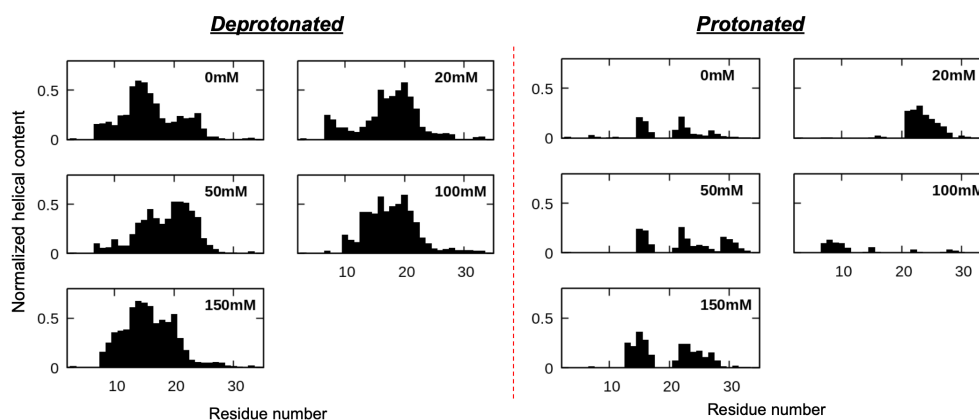


FIGURE 5.2: **Deprotonation of all acidic residues leads to high helical content.** *Left:* Per residue helical content for fully deprotonated pHLIP as a function of the salt concentration for deprotonated pHLIP. *Right:* Per residue helical content of protonated pHLIP as a function of salt concentration.

Our results suggest that the NaCl produces a shift in the helical content of deprotonated pHLIP. Specifically, the N-terminus of deprotonated pHLIP shows increase in helical content to around 45-60% for all N-terminus residues at high salt concentrations (100mM and 150mM), consistent with recent computational studies[17], while the C-terminus remains largely coiled. C-terminus lack of helicity of deprotonated pHLIP is consistent with results reported from a CD, fluorescence spectroscopy and all-atoms computational collaboration of state II pHLIP, in which they determined that helicity of C-terminus was hindered by increasing NaCl concentrations due to clustering of Na⁺ ions around acidic residues of C-terminus[35], disrupting protonation. Interestingly, protonated pHLIP remains highly unstructured throughout, suggesting that folding of the peptide is not only dependent on pH or salt, respectively, but a collective process involving lipid-peptide interactions and pH changes[32]. In addition, higher overall percentage of helicity is found in deprotonated systems compared to protonated ones. These results could be due to interactions between pHLIP residues in an attempt to stabilize the peptide, however further research into this phenomena needs to be performed.

5.4.2 Deprotonated pHLIP expands as a function of salt concentration.

IDPs are able to sample a wide range of conformational structures due to their fast dynamics and flexibility, and different types of conformations have an effect on the functionality of the peptide[36]. Conformationally packed secondary structures, such as helices, restrain movements along the peptide due to hydrogen bonding between residues, while unstructured systems have higher flexibility and fast paced dynamics that allow them to expand and contract freely. In order to further investigate the effects of salt on pHLIP’s conformation, we performed measurements of the radius of gyration of the peptide and the distance between residues 1 and 36 (**Fig 5.3**), using cpptraj commands, an AmberTools software[23]. Radius of gyration (RoG) has been used throughout the years as a means to detect conformational changes in biomolecules[37–39], hence is a useful tool that allows us to investigate possible changes in pHLIP’s secondary structure as a function of salt concentration.

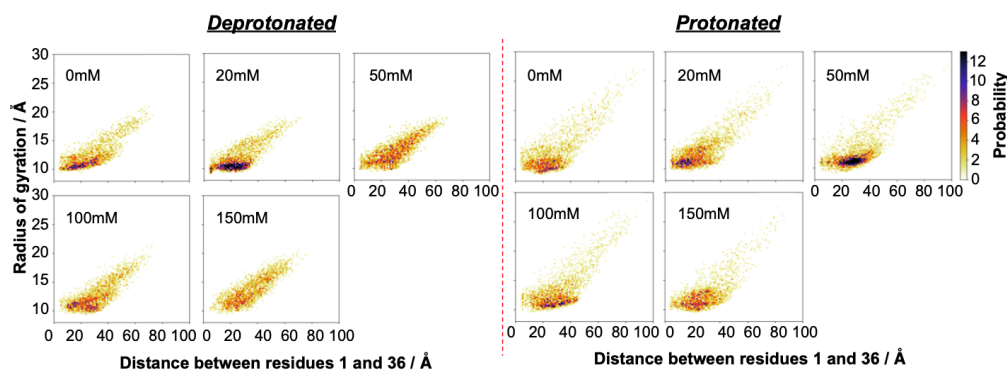


FIGURE 5.3: **Increased salt concentration induces extended conformations of deprotonated pHLIP.** *Left:* Radius of gyration of deprotonated pHLIP as a function of the distance between residues 1 and 36 of the peptide. *Right:* Radius of gyration of protonated pHLIP as a function of the distance between residues 1 and 36 of the peptide.

Our results show an increase in sampling of expanded deprotonated pHLIP at high salt concentrations, compared to lower concentrations (**Fig 5.3(left)**). Specifically, at 0mM and 20mM, deprotonated pHLIP remains mostly clustered with a radius of gyration (RoG) of around 10-15Å and a distance between residues of 4 to 40Å with a small percentage of data reaching $\text{RoG} \approx 20\text{Å}$ and distances of up to 70Å. However, as the salt concentration is increased to 50mM, 100mM and 150mM, a rise of the number of longer conformations is observed, becoming a more uniform sampling map. Contrary to these results, protonated pHLIP remains highly

clustered with RoG of around 10-15Å and distances between 5-45Å independently of salt concentration(**Fig 5.3(right)**). Interestingly, however briefly, protonated pHLIP is able to reach further distances (up to 95 Å) and RoG ($\approx 27\text{Å}$) in all 5 systems, independently of salt concentrations. These results suggest restriction of movement for deprotonated pHLIP at low NaCl concentrations, which is quickly resolved at higher ones. This behavior could be the result of helical content of the N-terminus, restricting the peptide, and extension of C-terminus to allow for efficient clustering of Na⁺ ions around acidic residues[35]. On the other hand, protonated results suggest high clustering of the peptide, could be an attempt of the system to shield protonated residues, as they are hydrophobic in nature and prefer to avoid solvent. This would explain why only small quantities of the peptide expand fully, even though helical content is low, and thus not a limiting factor.

5.4.3 Number of contacts increases with salt.

The importance of contacts between peptides and surrounding complexes is at the center of peptide functionality for biomedical applications[40–42]. Specifically, contacts between residues in proteins have been used in the past to determine secondary structure tendencies and functionality of proteins and peptides[43, 44]. Thus, here we made use of the native contacts command in cpptraj (Amber-Tools)[23] to quantify the average number of contacts occurring between pHLIP residues as a function of NaCl, and calculate the fraction of time of those contacts (**Fig 5.4**).

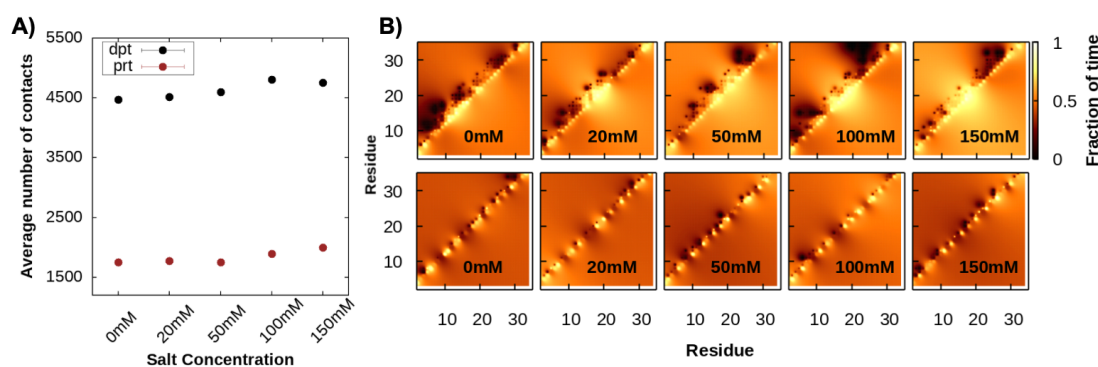


FIGURE 5.4: **Salt concentration directly affects contacts.** **A)** Average number of contacts as a function of salt concentration, for deprotonated (*black*) and protonated (*red*) pHLIP. **B)** Contact times for deprotonated (*top*) and protonated (*bottom*) pHLIP as a function of salt concentration.

Our results show an increase on the number of contacts as NaCl concentration increases (**Fig 5.4A**) for both protonated (*red*) and deprotonated (*black*) pHLIP. Direct comparison of trends between protonated and deprotonated pHLIP shows to be symmetrical, however deprotonated pHLIP has an average of ≈ 2800 contacts more than protonated simulations, independently of NaCl concentration. This is consistent with the higher degree of helical conformation observed for deprotonated versus protonated pHLIP (**Fig 5.2**). Contact times between residues (**Fig 5.4B**) also show a remarkable trend: Contact time between residues increases with salt concentrations for deprotonated simulations, while protonated systems do not show a significant change in contact time. The rise in contact time for residues 12-21 in deprotonated pHLIP is in parallel with the results per residue found in the helical content analysis, grounding the hypothesis that there is a direct correlation between contacts and secondary structure reported in previous studies of similar systems[43, 44]. On the other hand, the combination of lower average number of contacts and shorter contacts could indicate that the peptide has a conformation that allows for free movement and coordination between residues (i.e. not a well-defined secondary structure) which is consistent with the results reported in **figure 5.2**.

5.5 Conclusion

The goal of this project was to better understand the effect of NaCl concentration on pHLIP in state I. Our results show that deprotonated pHLIP is directly affected by increasing salt concentrations. Specifically, salt induces an increase in the helicity of the N-terminus of the peptide at concentrations approaching physiological level (150mM), while the C-terminus remains unstructured throughout. These results support the conviction that spontaneous folding of the peptide for insertion requires not only a drop in pH but the presence of a lipid bilayer. This conclusion is further reinforced by the results obtained for protonated pHLIP, which remained largely unstructured, independently on salt concentration. Discrepancies in RoG and distance between residues 1-36 of protonated and deprotonated pHLIP offer a different picture: increase in salt induces overall expansion of deprotonated pHLIP, while protonated pHLIP remains clustered. These results could be a direct effect of interactions between Na⁺ ions and acidic residues, and hydrophobic forces of protonated residues of pHLIP, respectively. Our contacts results support

our helicity conclusions, by showing increasing number of contacts with higher salt concentrations and longer interactions between residues. Overall, our results show that changes in salt concentration only affect deprotonated pHLIP, while protonated pHLIP remains undisturbed. This infers that there is a direct relationship between salt concentration and secondary structure of deprotonated pHLIP in state I. Further studies of the system need to be performed in order to gain further understanding of the fundamental interactions that govern its structure and functionality.

Bibliography

- [1] Luis Rivas et al. “Membrane-active peptides as anti-infectious agents”. en. In: *Journal of Applied Biomedicine* 8.3 (July 2010), pp. 159–167. ISSN: 1214021X, 12140287. DOI: [10.2478/v10136-009-0019-3](https://doi.org/10.2478/v10136-009-0019-3). URL: <http://jab.zsf.jcu.cz/doi/10.2478/v10136-009-0019-3.html> (visited on 08/09/2021).
- [2] Marc-Antoine Sani and Frances Separovic. “How Membrane-Active Peptides Get into Lipid Membranes”. en. In: *Accounts of Chemical Research* 49.6 (June 2016), pp. 1130–1138. ISSN: 0001-4842, 1520-4898. DOI: [10.1021/acs.accounts.6b00074](https://doi.org/10.1021/acs.accounts.6b00074). URL: <https://pubs.acs.org/doi/10.1021/acs.accounts.6b00074> (visited on 08/09/2021).
- [3] Fatma Gizem Avci, Berna Sariyar Akbulut, and Elif Ozkirimli. “Membrane Active Peptides and Their Biophysical Characterization”. en. In: *Biomolecules* 8.3 (Aug. 2018), p. 77. ISSN: 2218-273X. DOI: [10.3390/biom8030077](https://doi.org/10.3390/biom8030077). URL: <http://www.mdpi.com/2218-273X/8/3/77> (visited on 08/09/2021).
- [4] Zahra Vaezi et al. “Aggregation determines the selectivity of membrane-active anticancer and antimicrobial peptides: The case of killerFLIP”. en. In: *Biochimica et Biophysica Acta (BBA) - Biomembranes* 1862.2 (Feb. 2020), p. 183107. ISSN: 00052736. DOI: [10.1016/j.bbamem.2019.183107](https://doi.org/10.1016/j.bbamem.2019.183107). URL: <https://linkinghub.elsevier.com/retrieve/pii/S0005273619302536> (visited on 08/09/2021).
- [5] Priyanka Singh et al. “Membrane Active Peptides Remove Surface Adsorbed Protein Corona From Extracellular Vesicles of Red Blood Cells”. en. In: *Frontiers in Chemistry* 8 (Aug. 2020), p. 703. ISSN: 2296-2646. DOI: [10.3389/fchem.2020.00703](https://doi.org/10.3389/fchem.2020.00703). URL: <https://www.frontiersin.org/article/10.3389/fchem.2020.00703/full> (visited on 08/09/2021).

- [6] Jianguo Li et al. “Membrane Active Antimicrobial Peptides: Translating Mechanistic Insights to Design”. en. In: *Frontiers in Neuroscience* 11 (Feb. 2017). ISSN: 1662-453X. DOI: [10.3389/fnins.2017.00073](https://doi.org/10.3389/fnins.2017.00073). URL: <http://journal.frontiersin.org/article/10.3389/fnins.2017.00073/full> (visited on 08/09/2021).
- [7] Yu Zai et al. “Aggregation and Its Influence on the Bioactivities of a Novel Antimicrobial Peptide, Temporin-PF, and Its Analogues”. en. In: *International Journal of Molecular Sciences* 22.9 (Apr. 2021), p. 4509. ISSN: 1422-0067. DOI: [10.3390/ijms22094509](https://doi.org/10.3390/ijms22094509). URL: <https://www.mdpi.com/1422-0067/22/9/4509> (visited on 08/09/2021).
- [8] Federica Rinaldi et al. “Decoration of Nanovesicles with pH (Low) Insertion Peptide (pHLIP) for Targeted Delivery”. en. In: *Nanoscale Research Letters* 13.1 (Dec. 2018), p. 391. ISSN: 1931-7573, 1556-276X. DOI: [10.1186/s11671-018-2807-8](https://doi.org/10.1186/s11671-018-2807-8). URL: <https://nanoscalereslett.springeropen.com/articles/10.1186/s11671-018-2807-8> (visited on 03/18/2021).
- [9] Xiao Luo et al. “Highly Sensitive Hill-Type Small-Molecule pH Probe That Recognizes the Reversed pH Gradient of Cancer Cells”. en. In: *Analytical Chemistry* 90.9 (May 2018), pp. 5803–5809. ISSN: 0003-2700, 1520-6882. DOI: [10.1021/acs.analchem.8b00218](https://doi.org/10.1021/acs.analchem.8b00218). URL: <https://pubs.acs.org/doi/10.1021/acs.analchem.8b00218> (visited on 03/18/2021).
- [10] Alexander M. Demin et al. “Smart Design of a pH-Responsive System Based on pHLIP-Modified Magnetite Nanoparticles for Tumor MRI”. en. In: *ACS Applied Materials & Interfaces* (July 2021), acsami.1c07748. ISSN: 1944-8244, 1944-8252. DOI: [10.1021/acsami.1c07748](https://doi.org/10.1021/acsami.1c07748). URL: <https://pubs.acs.org/doi/10.1021/acsami.1c07748> (visited on 08/02/2021).
- [11] Oleg A. Andreev, Donald M. Engelman, and Yana K. Reshetnyak. “Targeting diseased tissues by pHLIP insertion at low cell surface pH”. en. In: *Frontiers in Physiology* 5 (Mar. 2014). ISSN: 1664-042X. DOI: [10.3389/fphys.2014.00097](https://doi.org/10.3389/fphys.2014.00097). URL: <http://journal.frontiersin.org/article/10.3389/fphys.2014.00097/abstract> (visited on 03/18/2021).
- [12] John F Hunt et al. “Spontaneous, pH-Dependent Membrane Insertion of a Transbilayer R-Helix”. en. In: (), p. 16.

- [13] M. An et al. “pH-(low)-insertion-peptide (pHLIP) translocation of membrane impermeable phalloidin toxin inhibits cancer cell proliferation”. en. In: *Proceedings of the National Academy of Sciences* 107.47 (Nov. 2010), pp. 20246–20250. ISSN: 0027-8424, 1091-6490. DOI: [10.1073/pnas.1014403107](https://doi.org/10.1073/pnas.1014403107). URL: <http://www.pnas.org/cgi/doi/10.1073/pnas.1014403107> (visited on 08/02/2021).
- [14] Oleg A. Andreev et al. “pH (Low) Insertion Peptide (pHLIP) Inserts across a Lipid Bilayer as a Helix and Exits by a Different Path”. en. In: *Proceedings of the National Academy of Sciences* 107.9 (Feb. 2010), pp. 4081–4086. ISSN: 0027-8424, 1091-6490. DOI: [10.1073/pnas.0914330107](https://doi.org/10.1073/pnas.0914330107).
- [15] Yana K. Reshetnyak et al. “A Monomeric Membrane Peptide that Lives in Three Worlds: In Solution, Attached to, and Inserted across Lipid Bilayers”. en. In: *Biophysical Journal* 93.7 (Oct. 2007), pp. 2363–2372. ISSN: 00063495. DOI: [10.1529/biophysj.107.109967](https://doi.org/10.1529/biophysj.107.109967). URL: <https://linkinghub.elsevier.com/retrieve/pii/S0006349507714911> (visited on 08/02/2021).
- [16] Chitrak Gupta and Blake Mertz. “Protonation Enhances the Inherent Helix-Forming Propensity of pHLIP”. In: *ACS Omega* 2.11 (Nov. 2017), pp. 8536–8542. ISSN: 2470-1343. DOI: [10.1021/acsomega.7b01371](https://doi.org/10.1021/acsomega.7b01371).
- [17] Nicolas Frazee and Blake Mertz. “Intramolecular interactions play key role in stabilization of α -pHLIP at acidic conditions”. en. In: *Journal of Computational Chemistry* 42.25 (Sept. 2021), pp. 1809–1816. ISSN: 0192-8651, 1096-987X. DOI: [10.1002/jcc.26719](https://doi.org/10.1002/jcc.26719). URL: <https://onlinelibrary.wiley.com/doi/10.1002/jcc.26719> (visited on 08/09/2021).
- [18] Victor Vasquez-Montes et al. “Comparison of Lipid-Dependent Bilayer Insertion of pHLIP and Its P20G Variant”. In: *Biochimica et Biophysica Acta (BBA) - Biomembranes* 1860.2 (Feb. 2018), pp. 534–543. ISSN: 0005-2736. DOI: [10.1016/j.bbamem.2017.11.006](https://doi.org/10.1016/j.bbamem.2017.11.006).
- [19] W. Humphrey, A. Dalke, and K. Schulten. “VMD: Visual Molecular Dynamics”. eng. In: *Journal of Molecular Graphics* 14.1 (Feb. 1996), pp. 33–38. ISSN: 0263-7855.
- [20] Saeed Izadi, Ramu Anandakrishnan, and Alexey V. Onufriev. “Building Water Models: A Different Approach”. In: *The Journal of Physical Chemistry Letters* 5.21 (Nov. 2014), pp. 3863–3871. ISSN: 1948-7185. DOI: [10.1021/jz501780a](https://doi.org/10.1021/jz501780a).

- [21] Callum J. Dickson et al. “Lipid14: The Amber Lipid Force Field”. eng. In: *Journal of Chemical Theory and Computation* 10.2 (Feb. 2014), pp. 865–879. ISSN: 1549-9626. DOI: [10.1021/ct4010307](https://doi.org/10.1021/ct4010307).
- [22] James A. Maier et al. “ff14SB: Improving the Accuracy of Protein Side Chain and Backbone Parameters from ff99SB”. eng. In: *Journal of Chemical Theory and Computation* 11.8 (Aug. 2015), pp. 3696–3713. ISSN: 1549-9626. DOI: [10.1021/acs.jctc.5b00255](https://doi.org/10.1021/acs.jctc.5b00255).
- [23] D.A. Case et al. *Amber18*. University of California, San Francisco. 2019.
- [24] Andreas W. Götz et al. “Routine Microsecond Molecular Dynamics Simulations with AMBER on GPUs. 1. Generalized Born”. In: *Journal of Chemical Theory and Computation* 8.5 (May 2012), pp. 1542–1555. ISSN: 1549-9618. DOI: [10.1021/ct200909j](https://doi.org/10.1021/ct200909j).
- [25] Tod D. Romo, Nicholas Leioatts, and Alan Grossfield. “Lightweight Object Oriented Structure Analysis: Tools for Building Tools to Analyze Molecular Dynamics Simulations”. en. In: *Journal of Computational Chemistry* 35.32 (Dec. 2014), pp. 2305–2318. ISSN: 1096-987X. DOI: [10.1002/jcc.23753](https://doi.org/10.1002/jcc.23753).
- [26] Schrödinger, LLC. “The PyMOL Molecular Graphics System, Version 1.8”. Nov. 2015.
- [27] J. D. Hunter. “Matplotlib: A 2D graphics environment”. In: *Computing in Science & Engineering* 9.3 (2007), pp. 90–95. DOI: [10.1109/MCSE.2007.55](https://doi.org/10.1109/MCSE.2007.55).
- [28] Thomas Williams and Colin Kelley. *Gnuplot 5.2: An Interactive Plotting Program*. 2020.
- [29] Oleg A. Andreev, Donald M. Engelman, and Yana K. Reshetnyak. “pH-sensitive membrane peptides (pHLIPs) as a novel class of delivery agents”. en. In: *Molecular Membrane Biology* 27.7 (Oct. 2010), pp. 341–352. ISSN: 0968-7688, 1464-5203. DOI: [10.3109/09687688.2010.509285](https://doi.org/10.3109/09687688.2010.509285). URL: <http://www.tandfonline.com/doi/full/10.3109/09687688.2010.509285> (visited on 08/02/2021).
- [30] Theyencheri Narayanan et al. “pHLIP Peptide Interaction with a Membrane Monitored by SAXS”. en. In: *The Journal of Physical Chemistry B* 120.44 (Nov. 2016), pp. 11484–11491. ISSN: 1520-6106, 1520-5207. DOI: [10.1021/acs.jpcc.6b06643](https://doi.org/10.1021/acs.jpcc.6b06643). URL: <https://pubs.acs.org/doi/10.1021/acs.jpcc.6b06643> (visited on 03/18/2021).

- [31] Victor Vasquez-Montes et al. “Divalent Cations and Lipid Composition Modulate Membrane Insertion and Cancer-Targeting Action of pHLIP”. en. In: *Journal of Molecular Biology* 431.24 (Nov. 2019), pp. 5004–5018. ISSN: 0022-2836. DOI: [10.1016/j.jmb.2019.10.016](https://doi.org/10.1016/j.jmb.2019.10.016).
- [32] F. N. Barrera, J. Fendos, and D. M. Engelman. “Membrane physical properties influence transmembrane helix formation”. en. In: *Proceedings of the National Academy of Sciences* 109.36 (Sept. 2012), pp. 14422–14427. ISSN: 0027-8424, 1091-6490. DOI: [10.1073/pnas.1212665109](https://doi.org/10.1073/pnas.1212665109). URL: <http://www.pnas.org/cgi/doi/10.1073/pnas.1212665109> (visited on 08/02/2021).
- [33] Gregory Slaybaugh et al. “Kinetics of pHLIP peptide insertion into and exit from a membrane”. en. In: *Proceedings of the National Academy of Sciences* 117.22 (June 2020), pp. 12095–12100. ISSN: 0027-8424, 1091-6490. DOI: [10.1073/pnas.1917857117](https://doi.org/10.1073/pnas.1917857117). URL: <http://www.pnas.org/lookup/doi/10.1073/pnas.1917857117> (visited on 08/02/2021).
- [34] Lukas S. Stelzl and Gerhard Hummer. “Kinetics from Replica Exchange Molecular Dynamics Simulations.” eng. In: *Journal of chemical theory and computation* 13.8 (Aug. 2017). Place: United States, pp. 3927–3935. ISSN: 1549-9626 1549-9618. DOI: [10.1021/acs.jctc.7b00372](https://doi.org/10.1021/acs.jctc.7b00372).
- [35] Justin Westerfield et al. “Ions Modulate Key Interactions between pHLIP and Lipid Membranes”. en. In: *Biophysical Journal* 117.5 (Sept. 2019), pp. 920–929. ISSN: 00063495. DOI: [10.1016/j.bpj.2019.07.034](https://doi.org/10.1016/j.bpj.2019.07.034). URL: <https://linkinghub.elsevier.com/retrieve/pii/S000634951930623X> (visited on 08/02/2021).
- [36] Mads Nygaard et al. “An Efficient Method for Estimating the Hydrodynamic Radius of Disordered Protein Conformations”. en. In: *Biophysical Journal* 113.3 (Aug. 2017), pp. 550–557. ISSN: 00063495. DOI: [10.1016/j.bpj.2017.06.042](https://doi.org/10.1016/j.bpj.2017.06.042). URL: <https://linkinghub.elsevier.com/retrieve/pii/S0006349517306926> (visited on 08/09/2021).
- [37] John J. Tanner. “Empirical power laws for the radii of gyration of protein oligomers”. en. In: *Acta Crystallographica Section D Structural Biology* 72.10 (Oct. 2016), pp. 1119–1129. ISSN: 2059-7983. DOI: [10.1107/S2059798316013218](https://doi.org/10.1107/S2059798316013218). URL: <http://scripts.iucr.org/cgi-bin/paper?S2059798316013218> (visited on 08/10/2021).

- [38] Zhouting Jiang et al. “Effects of an Electric Field on the Conformational Transition of the Protein: A Molecular Dynamics Simulation Study”. en. In: *Polymers* 11.2 (Feb. 2019), p. 282. ISSN: 2073-4360. DOI: [10.3390/polym11020282](https://doi.org/10.3390/polym11020282). URL: <http://www.mdpi.com/2073-4360/11/2/282> (visited on 08/10/2021).
- [39] M. Yu. Lobanov, N. S. Bogatyreva, and O. V. Galzitskaya. “Radius of gyration as an indicator of protein structure compactness”. In: *Molecular Biology* 42.4 (Aug. 2008), pp. 623–628. ISSN: 1608-3245. DOI: [10.1134/S0026893308040195](https://doi.org/10.1134/S0026893308040195). URL: <https://doi.org/10.1134/S0026893308040195>.
- [40] Jeffrey L. Jorgensen et al. “Mapping T-cell receptor–peptide contacts by variant peptide immunization of single-chain transgenics”. In: *Nature* 355.6357 (Jan. 1992), pp. 224–230. ISSN: 1476-4687. DOI: [10.1038/355224a0](https://doi.org/10.1038/355224a0). URL: <https://doi.org/10.1038/355224a0>.
- [41] Robert M. Parrish et al. “The Surprising Importance of Peptide Bond Contacts in Drug-Protein Interactions.” eng. In: *Chemistry (Weinheim an der Bergstrasse, Germany)* 23.33 (June 2017). Place: Germany, pp. 7887–7890. ISSN: 1521-3765 0947-6539. DOI: [10.1002/chem.201701031](https://doi.org/10.1002/chem.201701031).
- [42] David Cole. “Increased Peptide Contacts Govern High Affinity Binding of a Modified TCR Whilst Maintaining a Native pMHC Docking Mode”. In: *Frontiers in Immunology* 4 (2013), p. 168. ISSN: 1664-3224. DOI: [10.3389/fimmu.2013.00168](https://doi.org/10.3389/fimmu.2013.00168). URL: <https://www.frontiersin.org/article/10.3389/fimmu.2013.00168>.
- [43] Badri Adhikari and Jianlin Cheng. “Protein Residue Contacts and Prediction Methods”. en. In: *Data Mining Techniques for the Life Sciences*. Ed. by Oliviero Carugo and Frank Eisenhaber. Vol. 1415. Series Title: Methods in Molecular Biology. New York, NY: Springer New York, 2016, pp. 463–476. ISBN: 978-1-4939-3570-3 978-1-4939-3572-7. DOI: [10.1007/978-1-4939-3572-7_24](https://doi.org/10.1007/978-1-4939-3572-7_24). URL: http://link.springer.com/10.1007/978-1-4939-3572-7_24 (visited on 08/10/2021).
- [44] Vladimir Potapov, Marvin Edelman, and Vladimir Sobolev. “Residue-residue contacts: application to analysis of secondary structure interactions.” eng. In: *Methods in molecular biology (Clifton, N.J.)* 932 (2013). Place: United States, pp. 159–173. ISSN: 1940-6029 1064-3745. DOI: [10.1007/978-1-62703-065-6_10](https://doi.org/10.1007/978-1-62703-065-6_10).

Chapters/chapterV

Chapter 6

Future directions

The knowledge conveyed in the above projects can be applied to a wide range of systems, specially in biological systems that remain poorly understood. The RAS protein is a member of the small GTPase family of proteins, able to bind to guanosine nucleotide forms part of the signaling cascade responsible for cell growth. Localized mutations in RAS account for 20% of all cancer cases and treatment of such afflictions has not been found yet, hence the need to further understand the protein.

RAS has 2 states: on and off. In the deactivated state, RAS is bound to the nucleotide guanosine diphosphate (GDP), while activation of RAS when the protein switches the GDP for the nucleotide guanosine triphosphate (GTP). The activation and deactivation of RAS is a cyclic process, promoted by the exchange of GTP to GDP and vice versa. This binding and unbinding procedures are facilitated by 2 other types of proteins: guanosine nucleotide exchange factors (GEFs) and GTPase activating proteins (GAP's). While RAS can hydrolyze the GTP to GDP and become deactivated, the process is too long and hence, RAS binding to GAP proteins help speed the process to an efficient rate. Under normal conditions, this process is able to cycle around each time there is a need for new cells to be formed, or when the task is completed and cell proliferation is no longer required. However, in cancer cells, RAS possesses localized mutations that hinder the binding on RAS to GAP in order to speed the process and deactivate, and hence, producing uncontrollable cell growth.

Although proteins involved in this process, such as RAS, GAP and RAF (RAS effector protein) have been studied for several decades, there are characteristics of

the structure and functionality of each that remain poorly understood. In future studies we aim to use our methodology and expertise in molecular dynamics simulations to gain insights into how RAS works, how environmental factors, such as lipid composition, close proximity of RAS to other proteins, etc. affect functionality of RAS and capability to bind to GAP. Furthermore, we aim to explore drug discovery for RAS deactivation, therefore getting one step closer towards effective treatment to cancers caused by RAS mutations.